MULTIDISCIPLINARY CENTER FOR EARTHQUAKE ENGINEERING RESEARCH
A National Center of Excellence in Advanced Technology Applications

ISSN 1520-295X

Approaches for the Seismic Retrofit of Braced Steel Bridge Piers and Proof-of-Concept Testing of an Eccentrically Braced Frame with Tubular Link

by

Jeffrey W. Berman and Michel Bruneau
University at Buffalo, State University of New York
Department of Civil, Structural and Environmental Engineering
Ketter Hall
Buffalo, New York 14260

Technical Report MCEER-05-0004

April 21, 2005

This research was conducted at the University at Buffalo, State University of New York and was supported by the Federal Highway Administration under contract number DTFH61-98-C-00094.

NOTICE

This report was prepared by the University at Buffalo, State University of New York as a result of research sponsored by the Multidisciplinary Center for Earthquake Engineering Research (MCEER) through a contract from the Federal Highway Administration. Neither MCEER, associates of MCEER, its sponsors, the University at Buffalo, State University of New York, nor any person acting on their behalf:

a. makes any warranty, express or implied, with respect to the use of any information, apparatus, method, or process disclosed in this report or that such use may not infringe upon privately owned rights; or

b. assumes any liabilities of whatsoever kind with respect to the use of, or the damage resulting from the use of, any information, apparatus, method, or process disclosed in this report.

Any opinions, findings, and conclusions or recommendations expressed in this publication are those of the author(s) and do not necessarily reflect the views of MCEER or the Federal Highway Administration.

MULTIDISCIPLINARY CENTER FOR EARTHQUAKE ENGINEERING RESEARCH
A National Center of Excellence in Advanced Technology Applications

Approaches for the Seismic Retrofit of Braced Steel Bridge Piers and Proof-of-Concept Testing of an Eccentrically Braced Frame with Tubular Link

by

Jeffrey W. Berman[1] and Michel Bruneau[2]

Publication Date: April 21, 2005
Submittal Date: September 14, 2004

Technical Report MCEER-05-0004

Task Number 094-C-3.3

FHWA Contract Number DTFH61-98-C-00094

1 Graduate Student, Department of Civil, Structural and Environmental Engineering, University at Buffalo, State University of New York
2 Professor, Department of Civil, Structural and Environmental Engineering, University at Buffalo, State University of New York

MULTIDISCIPLINARY CENTER FOR EARTHQUAKE ENGINEERING RESEARCH
University at Buffalo, State University of New York
Red Jacket Quadrangle, Buffalo, NY 14261

Preface

The Multidisciplinary Center for Earthquake Engineering Research (MCEER) is a national center of excellence in advanced technology applications that is dedicated to the reduction of earthquake losses nationwide. Headquartered at the University at Buffalo, State University of New York, the Center was originally established by the National Science Foundation in 1986, as the National Center for Earthquake Engineering Research (NCEER).

Comprising a consortium of researchers from numerous disciplines and institutions throughout the United States, the Center's mission is to reduce earthquake losses through research and the application of advanced technologies that improve engineering, pre-earthquake planning and post-earthquake recovery strategies. Toward this end, the Center coordinates a nationwide program of multidisciplinary team research, education and outreach activities.

MCEER's research is conducted under the sponsorship of two major federal agencies, the National Science Foundation (NSF) and the Federal Highway Administration (FHWA), and the State of New York. Significant support is also derived from the Federal Emergency Management Agency (FEMA), other state governments, academic institutions, foreign governments and private industry.

The Center's Highway Project develops improved seismic design, evaluation, and retrofit methodologies and strategies for new and existing bridges and other highway structures, and for assessing the seismic performance of highway systems. The FHWA has sponsored three major contracts with MCEER under the Highway Project, two of which were initiated in 1992 and the third in 1998.

Of the two 1992 studies, one performed a series of tasks intended to improve seismic design practices for new highway bridges, tunnels, and retaining structures (MCEER Project 112). The other study focused on methodologies and approaches for assessing and improving the seismic performance of existing "typical" highway bridges and other highway system components including tunnels, retaining structures, slopes, culverts, and pavements (MCEER Project 106). These studies were conducted to:

- assess the seismic vulnerability of highway systems, structures, and components;
- develop concepts for retrofitting vulnerable highway structures and components;
- develop improved design and analysis methodologies for bridges, tunnels, and retaining structures, which include consideration of soil-structure interaction mechanisms and their influence on structural response; and
- develop, update, and recommend improved seismic design and performance criteria for new highway systems and structures.

The 1998 study, "Seismic Vulnerability of the Highway System" (FHWA Contract DTFH61-98-C-00094; known as MCEER Project 094), was initiated with the objective of performing studies to improve the seismic performance of bridge types not covered under Projects 106 or 112, and to provide extensions to system performance assessments for highway systems. Specific subjects covered under Project 094 include:

- development of formal loss estimation technologies and methodologies for highway systems;
- analysis, design, detailing, and retrofitting technologies for special bridges, including those with flexible superstructures (e.g., trusses), those supported by steel tower substructures, and cable-supported bridges (e.g., suspension and cable-stayed bridges);
- seismic response modification device technologies (e.g., hysteretic dampers, isolation bearings); and
- soil behavior, foundation behavior, and ground motion studies for large bridges.

In addition, Project 094 includes a series of special studies, addressing topics that range from non-destructive assessment of retrofitted bridge components to supporting studies intended to assist in educating the bridge engineering profession on the implementation of new seismic design and retrofitting strategies.

The research discussed in this report was performed within Project 094, Task C-3.3, "Steel Substructures." The report identifies, categorizes, and qualitatively compares several options for the seismic retrofit of truss braced steel bridge piers. Through these comparisons, two promising strategies that lacked fundamental research necessary for implementation were identified as follows:

- *Laterally stable links for eccentrically braced frames.*
- *Design of supplemental retrofit systems for protection of existing elements.*

An initial theoretical and experimental investigation on the first topic listed above, using links with hybrid rectangular cross-sections to achieve the desired performance, is described. Equations for plastic shear, plastic moment, link length, stiffener spacing, maximum flange compactness, and link overstrength were derived consistent with the development of the existing codified design equations for WF links in eccentrically braced frames (EBFs). A proof-of-concept test specimen was designed and tested under cyclic, quasi-static conditions. The test specimen met and exceeded performance objectives in terms of both link rotation and ductility. No signs of lateral torsional buckling of the link and link beam were observed. Comparison of the results of this single test specimen with the equations derived for design showed reasonable agreement in terms of strength calculations. It was then determined that the stiffener spacing equation derived here and web compactness limits from the AISC seismic provisions for webs of HSS sections are likely redundant (i.e., both may not need to be satisfied). Basic fractographic analysis of the failure surface of the link flange indicated a combination of ductile cyclic crack propagation followed by brittle fracture through the remaining material. Fracture was found to initiate at the toe of stiffener welds that were placed perpendicular to the longitudinal direction of the flange and seemed unaffected by the welds used to form the rectangular link cross-section from four plates. Finally, the energy dissipation of the link was shown to be stable with increasing energy dissipation per cycle up to failure.

ABSTRACT

There are many steel truss bridges in the United States and other countries that were constructed at a time when seismic design was not well understood. Many of these bridges are now considered to be seismically vulnerable. Contributing significantly to their undesirable seismic performance are the braced steel piers that support the superstructure. These piers typically have bracing members that are made up of channels or angles that are tied together with steel lacings and rivets. Recent experimental investigations have shown that such structural members can suffer severe local buckling, rapid strength degradation, and limited ductility, when subjected to cyclic loading. Therefore, it is necessary to develop retrofit strategies for these piers that focus on protecting, strengthening, or increasing the ductility of the existing brace members.

This report describes, categorizes, and uses selected qualitative measures to rate various retrofit strategies for steel truss bridge piers. Promising retrofit strategies which require fundamental research before they can be properly implemented are then identified. One such strategy is an eccentrically braced frame where the link is not subject to lateral torsional buckling. This is desirable since eccentrically braced frames have been shown to exhibit excellent seismic performance, and if lateral bracing of the link can be avoided, they can be easily implemented in bridge piers where lateral bracing can be difficult to provide.

Design equations are then derived for links of eccentrically braced frames with hybrid rectangular cross-sections (hybrid meaning that the webs and flanges may have different yield stresses) including compactness requirements and stiffener spacings. Using the derived design equations, a proof-of-concept experimental study is designed and conducted. It is found that the hybrid rectangular link shows stable and ductile cyclic behavior with no sign of lateral torsional buckling, in absence of lateral bracing. Recommendations are then given for further research on both hybrid rectangular links for eccentrically braced frames and selected other retrofit strategies for the braced steel piers of truss bridges.

ACKNOWLEDGMENTS

Sincere thanks to the staff of the Structural Engineering and Earthquake Simulation Laboratory at the University of Buffalo, Duane Kozlowski, Scot Weinreber, Dick Cizdziel, and Mark Pitman for their assistance and expertise.

This research was conducted by the State University of New York at Buffalo and was supported by the Federal Highway Administration under contract number DTFH61-98-C-00094 to the Multidisciplinary Center for Earthquake Engineering Research. However, any opinions, findings, conclusions, and recommendations presented in this paper are those of the authors and do not necessarily reflect the views of the sponsors.

TABLE OF CONTENTS

TABLE OF CONTENTS (CONTINUED)

TABLE OF CONTENTS (CONTINUED)

TABLE OF CONTENTS (CONTINUED)

LIST OF FIGURES

LIST OF FIGURES (CONTINUED)

LIST OF FIGURES (CONTINUED)

LIST OF TABLES

NOTATIONS

a	Stiffener spacing
A_g	Gross area of section
A_s	Shear area of section
b	Flange width
c	Fatigue ductility exponent
C	Constant for elastic flange buckling
C_B	Factor for stiffener spacing equation
d	Section depth
d_b	Beam depth
d_c	Column depth
d_s	Stiffener depth
D_i	Minor damage index
D_x	Plastic plate modulus in x direction
D_y	Plastic plate modulus in y direction
D_{xy}	Plastic plate modulus in x-y (shear) direction
e	Link length
e^*	Balanced link length
e_{fl}	Length of flange in compression
e_i	Distance from link end to inflection point
E	Young's modulus of elasticity
$(EI)_{fl}$	Flange rigidity
$(EI)_{st}$	Stiffener rigidity
F_{uf}	Ultimate stress of flanges
F_{uw}	Ultimate stress of webs
F_y	Yield stress
F_{yf}	Yield stress of flanges
F_{yo}	Yield stress of existing braces
F_{yr}	Yield stress of supplemental braces
F_{yst}	Yield stress of stiffeners

NOTATIONS (CONTINUED)

F_{yw}	Yield stress of webs
G	Elastic shear modulus
G_s	Secant shear modulus
G_t	Plastic shear modulus
h	Panel height and height of test specimen from lower clevis to link centerline
h^*	Distance from upper clevis to link centerline
I_{st}	Stiffener moment of inertia about the web
I_{stf}	Flange stiffener moment of inertia about it's major axis
$K_s(\alpha)$	Boundary condition coefficient for shear buckling
L	Bay width
l_h	Half buckling wavelength of a plate
l_y	Flange yield length
m	Number of equidistant spaces between stiffeners
M	Applied moment
M_{8e}	Link end moment at 0.08 rads of link rotation
M_A	Link moment at end A
M_h	General link end moment
M_L	Experimentally obtained link end moment
M_{maxe}	Maximum experimentally obtained link end moment
M_p	Plastic moment
M_{pr}	Plastic moment reduced for full plastic shear force
M_{pra}	Plastic moment reduced for full plastic shear force and axial force P
M_p^f	Local flange plastic moment considering flange axial force
$M_{po}^{\ f}$	Local flange plastic moment without considering flange axial force
M_p^V	Plastic moment reduced for plastic shear force V_p^M
M_{Vpe}	Link end moment at the experimentally obtained plastic shear force
$\mathrm{M}(x)$	Link moment at x
N_f	Number of cycles to failure
N_{fi}	Number of cycles to failure at i^{th} plastic strain amplitude

NOTATIONS (CONTINUED)

P	Axial force
P_{br}	Design brace axial force
P_f	Flange axial force due to the overall link moment
P_{fy}	Flange yield axial force
P_s	Tributary force resisted by one stiffener
P_y	Product of flange yield stress and gross area of section
Q	Cross-section parameter for shear-moment interaction
R_y	Ratio of expected to specified yield stress
t_{cf}	Column flange thickness
t_{cw}	Column web thickness
t_f	Flange thickness
t_f	Stiffener thickness
t_w	Web thickness
V	Applied shear force
V_{8e}	Experimentally obtained link shear at 0.08 rads of rotation
V_a	Applied actuator load
V_f	Shear force carried by the flanges
V_L	Applied link shear force
V_{maxe}	Experimentally obtained maximum link shear
V_p	Plastic shear force
V_{p1}	Maximum possible link shear strength - method 1
V_{p2}	Maximum possible link shear strength - method 2
V_{p3}	Maximum possible link shear strength - method 3
V_{panel}	Panel zone plastic shear
V_{pe}	Experimentally obtained link plastic shear
V_p^M	Plastic shear force reduced for moment M_p^V
w	Stiffener width
α	Ratio of axial force to shear force and stiffener spacing over clear web depth
β	Section depth over web thickness

NOTATIONS (CONTINUED)

Δ	Frame displacement
$\Delta\varepsilon_p$	Plastic strain amplitude
δ_{T2E}	Displacement measurement form instrument T2E
δ_{TV3}	Displacement measurement form instrument TV3
δ_{TV4}	Displacement measurement form instrument TV4
δ_y	Specimen yield displacement
ε'_f	Fatigue ductility coefficient
γ	Link rotation angle
γ_u	Design or ultimate link rotation angle
$\overline{\gamma}_b$	Rotation from previous point of zero shear to the onset of web buckling
$\eta(\tau)$	Plastic reduction factor
θ	Brace angle with the horizontal
ν	Poisson's ratio
ϕ_v	Resistance factor for shear
ρ	Normalized link length
σ	Normal stress
σ_A	Flange normal stress from axial load
σ_{av}	Average flange normal stress
σ_b	Plastic plate compressive buckling stress
σ_{bm}	Minimum plastic plate compressive buckling stress
σ_{yA}	Flange yield stress reduced by σ_A
τ	Shear stress
τ_b	Plastic shear buckling stress
τ_E	Elastic shear buckling stress
ψ	Ratio of stiffener to flange rigidity

ABBREVIATIONS

ADAS	Added Damping and Stiffness Devices
AISC	American Institute of Steel Construction
ASD	Allowable Stress Design
ASTM	American Society for Testing and Materials
ATC	Applied Technology Council
CBF	Concentrically Braced Frame
EBF	Eccentrically Braced Frame
HSS	Hollow Structural Section
LRFD	Load and Resistance Factored Design
MCEER	Multidisciplinary Center for Earthquake Engineering Research
SEESL	Structural Engineering and Earthquake Simulation Laboratory
TADAS	Triangular Added Damping and Stiffness Devices
UB	University at Buffalo or Unbonded Brace
UTM	Universal Testing Machine
WF	Wide-Flange

SECTION 1

INTRODUCTION

1.1 Statement of Problem and Objectives

There are many bridges in the United States and other countries that are considered to be seismically vulnerable. Steel truss bridges, which are often long span bridges and may carry critical transportation lifelines, are one category of bridges which can be vulnerable. The piers of these bridges, and particularly the pier brace members, have been identified in previous studies as elements which may contribute significantly to the poor seismic performance of these bridges. Typically, the brace members are composed of angles or channels tied together with steel lacings and rivets. Experimental studies have shown these members are subject to local buckling, leading to rapid strength degradation and limited ductility when subjected to large cyclic loads.

The retrofit of these piers and bracing members is paramount to insuring the adequate seismic performance of steel bridges. The objective of this report is to describe many of the options that are available to engineers for the retrofit of braced steel bridge piers. Using selected qualitative measures, these retrofit strategies are compared. Promising strategies, for which fundamental research is necessary before they can be implemented, are identified. One of these promising strategies, the use of eccentrically braced frames with links that are not subject to lateral torsional buckling and therefore do not require lateral bracing, is then developed further through the derivation of design equations and a proof-of-concept experiment.

1.2 Scope of Work

The research conducted and reported herein is outlined below:

- Develop a list of the different retrofit strategies possible for the truss piers of steel bridges. These strategies include those that rely on passive energy dissipation through metallic yielding devices or friction dampers, as well as strengthening approaches. Fluid viscous damping, base isolation, and controlled rocking strategies are beyond the scope of this study.
- Categorize and rate the considered retrofit strategies using selected qualitative measures.
- Identify promising strategies for which fundamental research is necessary.
- Derive design requirements and equations for hybrid rectangular links for eccentrically braced frames (hybrid indicates that the webs and flanges may have different yield stresses).
- Design and perform a proof-of-concept experiment to show that links with hybrid rectangular cross-sections are laterally stable and can meet performance objectives without the need for lateral bracing.
- Investigate the experimental results to judge the appropriateness of the derived design requirements and equations.
- Recommend additional research needs for the retrofit strategy of laterally stable eccentrically braced frames, as well as those for some other promising strategies.

1.3 Report Organization

Section 2 contains the categorization, development of qualitative measures, and rating of many retrofit strategies for the truss piers of steel bridges that focus on protecting or replacing the laced brace members. This section also includes the identification of strategies which require fundamental research.

Section 3 focuses on the derivation of design equations and recommendations for links with hybrid rectangular cross-sections for use in eccentrically braced frames.

Section 4 describes the design and setup of a proof-of-concept experiment of an eccentrically braced frame having a link with a hybrid rectangular cross-section. Coupon test results on the material for the webs and flanges of the link are given and expected link plastic shear and plastic moment capacities using those results are reported.

Section 5 contains a description of the loading protocol used in the experiment. This is followed by observations made regarding the specimen behavior during testing, accompanied by several figures illustrating the specimen deformation. The failure mode of the link is then explored in the context of basic fractographic analysis.

Section 6 discusses the results of the proof-of-concept experiment in a quantitative manner and examines how the derived design equations and recommendations effected performance. Finally, cumulative energy dissipation of the link is investigated.

Section 7 contains conclusions and recommendations for further research. The recommendations are given for eccentrically braced frames having links with hybrid rectangular cross-sections, and for some of the other promising retrofit strategies identified in Section 2 for which fundamental research is necessary prior to their implementation.

SECTION 2

APPROACHES FOR THE SEISMIC RETROFIT OF STEEL TRUSS BRIDGE PIERS

2.1 General

One of the major factors effecting the seismic safety of steel truss bridges is their steel piers, and more specifically the pier bracing members (Astaneh et al., 1993, Astaneh et al., 1995, Ingham et al., 1995, and Ritchie et al., 1999). Typically, the pier bracing members are built-up sections consisting of channel or angle shapes tied together by lacing and rivets as shown in figure 2-1. A recent experimental study examined the strength and ductility of several types of these bracing members, generally referred to as laced members, and showed that they do indeed have limited ductility and suffer rapid strength degradation when subjected to cyclic loading (Lee and Bruneau, 2004). Failure modes observed ranged from global buckling of the entire member, to local buckling of angles, channels, or lacing, as well as rivet fracture. This study compliments and adds to previous experimental studies that examined "as built" lattice members (Astaneh et al., 1994, Uang and Keiser, 1997, Astaneh et al., 1998, and Itani et al., 1998).

In this section, several options for the seismic retrofit of steel truss bridge piers with lattice bracing members will be categorized, discussed, and qualitatively compared. These comparisons will provide the basis for further investigation of specific strategies and techniques in more quantitative ways. As there are many seismic retrofit options available for engineers, including isolation systems, viscous damping systems, active control, added stiffness/strength, controlled rocking, and hysteretic energy dissipation systems, only

strategies that fall under the last two broad categories will be considered here. For example, retrofit options utilizing metallic yielding devices or friction dampers.

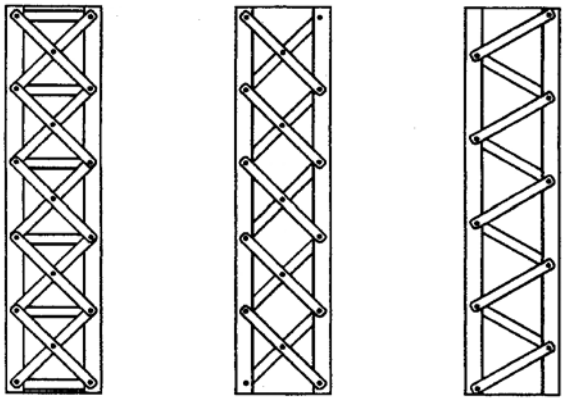

FIGURE 2-1 Typical Laced Member Types (Adapted from Ritchie et al., 1999)

2.2 Retrofit Classification

Retrofit strategies that stiffen, strengthen, and/or add hysteretic energy dissipation to existing braced steel truss bridge piers similar to that shown in figure 2-2 can focus on one of three major aspects, namely, the braces themselves, the brace connections, or the entire bracing system. Each focus is described in the following sections along with relevant specific retrofit strategies, which will facilitate the development of a large "matrix" of categorized retrofit options to help achieve useful qualitative comparisons.

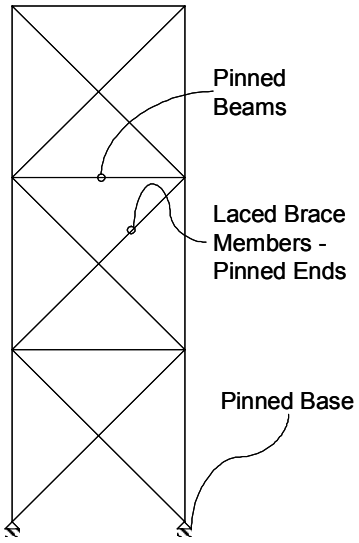

FIGURE 2-2 Typical Steel Truss Bridge Pier

2.2.1 Brace Retrofit

Retrofit of the braces can be broken down into two categories. First, the existing braces can be strengthened and/or made more ductile. Second, the existing braces could be replaced with new sections that have more desirable behavior without changing the overall brace configuration, load path, pier dimensions, beam sizes, etc.

Strategies identified in Ritchie et al. (1999) for increasing the strength and/or ductility of the existing laced braces consist of adding cover pates or replacing the lacing with solid or perforated plates. This approach has been implemented in some bridges (Ely and Birdy, 1997) and some specific configurations of cover plates have been tested (Dietrich and Itani, 1999). An alternative approach consists of wrapping the braces in a rubber or plastic material and encasing them in concrete to create a kind of unbonded brace.

Brace replacement is a fairly straightforward concept and be can be broken down further based on the type of new brace installed. For instance, the existing braces could be replaced with standard structural shapes (wide flange sections, or hollow structural sections), or they could be replaced with unbonded braces, which are becoming an appealing seismic retrofit option.

Using the above information, the options for brace retrofit can be illustrated with the tree diagram of figure 2-3.

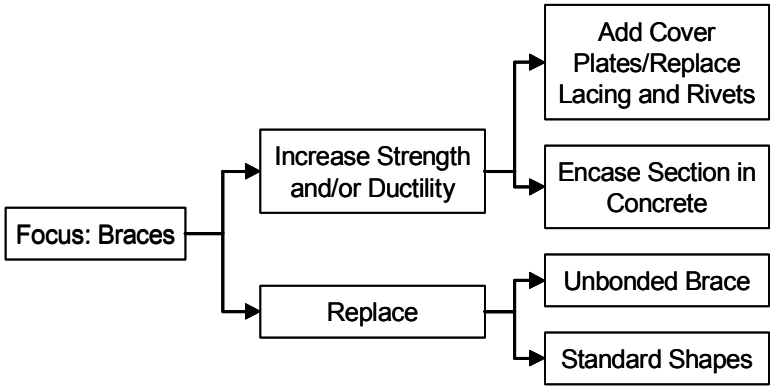

FIGURE 2-3 Brace Retrofit Tree Diagram

2.2.2 Brace Connection Retrofit

Options exist for retrofitting only the connections of the laced bracing members to the other pier members. In general, this retrofit focuses on inserting ductile energy dissipation devices, or structural fuses, either at brace intersection or end points. Many types of energy dissipation brace connection devices are available for this type of retrofit. For the purpose of this report, three major categories are defined, namely, those devices tested in a study by Rezai et al. (2000), the disposable knee brace (considered for the retrofit of brace endpoint connections), and all others. This broad categorization is acceptable because there are a large number of devices that for the most-part have the same qualitative pros and cons. The tree diagram of figure 2-4 is used to illustrate the retrofit options possible for brace connection retrofit.

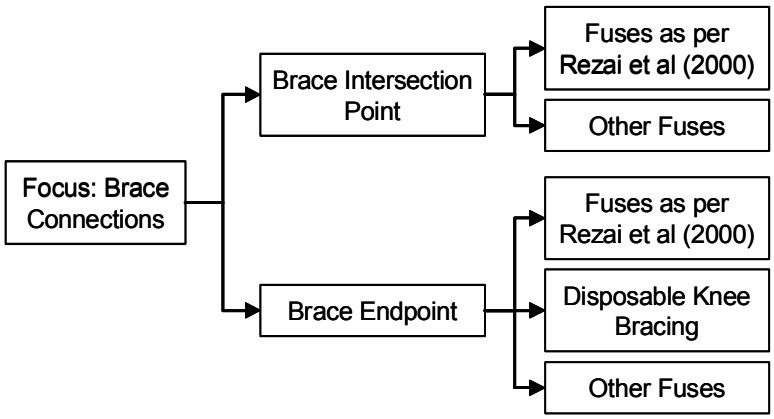

FIGURE 2-4 Brace Connection Retrofit Tree Diagram

2.2.3 Brace System Retrofit

The largest number of retrofit options available to engineers involve brace system retrofit. This includes retrofits in which the existing framing is left untouched and supplemented with additional framing which may or may not contain structural fuses: these will be known as "supplemental system" retrofit strategies here. Also included in the system retrofit category are options in which the existing braces, along with selected other pier components, are removed and replaced with a new system, these will be known as "replacement systems". In both cases the lateral load path through the pier could be modified which is the distinctive difference between this and the brace retrofit category.

Within the subcategory of supplemental systems, there are several possible specific retrofit types. For example, simple tension-only bracing could be added to the existing pier, or a supplementary concentrically braced frame could be added (these are lumped together and denoted external CBF here). Furthermore, external EBF's, shear panels, friction dampers, ADAS/TADAS devices, or unbonded braces could also be used as supplemental systems to the existing framing, and would work in parallel with it.

Many of the same retrofit systems considered as supplemental systems can be used to replace the existing braces. Unbonded braces, EBF's, CBF's using standard structural shapes, shear panels, or other ductile devices (such as ADAS, TADAS, or those reported by Rezai et al., 2000) are all viable possibilities for such replacement. Also, note that the replacement systems considered here are legitimate systems for new construction as well. Figure 2-5 shows the tree diagram of retrofit options considered in the category of brace configuration.

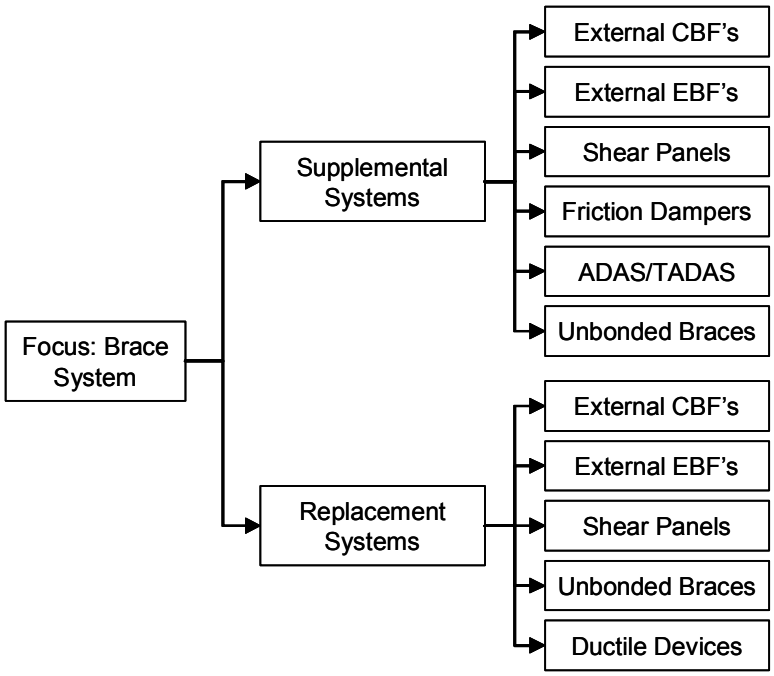

FIGURE 2-5 Brace System Retrofit Tree Diagram

TABLE 2-1 Matrix of Retrofit Options for Steel Truss Bridge Piers

Focus of Retrofit	Retrofit Strategy	Specific Retrofit Type	Modeling Challenges		Special Requirements			Adequate Local Ductility	Strength Increased	Pier Disp. Limited by Ex. Braces	Energy Diss. Prior to Ex. Brace Yield	Available Test Data	Aesthetic Concerns	Performance Rating	Relative Cost
			Retrofit	Existing Braces	Lateral Bracing	Capacity Check of Ex. Connections	Capacity Check of Ex. Columns								
Braces	Strengthen or Increase Ductility	Cover Plates	NA	ME1	No	Yes	Yes	Unknown	Yes	NA	NA	Limited	No	Unknown	Low-1
		Encase in Concrete	NA	ME2	No	Yes	Yes	Unknown	Yes	NA	NA	No	No	Unknown	Low-1
	Replace (Braces Only)	Unbonded Braces	MR1	ME3	No	Yes	Yes	Yes	Yes	NA	NA	Yes	No	Good	Low-1
		Standard Shapes	MR2	ME3	No	Yes	Yes	Yes	Yes	NA	NA	Yes	No	Fair	Low-1
Brace Connections	Brace Intersection	Rezai et al., 2000	MR1	ME4	No	No	No	No	No	No	Yes	Yes	No	Poor	Low
		Other	MR1	ME4	No	No	No	No	No	No	Yes	Yes	No	Poor	Low
	Brace Endpoint	Rezai et al., 2000	MR1	ME4	No	NA	No	No	No	No	Yes	Yes	No	Poor	Low
		Disposable Knee Brace	MR1	ME4	Yes: Link	NA	Yes	Yes	No	No	Yes	Yes	No	Good	Low-1
		Other	MR1	ME4	No	NA	No	No	No	No	Yes	Yes	No	Poor	Low
Brace System	Supplement	External CBF's/T-Only	MR2	ME4	No	No	Yes	Yes	Yes	Yes	No	Yes	Yes	Poor	Moderate
		External EBF's	MR1	ME4	Yes: Link	No	Yes	Yes	Yes	Yes	Yes-1	Yes	Yes	Fair	Moderate
		Shear Panels	MR1	ME4	No	No	Yes	Yes	Yes	Yes	Yes-1	Yes	Yes	Fair	Moderate
		Friction Dampers	MR1	ME4	No	No	Yes	Yes	Yes	Yes	Yes-1	Yes	Yes	Fair	Moderate
		ADAS/ TADAS	MR1	ME4	No	No	Yes	Yes	Yes	Yes	Yes-1	Yes	Yes	Fair	Moderate
		Unbonded Braces	MR1	ME4	No	No	Yes	Yes	Yes	Yes	Yes-1	Yes	Yes	Fair	Moderate
	Replace	CBF's	MR2	ME3	No	NA	Yes	Yes	Yes	NA	NA	Yes	No	Fair	High
		EBF's	MR1	ME3	Yes: Link	NA	Yes	Yes	Yes	NA	NA	Yes	No	Good	High
		Shear Panels	MR1	ME3	No	NA	Yes	Yes	Yes	NA	NA	Yes	No	Good	High
		Unbonded Braces	MR1	ME3	No	NA	Yes	Yes	Yes	NA	NA	Yes	No	Good	High
		Other Fuse Systems	MR1	ME3	No	NA	Yes	Yes	Yes	NA	NA	Yes	No	Good	High

2.3 Qualitative Measures

In order to compare the systems described above it is useful to define some qualitative measures that describe the relative advantages and disadvantages of various approaches. One may not be able to fully substantiate a final decision on selection of a retrofit type just from these measures, as a more in depth analysis of the different retrofit types may be necessary in order to determine which option is the most desirable in a certain situations, but these qualitative measures are nonetheless useful for providing a broad and general overview of the applicable options and trade-offs in comparing various approaches. As such, these measures will certainly provide a starting point for determining wether one retrofit is better suited than another for the seismic retrofit of steel truss bridge piers. Results are presented in the form of a table or a "matrix", with the retrofit options as rows and the qualitative measures as columns. General categories of qualitative measures are presented in the following sections. Filling in the body of the matrix is the subject of Section 2.4, however, the matrix shown in table 2-1 is referred to for the purpose of the following discussion.

2.3.1 Modeling Challenges

The first category of qualitative measures to be considered are "modeling challenges", i.e., whether accurate hysteretic models exist for a given retrofit type (or the structural fuse used in a retrofit type), and if so, what is their complexity relative to a simple elastic-perfectly plastic hysteretic model. For this purpose, three cases are considered, with the following notation for the purpose of table 2-1: "MR1", which refers to a simple bilinear hysteretic model; "MR2", which refers to a more complex brace buckling model that accounts of strength and stiffness degradation as a function of slenderness and width-to-thickness ratios of the member; and "not applicable" (NA) for cases where the retrofit only consists of modifying the existing braces.

Similarly, the modeling of the existing braces can also be assessed in terms of their relative complexity. Consider that in certain circumstances a linear model may be acceptable (i.e., if the existing brace is not expected to buckle), and in others more complicated hysteretic models may be necessary (i.e., if the existing brace is expected to buckle and loose strength).

For this purpose, four cases are considered for the existing brace model complexity: "ME1" refers to a complex brace buckling model that accounts for strength and stiffness degradation, similar to "MR2" above; "ME2" indicates an unknown model (i.e. member behavior is unknown and therefore the necessary model is unknown); "ME3" indicates that no modeling of the existing braces is necessary; and "ME4" refers to a linear elastic model with an accompanying knowledge of the buckling strength. In table 2-1, two columns are used for entries regarding the above, namely, the complexity of retrofit and existing brace modeling that may be required.

2.3.2 Special Requirements

Three Special Requirements that warrant consideration when selecting a retrofit option for steel truss bridge piers are incorporated as columns in the matrix of table 2-1. These are: lateral bracing needs (i.e., whether out-of-plane bracing will be needed for the retrofit to work properly); capacity checking of existing brace connections (i.e., whether the retrofit will require the capacity checking and possible strengthening of existing brace connections); and capacity checking of existing columns. Entries into table 2-1 under these columns consist of either "yes", "no", "NA" (not applicable).

2.3.3 Other Qualitative Measures

In addition to the columns described above, several other qualitative measures are incorporated as columns into the matrix and are described below.

First, the local ductility demand on the retrofits, especially those that involve structural fuses, is considered. When certain retrofit options are contemplated it is necessary to calculate the local ductility demand on a device or component for a given level of global ductility and then assess whether that device or component has the capacity to develop such local ductility. Using published analytical and experimental results where available, it is possible to determine whether the retrofit options considered here will typically be able to achieve a local ductility suitable for use in steel truss bridge piers. Therefore, entries into the matrix of table 2-1 under the "adequate local ductility" column indicate either "yes", "no", or "unknown".

Second, the strength of the retrofitted steel truss bridge pier is addressed. Each retrofit option will either increase the strength of the pier or make the system more ductile without increasing the strength. As such, entries under the column labeled "strength increased" are either "yes" or "no".

Next, consideration is given to whether the retrofit options will increase the ductile displacement capacity of the existing pier, or whether the displacement will still be limited by the ductile displacement capacity of the existing braces. For each retrofit option either "yes", "no", or "NA" is entered under the column "pier displacement limited by existing braces". A "yes" indicates that pier displacement capacity after retrofit is still limited by the existing braces; a "no" indicates that the retrofit pier displacement is not limited by the existing braces; and a "NA" indicates that the existing braces are modified or removed as part of the retrofit option.

The ability of the retrofit to dissipate energy prior to the existing braces reaching their displacement capacity should also be assessed when considering retrofit options for steel truss bridge piers and is therefore added as a column in the matrix of table 2-1. To simplify this assessment, the displacement capacity of the existing braces is conservatively taken as their yield displacement. Entries under this column are: "yes", when that the retrofit is able to dissipate energy prior to the existing braces reaching their yield displacement; "yes-1", indicates that energy dissipation not only occurs prior to existing braces reaching their displacement capacity, but this factor must be explicitly quantified as part of the retrofit concept; "no", when energy dissipation is not possible prior to existing brace yielding; and "NA", when the existing braces (modified or not) are the sole energy dissipation elements, or when the existing braces are removed.

Next, the question of whether there is available test data supporting the different retrofit options is addressed. Test data is necessary for calibrating analytical models, assessing strength and ductility capacity , and providing some level of confidence in the retrofit performance. Entries under this column are "yes", "no", or "limited", when adequate test

data in the literature is available, when it is not available, or when it is too limited to support implementation, respectively.

Some steel truss bridge piers support major bridges for which aesthetics are important to the community and many of the retrofit options considered here may alter the appearance of the piers. As such, a column is added to the matrix to address whether aesthetic concerns are likely to be important for each of the retrofit options. Entries in this column are either "yes" or "no" indicating that the retrofit option may or may not significantly alter the appearance of the piers.

Penultimately, a column is added for the relative rating of each retrofit option based on overall performance. This column can be considered a subjective assessment of the combined effectiveness of the local ductility, strength increase, increased displacement capacity, and energy dissipation prior to existing brace yielding columns. In other words, the entries under "relative performance rating" will depend on the entries in those other columns of the matrix. Ratings used are: "good", when stable hysteretic behavior and significant energy dissipation can be developed by the retrofit solution that also controls the maximum pier displacement; "fair", when stable hysteretic behavior and modest energy dissipation can be developed and the maximum displacement of the pier is limited by the existing braces; "poor", when either buckling of the retrofit braces or existing braces will occur as part of the intended hysteretic behavior, or when the large local ductility demands may be hard to satisfy with the retrofit strategy; and "unknown", when there is not there is enough published test data available on the retrofit option to judge its performance.

Finally, a column to account for a qualitative measure of cost is included. Although no cost estimating will be done, it is possible to use professional judgement to assess which retrofit types may be more expensive to construct than others. Possible entries in this column are: "low", for a relative inexpensive retrofit likely requiring little to no retrofit of existing columns, connections, beams, and foundations; "low-1", for relatively inexpensive retrofits that are more likely to require strengthening of columns, connections, beams, or foundations

due to increased demand imparted by the retrofit; "moderate", for retrofit options that have a high relative cost for the new materials but that may not require substantial strengthening of existing components; and "high", for retrofit options that may require substantial strengthening or replacement of existing components as well as having a high relative cost themselves.

2.4 The Matrix

Table 2-1 shows the matrix of retrofit options for steel truss bridge piers developed per the criteria outlined in the previous sections. Retrofit types are grouped together in rows per the categories in the tree diagrams of figures 2-3, 2-4, and 2-5, are the rows, while the qualitative measures are listed in the columns. This section discusses the reasoning for assigning most of values for the entries shown for each retrofit approach considered. To facilitate this discussion, the following sections are organized by retrofit strategy, in the order they appear in table 2-1, from top-to-bottom.

2.4.1 Brace Retrofit - Strengthen or Increase Ductility

The strategy described in Section 2.2.1 that consists of retrofitting the braces using cover plates retrofit type (which includes the options of lacing and/or rivet replacement) presents difficulties in several areas. Nonlinear analytical models that can account for the complex hysteretic behavior of braces as a function of changing slenderness ratios and width-to-thickness ratios that are calibrated to match experimental results are necessary to accurately represent seismic response, which accounts for the "ME1" rating in the column for "modeling challenges - existing braces" in table 2-1. Because this retrofit type may also increase the strength of the existing braces, which are still relied upon as the energy dissipating elements, it would be important to ensure that the strength of existing columns and connections is sufficient, in a capacity design perspective. Test data available in the literature regarding this type of retrofit is "limited" to some specific geometries and applications such as in Dietrich and Itani (1999), therefore, it is "unknown" whether the local ductility levels necessary can be achieved in a broad range of applications. If, as mentioned above, this retrofit increases the strength of the braces, then it could also increase the pier strength system. The cover

plate retrofit strategy receives a "NA" rating in both the "pier displacement limited by existing braces" and "energy dissipation prior to existing brace yield" columns of table 2-1 because it involves modification of the existing braces. There are limited aesthetic concerns for this retrofit because it leaves the geometry of the pier untouched. The performance rating is "unknown" and it has been assigned a relative cost of "low-1" because of the possibility of having to strengthen connections, columns, beams, and foundations to comply with capacity design principles.

The strategy that consists of encasing the braces in concrete, which is an attempt to effectively create the equivalent of unbonded braces, has similar matrix entries as those described for the cover plate retrofit. However, it is not known what type of analytical model would be appropriate as there is no experimental data available on the cyclic behavior of such members. Therefore, under "modeling challenges - existing braces", this retrofit strategy received a rating of "ME2". The lack of test data also leads to "unknown" entries under "adequate local ductility" and "performance rating". As for the previous case, because the brace strength would increase, the pier strength would also increase, and connection, column, and foundation capacity would have to be checked and possibly strengthened. This led to the relative cost assessment of "low-1". An additional concern not addressed in table 2-1 for this retrofit strategy is whether unbonding can really be achieved for such members, and whether the laces and rivets will prevent the unbonded brace from working properly (i.e. the rivets and laces may engage the concrete, forcing the concrete to take compression load which is not the intended purpose).

2.4.2 Brace Retrofit - Replace (Braces Only)

For the strategy of replacing the existing braces with buckling restrained braces (BRBs) while keeping the same overall pier configuration, no modeling of the existing braces, and only a simple bilinear hysteretic model for the new braces are necessary, leading to "ME3" and "MR2" entries in those columns of table 2-1 respectively. There exists ample test data on the excellent ductile behavior of unbonded braces, and unbonded braces could have a higher strength than the existing braces (this is likely case dependent), which would translate into

increased pier strength. These factors lead to a "performance rating" of "good". As in the cases above, the strength of the BRB could be larger than the braces it is replacing, thereby requiring column, connection, and foundation checking, which has resulted in the "low-1" relative cost.

Replacing the existing braces with standard structural shapes, such as wide flange shapes or hollow structural shapes, may require advanced modeling of the complex hysteretic behavior of the new braces to accurately determine if the retrofit is adequate since the limiting behavior remains brace buckling with strength and stiffness degradation, leading to the "MR2" rating under "modeling challenges - retrofit" in table 2-1. In this case, the new braces will likely increase the required strength of the pier and have adequate local ductility, however, the buckling of the new braces may lead to pinched hysteretic behavior and possible strength degradation. Therefore, this retrofit type receives only a fair performance rating. Furthermore, the strength increase will necessitate capacity checking and possible strengthening of pier connections and columns, leading to the "relative cost" assessment of "low-1".

2.4.3 Brace Connection Retrofit

With the exception of the disposable knee brace, all retrofit strategies in the category of brace connection retrofit, involve inserting devices to dissipate energy at the brace connection points (either the end or intersection points), and receive the same ratings in table 2-1. Typically, the hysteretic behavior of these devices may be represented with simple bilinear hysteretic models and only knowledge of the strength of the existing braces is necessary. Because devices are inserted in series with the existing braces, the forces equal to the device strength must be resisted by the braces without buckling, therefore; the strength of the system is equal or less than prior to retrofit, but the energy dissipation has been enhanced. However, to dissipate significant amounts of energy at low force values requires larger displacements and therefore, larger local ductility. For example, a device located at brace endpoints in a 7300 mm (24 ft) by 7300 mm X-braced panel the device would have to sustain local deformations of over 50 mm at a pier drift of 1%. Test data from Rezai et al. (2000),

Tremblay and Bouatay (1999a), Rezai et al. (1999), and Tremblay and Bouatay (1999b) indicates that the maximum device deformation reached for any of the full-scale connection fuses tested was about 15 mm, which corresponded to a device ductility (or local ductility) of 4. Therefore, it is difficult to design these relatively small devices in brace connection retrofit scenarios for steel truss bridge piers to meet their local deformation demands, resulting in a relative performance rating of "poor". Although these retrofit possibilities would be relatively cost-effective, would not require lateral bracing, and likely would not force the columns to be strengthened, they may not be feasible alternatives with the existing devices described in the literature.

In the case of disposable knee braces, such as those described in Balendra et al. (1997), it may be possible to reach the necessary drift demands prior to the knee brace reaching its local deformation capacity. Additionally, it has been shown that these systems have stable hysteretic behavior that can be modeled using simple bilinear elements, comparable to that of an EBF. There are however three drawbacks to this system. First, the strength of the system is not enhanced unless the existing braces are also replaced, which not only increases cost but also makes it less likely that this system would be chosen over replacing the braces with unbonded braces, which are easier to design and have already been used in many building retrofit instances. Second, the knee braces may require lateral bracing to avoid lateral torsional buckling of the link, which can be difficult to provide on a bridge pier. Finally, this system imparts large moments onto the beam and columns which would likely require significant strengthening (this leads to the "relative cost" assessment of "low-1").

2.4.4 Brace System Retrofit - Supplement

As described in Section 2.2.3, the supplemental brace system retrofit strategies introduce additional systems or braces which act in parallel with the existing braces in the bridge pier. These systems can be designed to dissipate energy prior to the buckling of the existing braces. In the case of adding external CBF's or tension-only bracing, it can be shown through compatibility of deformations that it is possible to yield the retrofit braces prior to the yielding of the existing braces (not buckling, which would occur at a smaller displacement) only under

certain (hard to obtain) conditions. For example, consider the two story bridge pier schematic shown in figure 2-6, which has a supplemental CBF in an x-brace configuration that extends over both stories of the pier. It can be shown for this case that the supplemental braces will yield prior to the existing braces yielding (assuming equal Young's moduli) if:

$$\frac{F_{yr}\left(L^2+4h^2\right)}{2F_{yo}\left(L^2+h^2\right)}<1.0 \qquad \textbf{(2-1)}$$

where F_{yr} is the yield stress of the supplemental braces, F_{yo} is the yield stress of the existing braces, L is the bay width, and h is the panel (or story) height. If $L = h$, this simplifies to:

$$\frac{F_{yr}}{F_{yo}}<\frac{4}{5} \qquad \textbf{(2-2)}$$

and if instead, $F_{yo} = F_{yr}$ is assumed, (2-1) simplifies to:

$$\sqrt{2}h<L \qquad \textbf{(2-3)}$$

Neither (2-2) or (2-3) represent inequalities that are satisfied in typical situations. For instance, a bridge pier may have been constructed in the 1950's using steel similar to A36 (F_{yo} = 250 MPa), which means it is difficult to find steel today that has a yield stress less than that of the existing braces. Additionally, these piers are typically made of panels that have aspect ratios close to one, in which case (2-3) would not be satisfied. The same has been found to be true for any configuration of supplemental CBF, whether the supplemental bracing is designed as a tension-only bracing system or a system in which both tension and compression are considered. Similar results are obtained for supplemental x-bracing added over half the panel height (i.e. two x's per panel). This has led to the "relative performance rating" of "poor". Additionally, as with all the supplemental system retrofit options, the extensive additional framing necessary for implementation, offset by the fact that the existing pier would likely not have to be temporarily shored, results in the "moderate" rating for "relative cost".

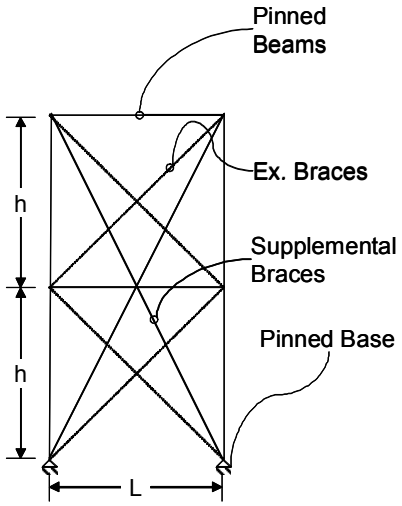

FIGURE 2-6 Two Story Pier with Supplemental CBF

The other supplemental systems in table 2-1 may be designed to yield prior to the existing braces yielding or buckling, but, because deformations at which the existing braces buckle are likely small, supplemental systems have only a limited deformation range over which energy can be dissipated. This has led to the "fair" performance rating for the remaining supplemental systems. If certain details are used to implement these supplemental systems the existing brace connections may not be subject to any additional load, and would not require retrofit. Only the capacity of the existing braces and simple bilinear hysteretic models of the retrofit devices would be needed to model these retrofit options, resulting in the "MR1" and "ME4" ratings for the "modeling challenges". Two drawbacks of the supplemental systems are additional column demands, which may necessitate column strengthening, and that these systems may not be aesthetically pleasing since they would significantly alter the pier's appearance. Despite these drawbacks, supplemental system retrofit strategies other than the CBF are viable retrofit options that could be designed to meet performance objectives. Figures 2-7a and 2-7b show schematics of the TADAS supplemental system and the unbonded brace supplemental system respectively. Note that the unbonded brace in the unbonded brace supplemental system of figure 2-7b must be oriented at a very shallow angle in order for it to yield well before the existing braces.

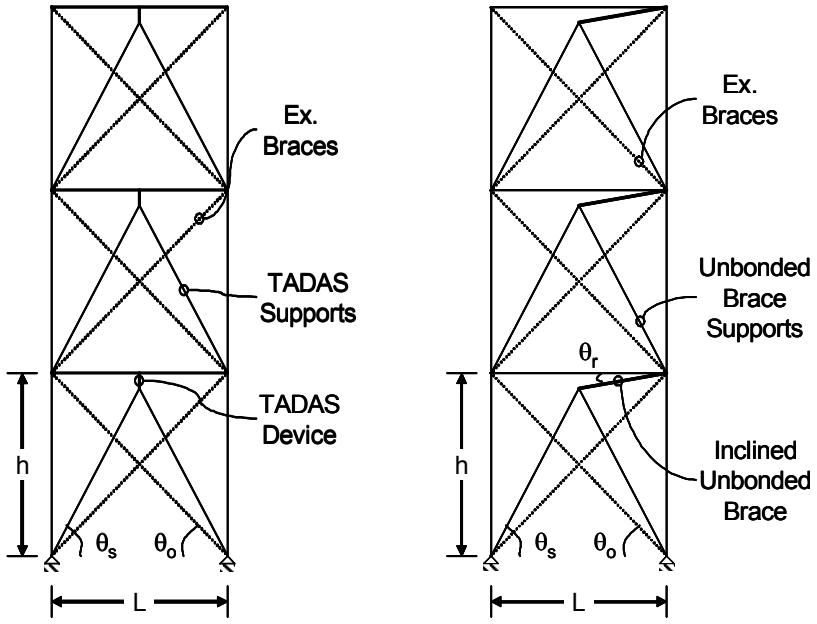

FIGURE 2-7 Supplemental Systems (a) TADAS (b) Buckling Restrained Braces (BRBs)

2.4.5 Brace System Retrofit - Replace

Certainly, an optimal seismic performance can be achieved when it is possible to replace the existing bracing system of a steel truss bridge pier with one specially designed to dissipate energy and behave in a ductile manner. However, full replacement of the bracing system, connections, and possibly the beams, as well as possibly strengthening columns and changing the load path for the pier could, in many cases, make these options cost prohibitive, regardless of their superior performance. In some cases though, especially when bridges on major transportation lifelines are considered, such a retrofit strategy may be warranted.

Replacing the bracing with a CBF using standard structural shapes receives only a "fair" performance rating due to the fact that the compression braces are still subject to buckling and strength degradation. The other retrofit options considered in this category can be analyzed using bilinear hysteretic models and test data demonstrates that they can dissipate energy in a stable and ductile manner.

For the EBF option, the requirement of lateral bracing of the link is a constraint that severely limits its use since that bracing is difficult to provide in a bridge pier. This is unfortunate because the EBF has been shown to be an excellent seismic load resisting system (Kasai and Popov, 1986a, and Englehardt and Popov, 1989, among others). Therefore, it is desirable to investigate the possibility of developing a new type of EBF that does not require lateral bracing of the link. Since the existing lateral bracing requirements of EBFs are meant to prevent lateral torsional buckling of the wide-flange sections used as the link beams, it may be possible to eliminate the lateral bracing requirements if sections that are not subject to lateral torsional buckling are used as links. This possibility is discussed and developed further in later sections.

2.5 Selection of Desirable Retrofit Strategies

Based on the results in table 2-1, certain retrofit strategies here are deemed unworthy of further consideration. For instance, it is judged that the brace connection strategies may not be practical at this time in a retrofit perspective. All of those strategies except the disposable knee brace, do not have the deformation capacity needed to meet the expected demands, and the disposable knee brace requires more complex detailing (including likely brace replacement) than other solutions, while imparting large moments on the beams and columns.

In the perspective of changing brace system, two retrofit strategies can be eliminated from consideration here. First, because it has been shown that the supplemental CBF or tension-only bracing retrofit strategy cannot be easily designed such that the new braces yield prior to the existing braces in most situations, this retrofit alternative is not studied further. Second, the retrofit option of replacing the bracing system with a new CBF system using standard structural sections is not considered further because systems with superior behavior exist, and much of the cost in this case is not determined by the type of new system used but by the replacement of the existing bracing system.

2.6 Research Areas

Using the matrix of table 2-1 as well as the discussions above, it is possible to identify some areas where fundamental research is necessary to either validate a retrofit strategy or enhance its performance. For instance, the development of an EBF that does not require lateral bracing seems desirable (and could be applicable to both new and retrofit construction) and will be the focus of the remainder of this report. There is also a need to develop simple design procedures for the supplemental systems where emphasis is placed on protecting the existing brace members while satisfying stiffness and energy dissipation criteria. Additionally, it may be advantageous to examine the cover plate retrofit alternative in an experimental study to determine what additional strength and ductility can be achieved for a wider variety of brace geometries and cross-sections than those considered in Dietrich and Itani (1999).

SECTION 3
THEORY AND DESIGN OF LINKS WITH HYBRID HOLLOW RECTANGULAR CROSS-SECTIONS

3.1 General

In this section the theory and design of eccentrically braced frame (EBF) links with hybrid hollow rectangular cross-sections is discussed. First, a shear-moment interaction theory is derived and an equation to determine the balanced link length is formulated. The limit state of flange buckling is then considered and an upper bound on the flange compactness ratio is proposed to avoid this failure mode. Next, equations are derived for the limit state of web buckling, and to achieve a conservative stiffener spacing to prevent it prior to the development of substantial web yielding. Equations are then developed for determining the stiffener sizes necessary to prevent web and flange buckling. Following this, the lateral torsional buckling of hybrid hollow rectangular links is discussed. The overstrength of links is then considered and three methods for calculating the maximum possible shear strength are described. Finally, capacity design of the framing and connections outside the link region is briefly discussed and references are given for more detailed information.

3.2 Shear-Moment Interaction and Link Length

In the case of eccentrically braced frames utilizing links with hybrid rectangular cross-sections (hybrid in this case is referring to a structural element having different flange and web yield stresses) the same three types of plastic mechanisms that can develop in wide-flange (WF) links are possible, namely:

- Moment hinges developing the full plastic moment, M_p, of the cross-section at the end of the links,

- Links developing the full plastic shear force, V_p, over their entire length (i.e. yielding in shear), with moments at the ends of the link less than the plastic moment (reduced to account for shear as described below), and,
- Links yielding in both shear and flexure, with one yielding mode developing after strain hardening from the other one.

Links which form the different types of plastic hinges as outlined above are generally referred to as flexural links, shear links, and intermediate links respectively. It has been shown in numerous experimental studies that shear links exhibit the most stable and ductile cyclic behavior (Hjelmstad and Popov, 1983; Kasai and Popov, 1986a; Kasai and Popov, 1986b; Ricles and Popov, 1989; and Engelhardt and Popov, 1989; among others).

Using the generic hybrid hollow rectangular cross-section of figure 3-1 (with webs spanning the full height of the box), the following expressions for the basic quantities of full plastic moment, M_p, full plastic moment in the presence of full plastic shear, M_{pr}, and the full plastic shear, V_p, can be developed:

$$M_p = F_{yf} t_f (b - 2t_w)(d - t_f) + F_{yw} \frac{t_w d^2}{2} \tag{3-1}$$

$$M_{pr} = F_{yf} t_f (b - 2t_w)(d - t_f) + 2F_{yw} t_f t_w (d - t_f) \tag{3-2}$$

$$V_p = \frac{2}{\sqrt{3}} F_{yw} t_w (d - 2t_f) \tag{3-3}$$

where F_{yf} and F_{yw} are the yield stresses of the flange and web material respectively, b is flange width, t_f is the flange thickness, d is the full depth of the cross-section, and t_w is the web thickness. Note that the above equations assume that shear yielding is constrained over the depth (d-$2t_f$), and that the complete flanges, over a width of b, contribute to the flexural strength which may not necessarily be the case. In later sections this assumption will be re-evaluated by comparison with experimental results.

The interaction between shear and moment in WF links has been studied by other researchers. Typical theoretical formulations of shear and moment interaction in wide flange

shapes, such as those given by Hodge (1959) or Neal (1961), produce interaction diagrams such as the curves in figure 3-2, the latter of which is given by:

$$\left(\frac{M-M_{pr}}{M_p-M_{pr}}\right)^2+\left(\frac{V}{V_p}\right)^2=1 \qquad for \qquad M\geq M_{pr} \tag{3-4}$$

$$V\approx V_p \qquad for \qquad M\leq M_{pr} \tag{3-5}$$

However, experimental results such as the points in figure 3-2, which represent the results of several test at Berkeley (Kasai and Popov, 1986a), suggest that the interaction could be neglected.

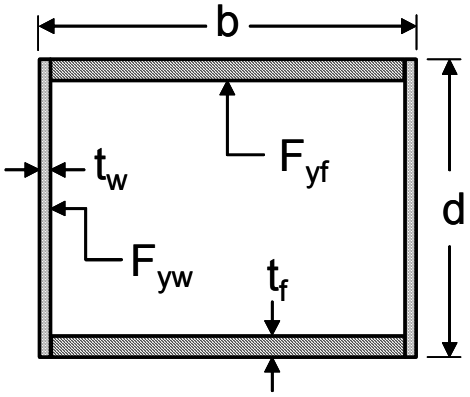

FIGURE 3-1 Hollow Hybrid Rectangular Cross-Section

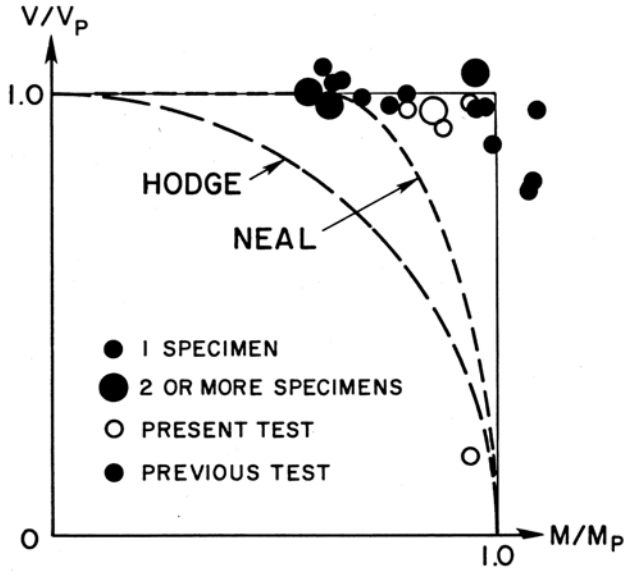

FIGURE 3-2 Shear-Moment Interaction for WF Links (Kasai and Popov, 1986a)

Possible reasons for the difference between experimental and theoretical shear-moment interaction have been given by Kasai and Popov (1986a), and Roeder and Popov (1977) as:

- The theoretical formulations do not include strain hardening and assume a given plasticity model, which are approximations.
- The stress condition at the link ends could shorten the yield plateau and cause immediate strain hardening.
- The stress distribution on the cross-section may be different than assumed because the flange shear may become large due to the warping restraint at the link ends.

However, none of these hypotheses have been demonstrated analytically, and for the purposes of developing design rules for WF links, Kasai and Popov (1986a) proposed neglecting the effect of possible shear-moment interaction, as it agreed with the experimental data. This has since been implicitly adopted in the AISC seismic provisions (AISC, 2002) governing the design of eccentrically braced frames for buildings.

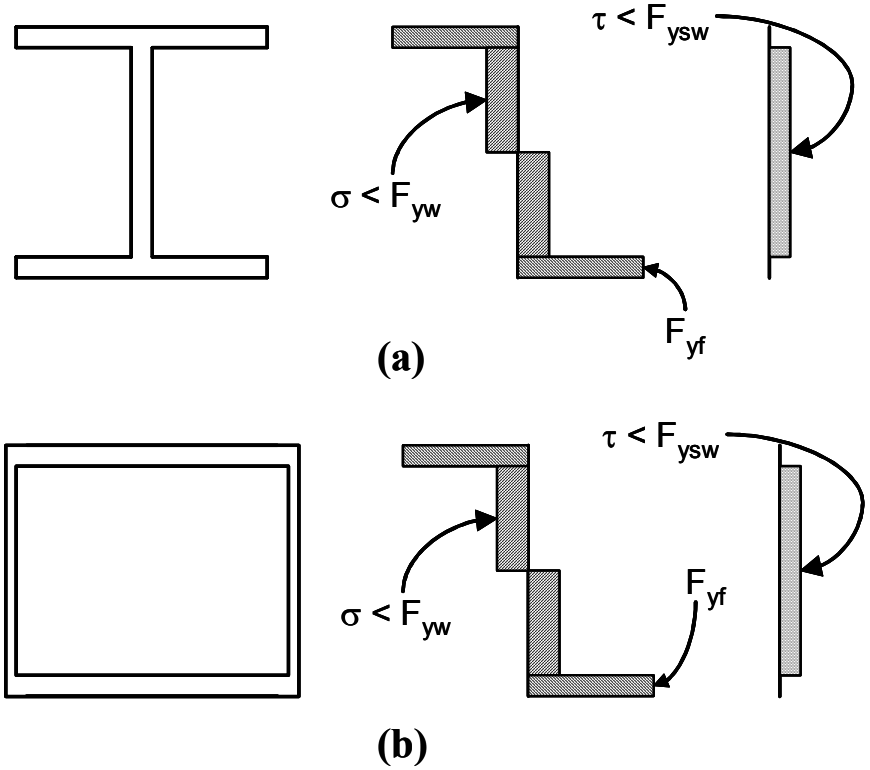

FIGURE 3-3 Assumed Stress Distributions

(a) WF Link (b) Rectangular Link

In the case of links with hybrid rectangular cross-sections, there is no experimental evidence to support neglecting possible shear-moment interaction (although the experiment performed

and presented in this study may provide one such data point). It is therefore necessary, for specimen design and other initial phases of this study, to develop a shear-moment interaction equation for such a structural member. Mrazik et al. (1987) presents the derivation of a shear-moment interaction equation for hybrid I-sections based on the stress distribution shown in figure 3-3a (where F_{ysw} is the shear yield stress of the web). Using a similar stress distribution (shown in figure 3-3b) and the hybrid cross-section of figure 3-1, the following equations can be written:

$$V_p^M = 2\tau t_w(d - 2t_f) \tag{3-6}$$

$$M_p^V = F_{yf} t_f (b - 2t_w)(d - t_f) + \sigma \frac{t_w d^2}{2} \tag{3-7}$$

where V_p^M is the plastic shear force in the presence of the reduced plastic moment M_p^V, which can be larger than M_{pr} which in turn would cause V_p^M to be less than V_p, τ is the shear stress on the web, σ is the normal stress on the web, and all other parameters are as previously defined. Assuming that τ and σ in (3-6) and (3-7) satisfy the Von-Mises yield criteria for plane stress in the web, namely:

$$F_{yw} = \sqrt{\sigma^2 + 3\tau^2} \tag{3-8}$$

Rewriting (3-3) and (3-6), which was an equation for plastic shear with applied moments less than M_{pr}, as:

$$\tau = \frac{V_p^M}{2t_w(d - 2t_f)} \tag{3-9}$$

$$t_w(d - 2t_f) = \frac{\sqrt{3}}{2} \frac{V_p}{F_{yw}} \tag{3-10}$$

and substituting first (3-9) and then (3-10) into (3-8) results in the following equation for the normal stress in the web:

$$\sigma = F_{yw} \sqrt{1 - \left(\frac{V_p^M}{V_p} \right)^2} \tag{3-11}$$

Substituting (3-11) into (3-7) gives:

$$M_p^V = F_{yf} t_f \left(b - 2t_w\right)\left(d - t_f\right) + \frac{t_w d^2}{2} F_{yw} \sqrt{1 - \left(\frac{V_p^M}{V_p}\right)^2} \tag{3-12}$$

Next, (3-1) is rewritten in two different forms, namely:

$$F_{yf} t_f \left(b - 2t_w\right)\left(d - t_f\right) = M_p - F_{yw} \frac{t_w d^2}{2} \tag{3-13}$$

$$M_p = F_{yw} \frac{t_w d^2}{2} \left(1 + 2 \frac{F_{yf}}{F_{yw}} \frac{t_f \left(b - 2t_w\right)\left(d - t_f\right)}{t_w d^2} \right) \tag{3-14}$$

the second of which is rearranged again as:

$$\frac{F_{yw} t_w d^2}{2} = \frac{M_p}{\left(1 + 2 \frac{F_{yf}}{F_{yw}} \frac{t_f \left(b - 2t_w\right)\left(d - t_f\right)}{t_w d^2} \right)} \tag{3-15}$$

Finally, (3-14) and (3-15) are substituted into (3-12), which results in the following shear-moment interaction equation for a non-homogeneous hollow rectangular cross-section:

$$\frac{M_p^V}{M_p} + \frac{1}{\left(1 + 2 \frac{F_{yf}}{F_{yw}} \frac{t_f \left(b - 2t_w\right)\left(d - t_f\right)}{t_w d^2} \right)} \left(1 - \sqrt{1 - \left(\frac{V_p^M}{V_p}\right)^2} \right) = 1 \tag{3-16}$$

For simplicity the cross-section parameter, Q, will be defined as:

$$Q = \frac{t_f \left(b - 2t_w\right)\left(d - t_f\right)}{t_w d^2} \tag{3-17}$$

and the interaction equation can then be rewritten as:

$$\frac{M_p^V}{M_p} + \frac{1}{\left(1 + 2 \frac{F_{yf}}{F_{yw}} Q \right)} \left(1 - \sqrt{1 - \left(\frac{V_p^M}{V_p}\right)^2} \right) = 1 \tag{3-18}$$

Figure 3-4 shows shear-moment interaction curves for hybrid hollow rectangular cross-sections with various values of the yield stress ratio (F_{yf}/F_{yw}) and the cross-section parameter

(*Q*). From this figure it is evident that more shear-moment interaction should be expected when lower values of the yield stress ratio and cross-section parameter are used. This notion will be compared with experimental results in later sections.

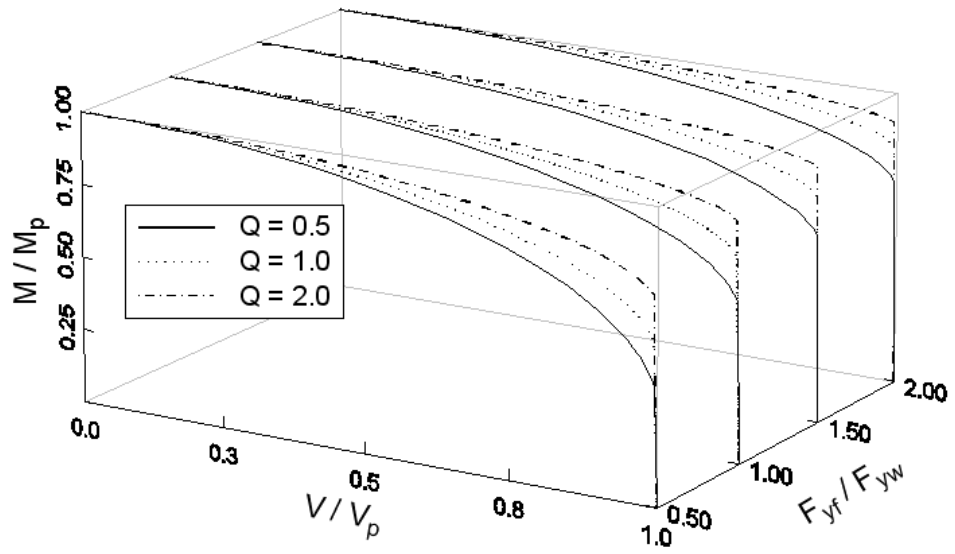

FIGURE 3-4 V-M Interaction for Cross-Section of Figure 3-1

As mentioned above, shear links exhibit the most stable and ductile hysteretic behavior; therefore, it is necessary to derive the link length at which the transition from shear link to flexural link occurs. Consider the free body diagram of a link of length *e** as shown in figure 3-5. The link length can be written in terms of the shear forces and moments at the link ends as:

$$e^* = \frac{2M_p^V}{V_p^M} \tag{3-19}$$

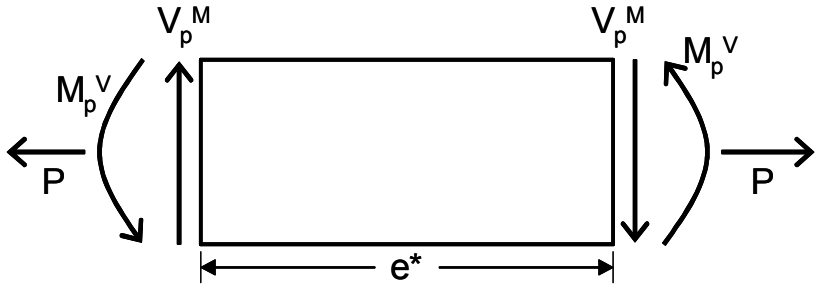

FIGURE 3-5 Link Free Body Diagram

In order to obtain the link length at which the transition from shear to flexural behavior occurs (known as the balance link length), the full plastic shear (V_p) given by (3-3) and the plastic moment reduced for the full plastic shear (M_{pr}) given by (3-2) can be substituted in (3-19) for V_p^M and M_p^V respectively (the effect of the axial force, P, is neglected). The resulting balanced link length for a hybrid hollow rectangular link is:

$$e^* = \frac{\sqrt{3}\left[F_{yf}t_f(b-2t_w)(d-t_f)+2F_{yw}t_f t_w(d-t_f)\right]}{2F_{yw}t_w(d-2t_f)} \tag{3-20}$$

where all terms are as previously defined. Assuming bi-linear elasto-plastic material properties, a link with length less than e^* will develop the full plastic shear prior to developing the reduced plastic moment and a link with length greater than e^* will develop flexural yielding of the link ends prior to developing the full plastic shear. When strain hardening is considered, a safety factor for (3-20) may be needed to insure full shear or full flexural yielding. This will be addressed in later sections. Also, a normalized link length will be used in later sections and is defined as $\rho = e/(M_p/V_p)$, where e is the designed link length (note that M_p is used in lieu of M_{pr} for consistency with current design codes). Currently, for code-based design of WF links, a shear link is considered to have $\rho \leq 1.6$, an intermediate link is considered to have $1.6 < \rho \leq 2.6$, and a flexural link is considered to $2.6 < \rho$.

Using the rectangular and square standard hollow structural sections (HSS) listed in the AISC LRFD Manual of Steel Construction (AISC, 1998) that meet the AISC seismic provision limits for width-to-thickness ratio, the maximum link length for a shear link given by (3-20) would be 460 mm (18 in) and would be obtained with a HSS 250x250x16 (10x10x5/8). With a 460 mm link length and a 7.3 m (24 ft) wide by 3.7 m (12 ft) tall frame the drift at a plastic rotation of 0.08 rad (the maximum allowed by the AISC seismic provisions) is only 0.5%, from (Bruneau et al., 1998):

$$\theta = \gamma \frac{e}{L} \tag{3-21}$$

where θ is the drift, L is the bay width, and e is the link length. There may be instances where ductility demand exceeds this drift value. Additionally, a short link has greater

stiffness, which can translate into increased seismic demands on the structure. Furthermore, as a minor point, short links can cause congested details and fabrication difficulties. To avoid these problems, a hybrid cross-section can be used. The advantage of a hybrid cross-section is the ability to vary the M_p over V_p ratio by changing the flange and web width and depth to thickness ratios independently, allowing longer link lengths while still having a shear link and the desired shear strength.

3.3 Flange Buckling

Flange buckling has been shown to be an undesirable behavior in links in eccentrically braced frames because it can lead to high strains which in turn can cause premature fractures, as well as trigger lateral torsional buckling or web buckling, all of which cause significant strength degradation and limit ductile behavior. Kasai and Popov (1986a) derived a limiting flange compactness ratio (b/t_f) for which flange buckling could be avoided in WF links. Based on that result, they concluded the existing flange compactness ratio limit given for plastic design in the, then current, AISC ASD specifications (1980) was slightly conservative and recommended that it be adopted as the limit for WF EBF links. Since then the limit flange compactness ratio has been reduced for WF sections.

A similar approach to that used for WF links by Kasai and Popov can be followed to assess the flange buckling of a hollow rectangular section of the type shown in figure 3-1. First the flange yield length is determined. This value is then introduced in a plastic plate buckling equation to determine the critical buckling stress of the flange element, which in turn is compared with an estimate of the average flange stress in the flange yield zone.

3.3.1 Flange Yield Length

Consider the free body diagram of figure 3-6 in which M_A and M_B are the link end moments, V is the link shear, α is the ratio of axial force to link shear, and γ is the link rotation angle. From this free body diagram, the moment diagram of figure 3-7 may be developed, where $M(x)$ is the moment at a distance x from end A, and e_i is the distance from end A to the point of zero moment (which is not the link length divided by 2 if $M_A \neq M_B$). From this moment diagram the following equations may be written:

$$V = \frac{M_A}{e_i} \qquad \textit{and} \qquad M(x) = M_A\left(\frac{e_i - x}{e_i}\right) = M_A\left(1 - \frac{x}{e_i}\right) \tag{3-22}$$

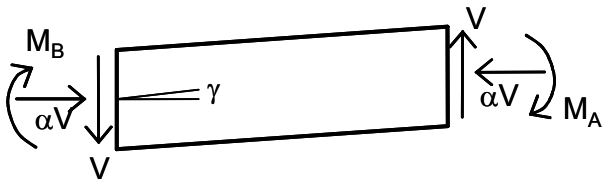

FIGURE 3-6 Link Free Body Diagram for Flange Buckling Derivation

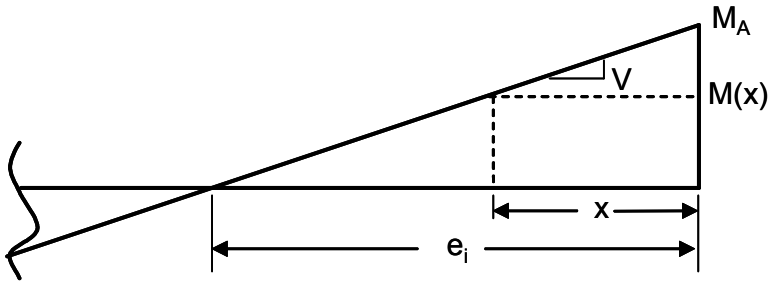

FIGURE 3-7 Link Moment Diagram

Next, in order to find the plastic moment capacity in the presence of axial force, the flange yield stress is reduced by the average flange stress due to the axial force, σ_A, which can be written as:

$$\sigma_{yA} = F_{yf} - \sigma_A = F_{yf} - \frac{\alpha V}{A_g} \tag{3-23}$$

where A_g is the gross cross-sectional area, and all other terms are as previously defined. Note that (3-23) assumes that the axial force is resisted by the entire cross-section. Substituting the expression for V in (3-22) into (3-23) and normalizing by the flange yield stress, F_{yf}, gives:

$$\frac{\sigma_{yA}}{F_{yf}} = 1 - \frac{\alpha M_A}{e_i P_y} \tag{3-24}$$

where P_y is the product of the flange yield stress and the gross area (which may differ from the axial force required to yield the entire cross-section in the case of a hybrid section). The plastic moment reduced for both the fully plastic shear and the presence of axial force can then be estimated as:

$$M_{pra} = M_{pr}\frac{\sigma_{yA}}{F_{yf}} = M_{pr}\left(1 - \frac{\alpha M_A}{e_i P_y}\right) \tag{3-25}$$

Assuming that M_A is greater than or equal to M_{pr}, the flange stress diagram due only to the moments may be constructed as in figure 3-8, where l_y is the flange yield length.

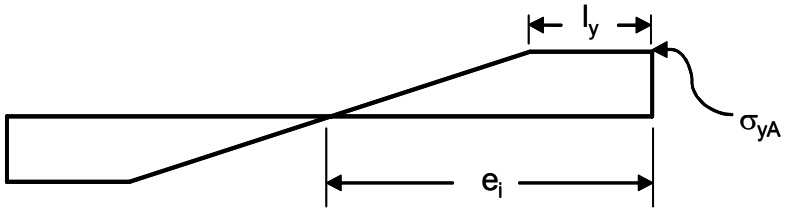

FIGURE 3-8 Flange Stress Diagram

Considering figures 3-7 and 3-8, the moment at $x = l_y$, which is M_{pra}, can be written as:

$$M(x = l_y) = M_A\left(1 - \frac{l_y}{e_i}\right) = M_{pra} \tag{3-26}$$

Substituting (3-25) into (3-26) results in the following equation for the flange yield length:

$$l_y = e_i\left(1 - \frac{M_{pr}}{M_A}\right) + \frac{\alpha M_{pr}}{P_y} \tag{3-27}$$

The corresponding moment diagram is shown in figure 3-9.

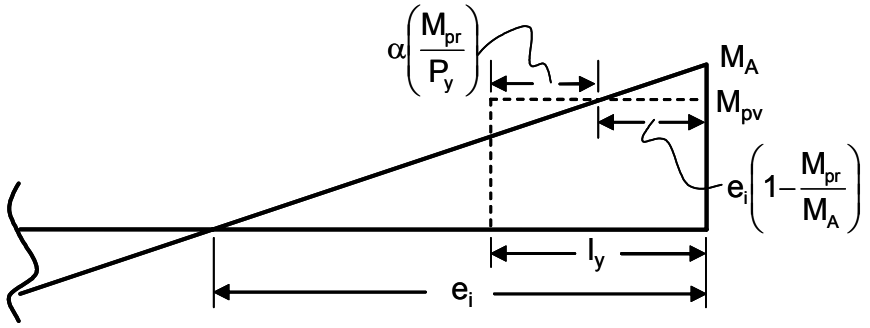

FIGURE 3-9 Link Moment Diagram

Note that (3-23), (3-24), and (3-25) assume that the entire flange width has a yield stress of F_{yf}, while when considering the cross-section of figure 3-1 the corner regions have a yield stress of F_{yw}. Depending on the ratio of F_{yw} to F_{yf} this assumption may yield conservative or unconservative results in terms of flange yield length (conservative if F_{yw} is less than F_{yf}, and vice-versa), but, in most cases will not lead to errors in the reduced plastic moment M_{pra} or flange yield length of more than 5%. For instance, for a flange yield stress of 310 MPa (45 ksi), web yield stress of 413 MPa (60 ksi) and flange width-to-web thickness ratio of 19

the average flange yield stress (considering the corners to have F_{yw}) is 321 MPa (46.6 ksi). In this case using the F_{yf} results in a M_{pra} that is 3.6% larger than if the average yield stress is used. From (3-27) the error in the flange yield length is the same as that for F_{yf} and M_{pra}. Furthermore, this flange yield length is also applicable to flexural links since the only restriction made on the end moment, M_A, was that it was larger than M_{pr}.

3.3.2 Plastic Plate Buckling Equation

In their derivation of the flange buckling strength of WF links, Kasai and Popov used a plastic plate buckling equation for plates having one unloaded edge free and the other unloaded edge hinged (which conservatively neglects the restraint provided by the web). Here, for the cross-section shown in figure 3-1, the flanges are assumed to have both unloaded edges hinged. Haaijer (1957) derived the following equation for the plastic buckling stress, σ_b, of compressed plates with finite length and such boundary conditions:

$$\sigma_b = \left(\frac{t_f}{b}\right)^2 \frac{\pi^2}{12}\left[D_x\left(\frac{b}{l_h}\right)^2 + D_y\left(\frac{l_h}{b}\right)^2 + D_{xy} + D_{yx} + 4G_t\right] \tag{3-28}$$

where D_x, D_y, D_{xy}, and D_{yx} are plastic plate modulii in the longitudinal (x) and transverse (y) and shear (xy and yx) directions, G_t is the plastic shear modulus, and l_h is the half wavelength of the buckled plate. Based on numerous compression tests, Haaijer determined the following values to be appropriate for the above modulii; D_x = 20700 MPa (3000 ksi); D_y = 226000 MPa (32800 ksi); D_{xy} = D_{yx} = 55850 MPa (8100 ksi); G_t = 16550 MPa (2400 ksi). (3-28) can be used to calculate the plastic flange buckling stress of links with cross-sections corresponding to figure 3-1, with the half wavelength taken as the smaller of the stiffener spacing or $l_y/2$, where l_y is given by (3-27).

3.3.3 Average Flange Stress

To check for the occurrence of flange buckling an estimate of the average flange stress, σ_{av}, in the flange yield zone can be used. From figures 3-8 and 3-9 it can be shown that:

$$\sigma_{av} = F_{yf} \frac{\left(1 + \frac{M_A}{M_{pr}}\right)}{2} \tag{3-29}$$

In order to match the results of strain recordings from experimental WF link tests, Kasai and Popov modified (3-29) to be:

$$\sigma_{av} = F_{yf} \frac{\left(1 + \frac{1.1\,M_A}{M_{pr}}\right)}{2} \tag{3-30}$$

where if equal end moments, 35% strain hardening of the link before flange buckling, and a shear link are assumed, then:

$$M_A = 1.35\,V_p \frac{e}{2} \tag{3-31}$$

Otherwise, for a flexural link, the end moment, M_A, should be M_p multiplied by a factor to account for strain hardening. Using (3-30) and (3-31) to approximate the average stress in the flange yield zone, as well as (3-27) and (3-28) to approximate the flange yield length and plastic buckling stress, the limit state of flange buckling of EBF links with hollow rectangular cross-sections can be avoided by checking that σ_{av} is less than σ_b.

3.3.4 Simplified Procedure for Shear Links

Further simplification of the flange buckling problem for shear links is possible with some additional assumptions. First, if the link length, e, of (3-31) is conservatively assumed to be the balanced link length, e^* (this is conservative because (3-31) represents the end-moment for a shear link and e^* is the length of the longest possible shear link), where:

$$e^* = \frac{2\,M_{pr}}{V_p} \tag{3-32}$$

Substituting (3-32) and (3-31) into (3-30) gives:

$$\sigma_{av} = 1.243 F_{yf} \tag{3-33}$$

which represents a reasonable upper bound on the average flange stress.

Next, Haaijer showed that the minimum value of plastic buckling stress as given by (3-28) is obtained when:

$$\frac{l_h}{b} = \sqrt[4]{\frac{D_x}{D_y}} \tag{3-34}$$

and the corresponding minimum plastic buckling stress, σ_{bm}, is:

$$\sigma_{bm} = \left(\frac{t_f}{b}\right)^2 \frac{\pi^2}{12}\left(2\sqrt{D_x D_y} + D_{xy} + D_{yx} + 4G_t\right) \tag{3-35}$$

Substituting the previously discussed values for D_x and D_y into (3-34) gives:

$$l_h = 0.55 b \tag{3-36}$$

which is the half wavelength that produces the minimum value of the plastic buckling stress. Therefore, it is conservative to use (3-35) to calculate the plastic plate buckling stress of flanges in EBF links. Limiting the upper value of the average flange stress of (3-33) to the minimum buckling stress of (3-35) and solving for the flange compactness ratio, b/t_f, results in:

$$\frac{b}{t_f} \le \sqrt{\frac{1}{1.243 F_{yf}} \frac{\pi^2}{12}\left(2\sqrt{D_x D_y} + D_{xy} + D_{yx} + 4G_t\right)} \tag{3-37}$$

Inserting the values for the moduli D_x, D_y, D_{xy}, and D_{yx} reported by Haaijer gives the following limit for flange compactness necessary to prevent buckling in shear links:

$$\frac{b}{t_f} \le 1.02\sqrt{\frac{E}{F_{yf}}} \tag{3-38}$$

For flexural links, setting $M_A = 1.2M_p$ to account for 20% strain hardening, and assuming $M_p = 1.2M_{pr}$, results in $\sigma_{av} = 1.292F_{yf}$. Making this adjustment results in a limit flange compactness ratio for flexural links of:

$$\frac{b}{t_f} \le 1.00\sqrt{\frac{E}{F_{yf}}} \tag{3-39}$$

The current limits in the AISC LRFD seismic provisions (AISC, 2002) are from work by Lee and Goel (1987) and Hassan and Goel (1991) on fracture and local buckling prevention in concentrically braced frames and are based on test results using hollow rectangular and square members in compression or combined compression and flexure. Comparing the AISC limit:

$$\frac{b}{t_f} \leq 0.64\sqrt{\frac{E}{F_{yf}}} \tag{3-40}$$

with the limit in (3-38) suggests that the limits currently in use for the design of square or rectangular cross-sections as compression or flexural members in seismic applications are theoretically conservative for use in the design of links of similar cross-sections. While the derivation of the limit of (3-38) used some conservative assumptions, it should still be verified experimentally.

3.4 Web Buckling and Stiffener Spacing

Web buckling has also been shown to be an undesirable failure mode for links in EBFs as it causes rapid strength and stiffness degradation and significantly impedes the energy dissipation capabilities of the system. Therefore, the spacing of stiffeners to avoid web buckling is a critical design issue for EBF links of any cross-section. Kasai and Popov (1986a) derived the stiffener spacing formula for WF links which appears in the AISC LRFD seismic provisions. The following derivation of a stiffener spacing formula for links of hollow rectangular cross-sections is similar to that for WF links, modified to represent the boundary conditions for the webs of a cross-section such as that of figure 3-1. Fully restrained boundary conditions for the web sides adjacent to the flanges were used in Kasai and Popov because of the presence of flange sections on both sides of the web and the high moment gradient. In the case of a hollow rectangular cross-section, there is flange on only one side of each web, therefore, simply supported boundary conditions are reasonable. Furthermore, simply supported boundary conditions are what has been traditionally used for web buckling considerations in plate and box girders.

The problem of web buckling in EBF links is generally an inelastic buckling problem for which the assumed form of the shear buckling stress, τ_b, is:

$$\tau_b = \eta(\tau)\,\tau_E \tag{3-41}$$

where $\eta(\tau)$ is a plastic reduction factor and is a function of the strain history, and τ_E is the elastic shear buckling stress for a plate given by (Basler, 1961):

$$\tau_E = \frac{\pi^2 E}{12(1-\nu^2)} K_s(\alpha)\left(\frac{1}{\beta}\right)^2 \tag{3-42}$$

where ν is Poisson's ratio, $K_s(\alpha)$ is a buckling coefficient which is a function of the boundary conditions and the panel aspect ratio, α, itself defined as the stiffener spacing, a, over the web depth, d-$2t_f$, and β is the web conpactness defined as the web depth over the web thickness, t_w.

The plastic reduction factor, η, was found by Kasai and Popov for WF links from tests on 30 specimens having different yield strengths, strain hardening modulii, aspect ratios, and web compactness ratios, and subjected to various cyclic displacement histories. From these tests:

$$\eta = 3.7\frac{G_s}{G} \tag{3-43}$$

where G_s is the secant shear modulus, and G is the elastic shear modulus. The secant shear modulus is defined as:

$$G_s = \frac{\tau}{\bar{\gamma}} = \frac{\tau_b}{\bar{\gamma}_b} \tag{3-44}$$

where $\bar{\gamma}_b$ is defined as the rotation of the link from the last point of zero shear force to the onset of web buckling and τ_b is the shear stress at web buckling, which is defined as the shear force divided by the web area. Substituting (3-42), (3-43), (3-44), and:

$$G = \frac{E}{2(1-\nu)} \tag{3-45}$$

into (3-41) and solving for $\bar{\gamma}_b$ gives:

$$\bar{\gamma}_b = 8.7 K_s(\alpha)\left(\frac{1}{\beta}\right)^2 \tag{3-46}$$

Kasai and Popov found that $\bar{\gamma}_b$ can be conservatively approximated by $2\gamma_u$, where γ_u is the ultimate link rotation. Finally, Galambos (1998) gives the expression for $K_s(\alpha)$ for a plate

simply supported on 4 sides (which is somewhat conservative because it neglects rotational restraint provided by the flanges) as:

$$K_s(\alpha) = 5.34 + \frac{4}{\alpha^2} \qquad if \qquad \alpha \geq 1$$
$$K_s(\alpha) = 4 + \frac{5.34}{\alpha^2} \qquad if \qquad \alpha < 1 \tag{3-47}$$

Setting the maximum panel aspect ratio to 1, substituting the appropriate expression for $K_s(\alpha)$ into (3-46), and solving for α gives:

$$\alpha = \sqrt{\frac{5.34}{\left(\frac{\gamma_u \beta^2}{4.35}\right) - 4}} \tag{3-48}$$

Note that for a panel aspect ratio of greater than 1, the constants 4 and 5.34 in (3-48) switch places. Solving (3-48) for a ($\alpha = a/d\text{-}2t_f$) can be conservatively approximated by solving for a from:

$$\frac{a}{t_w} + \frac{1}{8}\frac{d}{t_w} = C_B \qquad (a \leq d) \tag{3-49}$$

where C_B is 20 and 37 for ultimate link rotations of 0.08 rads (which is the maximum allowed for WF links in the AISC LRFD seismic provisions) and 0.02 rads respectively, and the web depth (d-2t$_f$) has been replaced by the section depth d. As explained in the Appendix, (3-49) has approximately the same degree of conservatism as the stiffener spacing equations for WF links that appear in the AISC LRFD seismic provisions. Shear links with hollow, rectangular cross-sections utilizing stiffener spacings satisfying (3-49) and stiffener sizes as described in the next section should not suffer web buckling when experiencing plastic rotations of up to 0.08 rads.

The above stiffener spacing requirements are applicable for shear and intermediate links ($\rho \leq 2.6$). For flexural links ($\rho > 2.6$), the requirements for stiffener spacing for WF links is likely adequate, namely, stiffeners required only at 1.5b from each end of the link.

3.5 Stiffener Sizing

The stiffeners on a link of hollow rectangular cross-section in an EBF must be designed to prevent both flange and web buckling. These two buckling cases are treated separately below, resulting in two sets of design equations. Furthermore, the stiffeners may be placed on either interior or exterior faces of the flanges and webs of a hollow rectangular cross-section. The following derivations are valid for both interior or exterior stiffener, however, the figures used will depict exterior stiffeners only.

3.5.1 Web Stiffeners

Consider a single eccentrically loaded stiffener on each of the webs as shown in figure 3-10. The solid line shows the size of stiffeners considered in the following, although the dotted lines show a likely shape for the complete stiffener system. Solmon and Johnson (1996) present a derivation for the required size of eccentrically loaded stiffeners for plate girders and Popov and Malley (1983) applied a similar procedure to WF shear links. Here the procedure will be modified for application to hollow rectangular shear links.

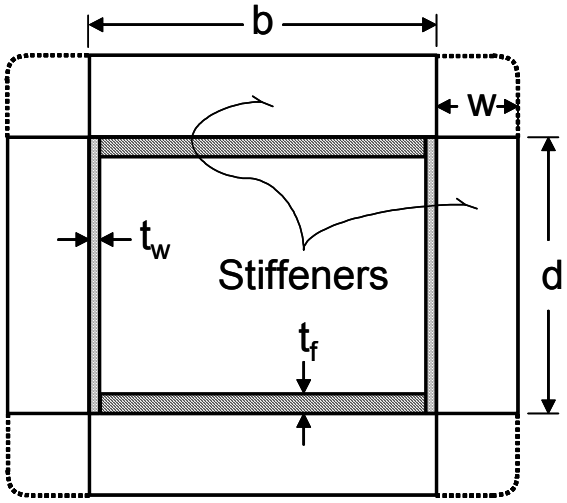

FIGURE 3-10 Cross-Section with Stiffeners

The force tributary to one stiffener, P_s, is resisted by the stress in the stiffener, which will be allowed to reach yield, F_{yst}, as shown in figure 3-11. From summation of moments about the point of application of P_s in figure 3-11, and neglecting the thickness of the tube wall, it can be shown that:

$$\frac{(w-x)^2}{2} = wx - \frac{x^2}{2} \tag{3-50}$$

where w is the stiffener width and x is the distance from the outer stiffener edge to the point at which the stiffener stress changes sign. Solving (3-50) for x gives $x = 0.293w$. Setting the force, P_s, equal to the sum of the vertical stresses times the stiffener thickness, t_s, and corresponding lengths (x and w-x) shown in figure 3-11, and substituting the resulting value for x given above, results in the stiffener yield limit state:

$$P_s = 0.414 w t_s F_{yst} \tag{3-51}$$

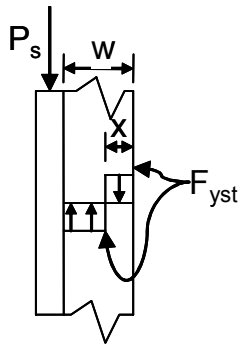

FIGURE 3-11
Stiffener Force
and Stresses

The link is designed such that the web is not allowed to buckle and tension field action will not occur. However, because of the complexity of inelastic web buckling, Popov and Malley found it convenient to use tension field action of the web plates as a reasonable approximation to determine the stiffener force, P_s. Considering the tension field forces and panel geometry shown in figure 3-12, it can be shown that (Solmon and Johnson, 1996):

$$P_s = \frac{1}{2}\sigma_t t_w a \left(1 - \frac{\frac{a}{h}}{\sqrt{1+\left(\frac{a}{h}\right)^2}} \right) \tag{3-52}$$

where σ_t is the tension field stress, h is the clear web depth and all other parameters are as previously defined. Popov and Malley set the tension field stress equal to the ultimate tensile stress of the web material, F_{uw}, to account for strain hardening. Making this

substitution, setting (3-51) and (3-52) equal to each other, and solving for the stiffener area, $A_{st} = wt_s$, gives:

$$A_{st} = \frac{F_{uw} t_w a}{0.828 F_{yst}} \left(1 - \frac{\frac{a}{h}}{\sqrt{1 + \left(\frac{a}{h}\right)^2}} \right) \tag{3-53}$$

Additionally, to prevent stiffener buckling, web stiffeners should satisfy the minimum moment of inertia requirements given in Appendix F2.3 of the AISC LRFD specifications, namely:

$$I_{st} \geq j a t_w^3 \qquad where \qquad j = \frac{2.5}{\left(\frac{a}{h}\right)^2} \geq 0.5 \tag{3-54}$$

and I_{st} is the stiffener inertia taken about the web, i.e. $t_s w^3/3$.

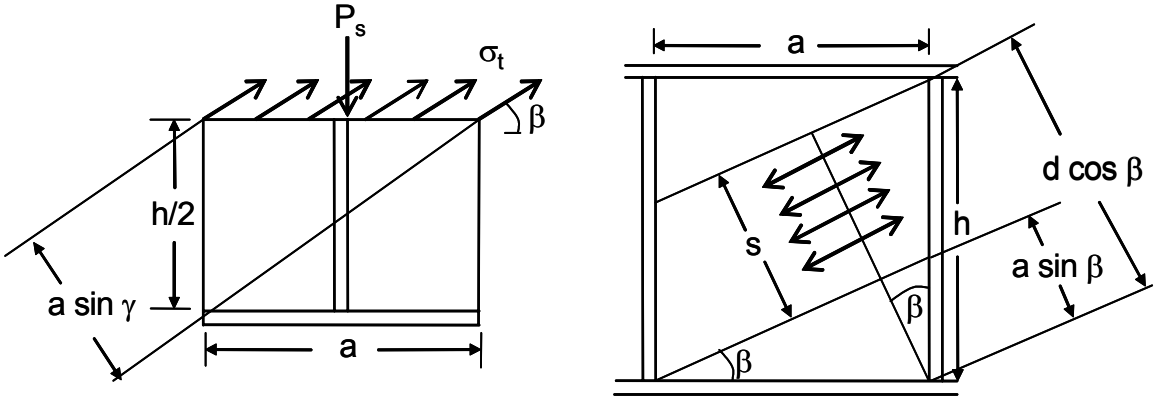

FIGURE 3-12 Panel Forces and Geometry (Adapted from Solmon and Johnson, 1996)

3.5.2 Flange Stiffeners

The flange stiffeners of an EBF link with a hollow rectangular cross-section must be designed to resist the force needed to prevent inelastic longitudinal buckling of the flange. A top view of the flange in compression with m+1 stiffeners and m equidistant spaces between them is shown in figure 3-13 (note it is assumed that there are stiffeners at each end of the link, if this is not the case there are m-1 stiffeners). Timoshenko and Gere (1961) made the conservative analogy of modeling this stiffened plate as a column on elastic supports. The ratio of stiffener to flange rigidity, ψ, is:

$$\psi = \frac{(EI)_{st}}{b(EI)_{fl}} \tag{3-55}$$

where $(EI)_{st}$ is the stiffener rigidity (EI_{st}), and $b(EI)_{fl}$ is the flange rigidity. The flange rigidity is given by:

$$(EI)_{fl} = \frac{E t_f^2}{12(1-\nu^2)} \tag{3-56}$$

where E is Young's modulus and all other terms are as previously defined. Timoshenko and Gere showed that in order to prevent stiffener deformation, the rigidity ratio, ψ, should be:

$$\psi \geq \frac{m^3}{\pi^2 C \left(\frac{e_{fl}}{b}\right)^3} \tag{3-57}$$

where e_{fl} is the length of the flange in compression, which can be taken as ½ the link length for shear links and 3b for flexural links (since outside these regions the compression vanishes or becomes small due to the moment gradient), and C is:

$$C = 0.25 + \frac{2}{m^3} \tag{3-58}$$

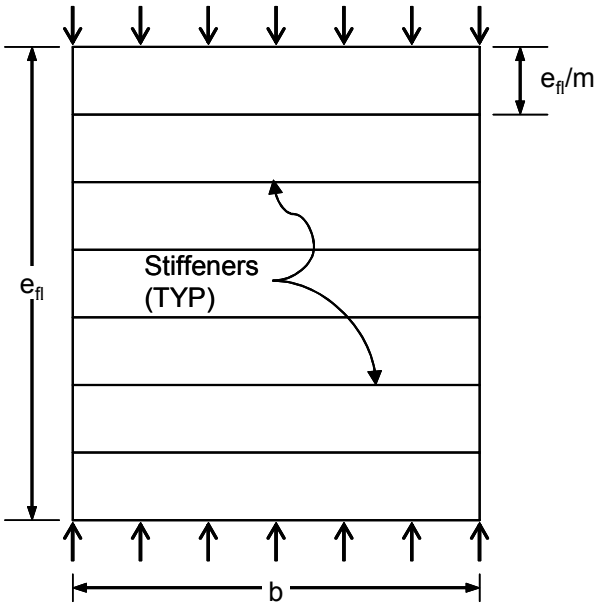

FIGURE 3-13 Top View of Compression Section of Flange and Stiffeners

Equating (3-55) and (3-57), substituting (3-56) and assuming that E is the same for the stiffeners and flange gives:

$$I_{stf} \geq \frac{m^3 b}{\pi^2 C \left(\frac{e_{fl}}{b} \right)^3} \left(\frac{t_f^3}{12(1-\nu^2)} \right) \tag{3-59}$$

where I_{stf} is the stiffener moment of inertia about it's major axis ($d_s^3 t_s/12$), and d_s is the stiffener depth. Inserting (3-58) and a Poisson's ratio, ν, of 0.3 gives the following equation governing the flange stiffener dimensions:

$$d_s^3 t_s \geq \frac{1.1 m^3 t_f^3 b}{\pi^2 \left(0.25 + \frac{2}{m^3} \right) \left(\frac{e_{fl}}{b} \right)^3} \tag{3-60}$$

3.5.3 Stiffener Connections

Since yielding of the stiffeners is possible because the derivation of the minimum stiffener size equation uses the stiffener yield as the limit state, the welds connecting the stiffeners to the link should be designed to develop the full yield strength of the stiffener. This philosophy is consistent with the current standards in the AISC LRFD seismic provisions for WF links.

3.6 Lateral Torsional Buckling

In the design of EBFs with WF links, lateral bracing of the link is necessary to prevent lateral torsional buckling, which has been shown experimentally to cause rapid strength degradation of the link and corresponding loss of its energy dissipation capabilities. However, hollow rectangular cross-sections are inherently more stable then WF sections in the context of lateral torsional buckling. In fact, the geometry of the cross-section could be selected such that the link beam is bent about its minor axis and lateral torsional buckling does not occur. Even a rectangular cross-section bent about its major axis is generally not subject to lateral torsional buckling, especially at the short lengths and high moment gradients encountered when used as a link in an EBF. For example, as shown in the AISC Hollow Structural Sections Specifications (AISC, 1997), a HSS 510x100x8 (20x4x5/16), which has the largest depth-to-width ratios of standard HSS, can achieve M_p,, at unbraced lengths of up to 2.7 m (8.7 ft) when bent about its major axis. Experimental verification however, will insure that these critical components do indeed behave in a ductile manner

without developing lateral torsional buckling in the absence of lateral bracing. Good ductile performance without lateral bracing is most desirable for their application in bridge piers where lateral bracing is difficult to provide.

3.7 Link Overstrength

Aside from (3-3) there are three other possible means of calculating the plastic shear strength of a hybrid shear link in an EBF. These other methods all give plastic shear strengths above that determined from (3-3) and may be useful in determining the expected overstrength of the shear link, i.e., in determining the maximum possible shear strength.

3.7.1 Method 1 - Corner Region Consideration

As opposed to (3-3), in which the corner regions of the link are assumed to contribute to the moment capacity of the section, the first method considered for evaluating the maximum possible link shear strength simply assumes that those regions act in shear. Therefore, the shear area of the link is $t_w d$ rather than $t_w(d\text{-}2t_f)$ and the maximum link shear strength, V_{p1}, is:

$$V_{p1} = \frac{2}{\sqrt{3}} F_{yw}\, t_w d \tag{3-61}$$

The shear strength from (3-61) may or may not be substantially different from that determined from (3-3) depending on the flange thickness. Thicker flanges will result in a larger difference between (3-61) and (3-3) while thin flanges will result in a small difference.

3.7.2 Method 2 - Flange Shear Consideration

The second method considered for evaluating the maximum possible shear strength of a hybrid rectangular link assumes that after flexural hinges form in the flanges, they begin to carry some shear by themselves (Richards and Uang (2002) for wide-flange links). Therefore, the maximum possible shear strength calculated for Method 2, V_{p2}, can be thought of as:

$$V_{p2} = V_p + 2V_f \tag{3-62}$$

where V_p is the shear strength given by (3-3) and V_f is the flange shear. Considering figure 3-14 it is clear that:

$$V_f = \frac{2M_p^f}{e} \tag{3-63}$$

where M_p^f is the flange plastic moment which, considering the presence of flange axial force, can be expressed as:

$$M_p^f = \left[1 - \left(\frac{P_f}{P_{yf}}\right)^2\right] M_{po}^f \tag{3-64}$$

where P_f is the flange axial force due to the overall link moment, P_{yf} is the flange yield axial force given by:

$$P_{yf} = F_{yf}(b - 2t_w)t_f + F_{yw}t_w t_f \tag{3-65}$$

and M_{po}^f is the flange plastic moment without the presence of axial force, namely:

$$M_{po}^f = \frac{F_{yf}(b - 2t_w)t_f^2}{4} + \frac{F_{yw}t_w t_f^2}{2} \tag{3-66}$$

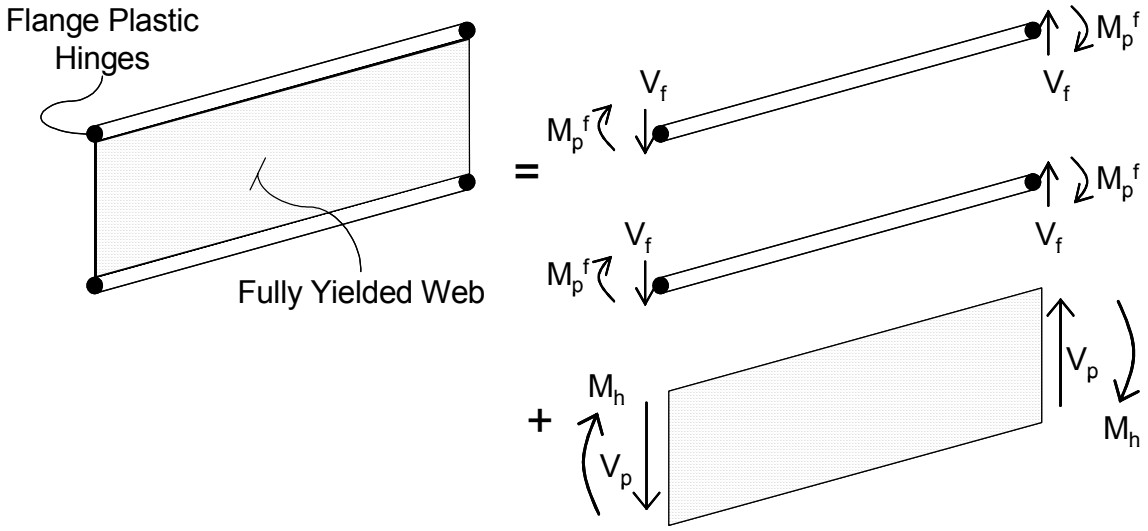

FIGURE 3-14 Formation of Flange Hinges at Link Ends

(Adapted from Richards and Uang, 2002)

Next, for simplicity, the flange axial force is approximated by assuming that 85% of the link end moment, M_h, is carried by the flanges (which is typical for WF sections but may need modification for hollow rectangular cross-sections), or:

$$P_f = \frac{0.85 M_h}{d - t_f} \tag{3-67}$$

Then, the link end moment just after the web has fully yielded is:

$$M_h = \frac{V_p e}{2} \tag{3-68}$$

where V_p is given by (3-3).

The above procedure can be simplified into a single equation, which is easier for design code implementation, with the assumption of equal flange and web yield stresses, i.e. $F_{yf} \approx F_{yw} \approx F_y$. With this assumption, (3-68) can be rewritten as:

$$M_h = \frac{F_y (d - 2t_f) t_w e}{\sqrt{3}} \tag{3-69}$$

Inserting (3-69) into (3-67) gives:

$$P_f = \frac{0.49 F_y (d - 2t_f) t_w e}{d - t_f} \tag{3-70}$$

Assuming that $d\text{-}2t_f \approx d\text{-}t_f$, rewriting (3-65) as $P_{yf} \approx F_y b t_f$, rewriting (3-66) as:

$$M_{po}^f = \frac{F_y b t_f^2}{4} \tag{3-71}$$

and inserting these and (3-70) into (3-64) results in:

$$M_p^f = \left[1 - \frac{t_w^2 e^2}{4 b^2 t_f^2}\right] \frac{F_y b t_f^2}{4} \tag{3-72}$$

Finally, (3-72) can be substituted into (3-63), which results in the following expression for the flange shear force, V_f:

$$V_f = \frac{F_y b t_f^2}{2e} - \frac{F_y t_w^2 e}{8b} \tag{3-73}$$

3.7.3 Method 3 - Panel Zone Application

The panel zone shear strength equation derived by Krawinkler et al. (1971) for columns in moment frames is the third method considered for calculating the maximum possible link shear force, namely:

$$V_{panel} = 0.55 F_y d_c t_{cw} \left(1 + \frac{3.45 b_c t_{cf}^2}{d_b d_c t_{cw}} \right) \tag{3-74}$$

where d_c is the column depth, t_{cw} is the column web thickness, b_c is the column flange width, t_{cf} is column flange thickness, F_y is the column yield stress, and d_b is the beam depth. In order to apply this equation to shear links the following substitutions are made; $F_y = F_{yw}$, $d_c = d$, $t_{cw} = 2t_w$, $b_c = b$, $t_{cf} = t_f$, and $d_b = e$, where all parameters are as previously defined. The resulting expression for the maximum possible link shear force, V_{p3}, calculate by this third method is then:

$$V_{p3} = 1.1 F_{yw} d t_w \left(1 + \frac{1.725 b t_f^2}{e d t_w} \right) \tag{3-75}$$

The three methods presented above give different results for the maximum possible shear strength of hybrid hollow rectangular links. In all three methods the web yield stress could be replaced with the ultimate stress, or factored for strain hardening. It is unclear at this point which one, if any, gives accurate results; therefore, in later sections, these methods will be compared with experimental results.

3.8 Design of Framing Outside the Link

As is currently the state of practice, capacity design of the framing and connections outside the link should be performed. Factors to account for the difference between the nominal and expected values of the link material's yield stress (and in the case of hybrid cross-sections the difference in yield stresses in the different materials) and strain hardening should also be considered. Bruneau et al. (1998), Naiem (2001), and the AISC seismic provisions provide summaries of methods and requirements for the design of framing and connections outside the link region. Furthermore, the most accurate method to assess the maximum possible shear strength of hybrid rectangular links, should be used for capacity design of the surrounding framing.

3.9 Summary

In this section design rules for links in EBFs with hybrid hollow rectangular cross-section were derived. First, the shear-moment interaction equation for such cross-sections was given, (3-18), then, the balanced link length (i.e. the link length for which the reduced plastic

moment and the plastic shear occur simultaneously) was formulated in terms of cross-section dimensions (3-20). Next, the b/t_f limits of the AISC seismic provisions for rectangular hollow structural sections were found to be adequate to prevent flange buckling according to a theory developed by Kasai and Popov for WF links and applied here to hollow rectangular links. Next, a stiffener spacing equation was proposed (3-49), again based on work done by Kasai and Popov on web buckling of WF shear links and adapted here to shear links with hollow rectangular coss-sections. Following this, equations for the minimum stiffener dimensions for both web and flange stiffener were derived, (3-53), (3-54), and (3-60), and recommendations for the design of the stiffener connections to the link were given. Lateral torsional buckling of hollow rectangular links was discussed and it was determined that lateral bracing is likely not needed (however, this conclusion is subject to experimental verification). Three methods for calculating the maximum possible shear strength of rectangular links were also presented, although it is not clear at this point which one is the most reliable. Finally, capacity design of the framing and connections outside the link was briefly discussed and references were given for further recommendations.

SECTION 4
EXPERIMENTAL DESIGN AND SETUP

4.1 General

This section describes the design and setup of a quasi-static cyclic test on a single story eccentrically braced frame (EBF) utilizing a link beam with a hybrid rectangular cross-section. The design of the test specimen is based on the maximum capacity of the hydraulic actuator available in the Structural Engineering and Earthquake Simulation Laboratory (SEESL) at the University at Buffalo (UB) and the theories developed in Section 3. The framing outside the link region is designed using capacity principles and appropriate safety factors. Tension test results on the material used to construct the link beam are given, and the setup, including the foundation beam, lateral bracing, and instrumentation are described. This first test specimen involving a hybrid rectangular link will be denoted the proof-of-concept specimen.

4.2 Frame Dimensions

Due to the constraints of available equipment in the SEESL, the overall test specimen dimensions were set to a height of 3150 mm and width, L, of 3660 mm. A general schematic of the test setup is shown in figure 4-1. As shown, a loading beam was necessary at the top of the specimen to evenly distribute the actuator force to the two columns (a small variation in the load to each column is expected due to the axial flexibility of the loading beam). Excluding the loading beam and clevis heights, the actual height of the specimen from the centerline of the link beam to the centerline of the lower clevises, h, was set at 2360 mm. Denoting the distance from the centerline of the link beam to the centerline of the upper clevises as h^*, assuming zero moments at the clevis centerlines and the middle of the link, and assuming that the actuator load is evenly distributed to the two columns, the free body

diagram of figure 4-2 can be used to determine the link shear force, V_L, in terms of the applied actuator load, V_a, as:

$$V_L = V_a \frac{h+h^*}{L} \tag{4-1}$$

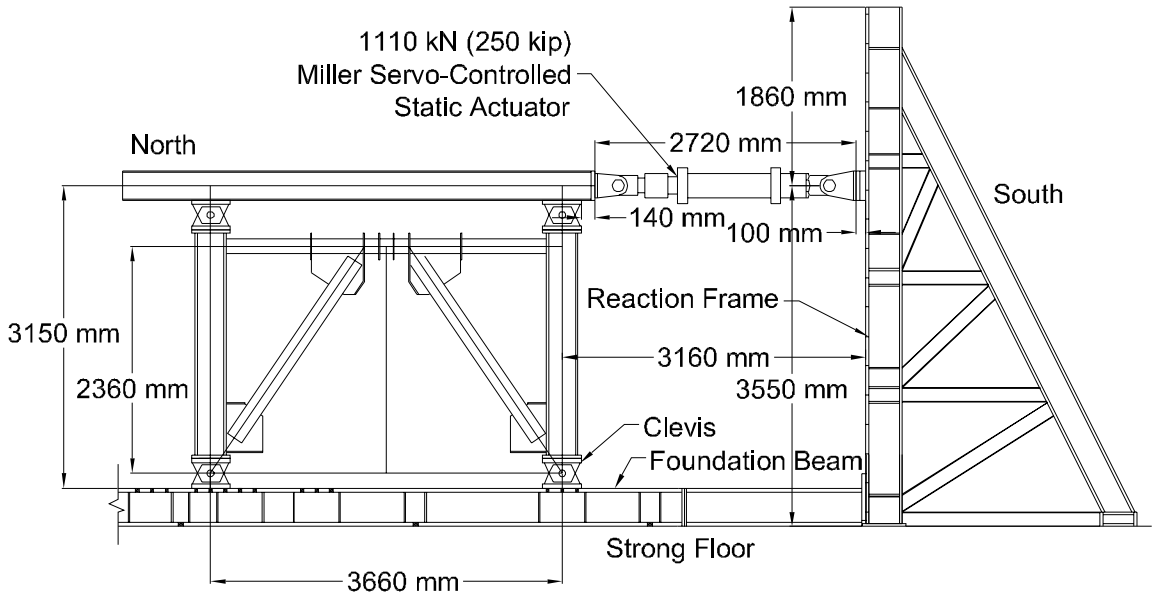

FIGURE 4-1 Test Setup Schematic

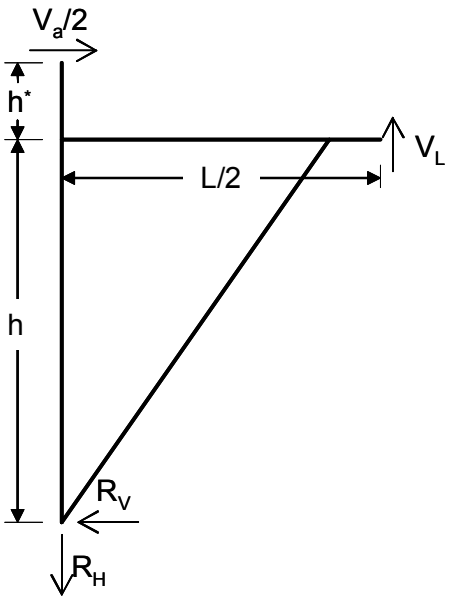

FIGURE 4-2 Free Body Diagram of North Half of Specimen

4.3 Link Design

The hybrid link must be designed to satisfy several conditions simultaneously. It must have the desired shear strength, flexural strength, and link length, while meeting the seismic limits for flange compactness (b/t_f) and web compactness (d/t_w). Additionally, a frame drift-to-link rotation ratio must be selected so that adequate energy dissipation can be achieved prior to the link rotation reaching 0.08 rad. Finally, the beam outside the link must be able to resist large axial forces and moments acting simultaneously. What follows is an outline of the procedure used to size the link cross-section for the experimental test specimen.

- To insure the actuator would have the capacity to push the specimen well into the strain hardening range, and to account for possible material yield stresses that were higher than specified, the maximum actuator force, V_a, was set to 445 kN.
- Using (4-1) the required link shear force, V_L, was found to be 327 kN for V_a of 445 kN, h of 2360 mm, and h^* of 326 mm.
- The required shear area, $A_s = (d-2t_f)t_w$, was found to be 880 mm^2 from (3-3) rearranged as:

$$(d-2t_f)t_w = \frac{\sqrt{3}\,V_p}{2\phi_v F_y} \tag{4-2}$$

  Note that a resistance factor, ϕ_v, of 0.9 was considered, the link plastic shear force V_p was taken as V_L from above, and the yield stress, F_y, was assumed to be 345 MPa (50 ksi).
- Next, the minimum link length was determined to achieve a link rotation, γ_u, of 0.08 radians at a minimum drift, Δ/h, of 1% . Using the following relationship for link length, drift, link rotation, and bay width:

$$\frac{\Delta}{h} = \gamma_u \frac{e}{L} \tag{4-3}$$

  the minimum link length was determined to be 460 mm (18 in).
- Next, the shear link length, e^*, was determined from (3-19) with a few conservative modifications. The first modification was to neglect any shear-moment interaction (i.e. assuming both M_p and V_p can be developed simultaneously). Then, to account

for strain hardening, the maximum possible link end moment and the maximum plastic shear were assumed to be $1.2M_p$ and $1.5V_p$ respectively, based on the work of Kasai and Popov (1986a). Finally, the plastic moment was multiplied by a resistance factor, ϕ_b, of 0.9, and the plastic shear was multiplied by the R_y for plate material of 1.1 which is the ratio of expected to specified yield stress (AISC, 2002). The resulting conservative equation for the maximum shear link length was:

$$e^* = \frac{1.31 M_p}{V_p} \tag{4-4}$$

Substituting (3-1) and (3-3) into (4-4), and assuming the flange and web yield stresses to be equal gives:

$$e^* = \frac{1.13\left[t_f\left(b-2t_w\right)\left(d-t_f\right)+\frac{t_w d^2}{2}\right]}{t_w\left(d-2t_f\right)} \tag{4-5}$$

- Assuming a yield stress of 345 MPa, and using the results of (4-3) to define the minimum e^*, the results of (4-5) to define the maximum e^* (to maintain a shear link), the results of (4-2) for the minimum required shear area, and the limits of the AISC seismic provisions (AISC, 2002) for both web and flange compactness, given by:

$$\frac{b-2t_w}{t_f} \text{ or } \frac{d-2t_f}{t_w} \le \frac{290}{\sqrt{F_y}} \quad F_y \text{ in MPa} \tag{4-6}$$

the following link cross-section dimensions and length were chosen: $d = b = 150$ mm (6 in), $t_f = 16$ mm (0.625 in), $t_w = 8$ mm (0.3125 in), and $e = 460$ mm (18 in). Using these values the anticipated plastic shear force, plastic moment, and plastic base shear were 381 kN, 120 kN-m, and 519 kN respectively.

4.4 Framing Outside the Link

Once the link dimensions were determined, capacity design principles were used to size the surrounding frame. The beam outside the link region was conservatively designed assuming it would have to resist 85% of the link end moment ($V_p e/2$) simultaneously with an axial force of $V_p L/2h$, both amplified by a 1.1 factor to represent expected strain hardening and another 1.1 factor to represent the expected versus specified yield stress. The corresponding moment

and axial force for the beam outside the link were 90 kN-m and 357 kN respectively. An effective length factor of 1.0 was assumed for each segment of the beam outside the link, which had lengths of 1600 mm (63 in), and the resistances of the segments were checked using standard AISC LRFD beam-column formulas and found to be adequate.

The eccentric braces were also designed as beam-columns. First, the design axial load, P_{br}, was found from simple statics (conservatively assuming the beam moment at the column was face zero) as:

$$P_{br} = \frac{V_p L}{(L-e)\sin\theta} \tag{4-7}$$

where θ is the brace angle with respect to the horizontal (55.9°) and all other terms are as previously defined. This load was then arbitrarily doubled to ensure elastic behavior of the braces. Second, the moment used for design of the braces was found using moment distribution factors based on a preliminary brace size and the actual size of the link-beam (resulting in approximately 44% of the link end moment, $V_p e/2$, assumed to go to each brace). This moment was then factored by 1.25 and 1.1 to account for strain hardening of the link and the expected versus specified yield stress of the link respectively. The effective length factor was conservatively taken as 1.0 and a HSS 178x178x12.7 (7x7x1/2) brace size was specified to resist the 1050 kN (236 kip) axial force and 53 kN-m (39 kip-ft) moment demands.

The columns for the specimen were W 310x143 (12x96) recycled from a previous experiment. With the member sizes described above, a SAP2000 (CSI, 1997) model was developed for pushover analysis. A shear hinge was placed in the middle of the link and assigned a bilinear force-rotation curve with a strain hardening slope of 10% of the elastic stiffness. Resulting loads were used to check the framing members again, verifying the above design. Figure 4-3 shows the test specimen with dimensions and member sizes.

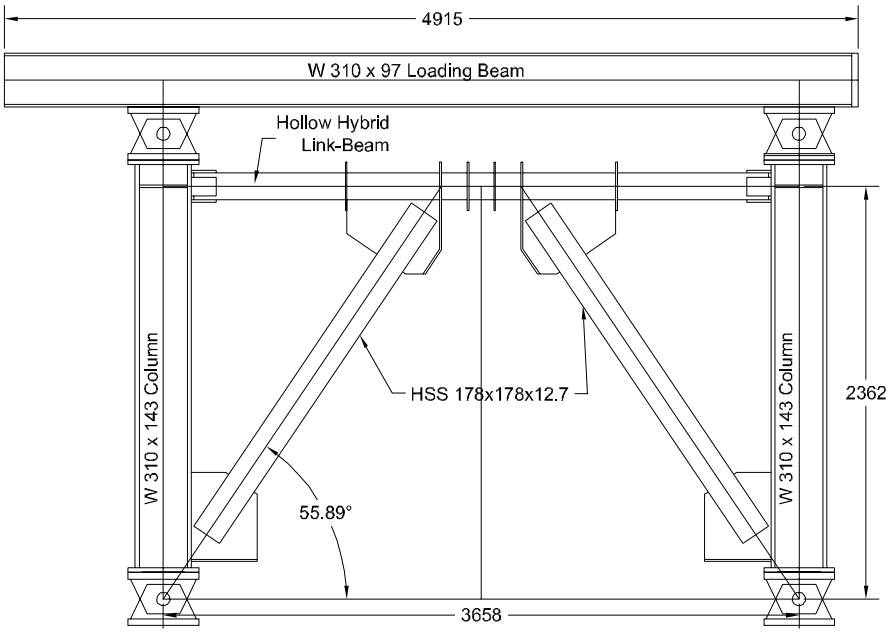

FIGURE 4-3 Test Specimen Dimensions and Member Sizes

4.5 Link Detailing

Discussed in this section are the link details shown in figures 4-4 and 4-5. First, the link stiffener spacing and stiffener sizes were designed using the equations of Section 3. From (3-49) a stiffener spacing of 150 mm (6 in) was calculated, then using (3-53), (3-54), and (3-60), a minimum stiffener thickness of 10 mm (0.375 in) and minimum stiffener width of 64 mm (2.5 in) were selected. Note that the stiffener width (i.e. the distance from the surface of the link to the edge of the stiffener), was kept constant around the entire cross-section (see figure 3-10). Assuming ASTM A572 Gr. 50 steel with a yield stress of 345 MPa (50 ksi) for the stiffeners, a 6.5 mm (0.25 in) fillet weld on both sides of each stiffener and all-around the link to stiffener interface was designed to resist the full yield strength of the stiffeners.

A full penetration groove weld was chosen to join the 4 plates (2 webs and 2 flanges) that were used to build the link's hybrid cross-section. The maximum weld shear flow, f, was determined from the equation:

$$f = \frac{VQ}{I_x} \tag{4-8}$$

where V is the shear force in the link, taken to be $2V_p$ for conservativeness, Q is the first moment of area of the flange about the neutral axis, and I_x is the moment of inertia of the entire link cross-section. Half of that shear flow was considered for the designs of each of the two lines of weld joining the webs to each flange.

As shown in figure 4-5, the flanges were designed with 45° bevels to accommodate the full penetration groove weld. This detail was selected over one in which the webs were beveled because, the flanges being thicker than the web, it allowed for a larger base-metal to weld-metal contact area for the same bevel angle.

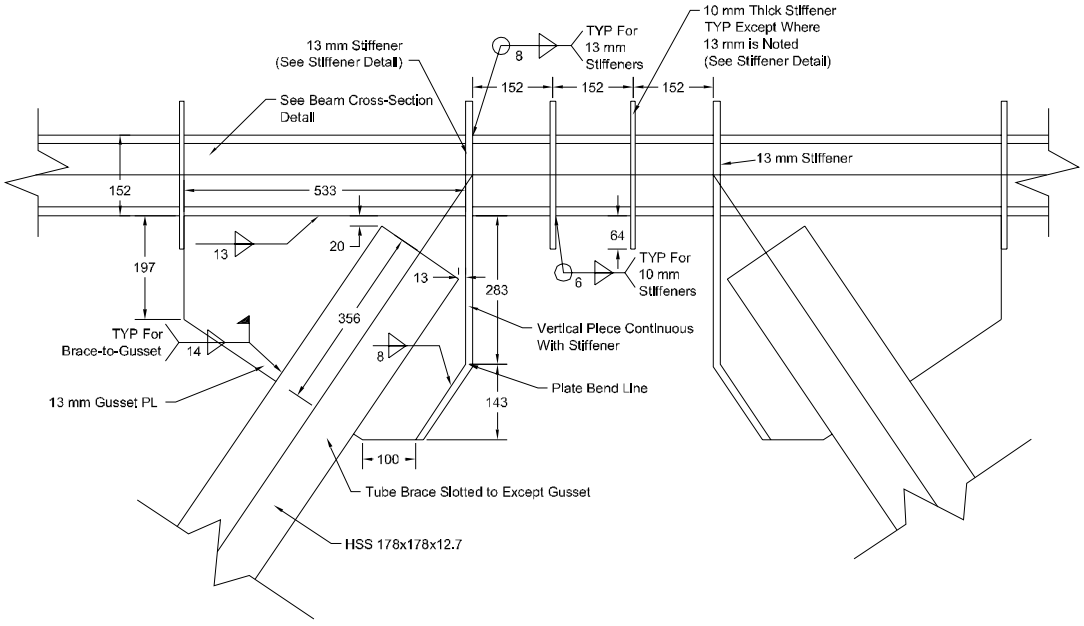

FIGURE 4-4 Link and Stiffener Detail

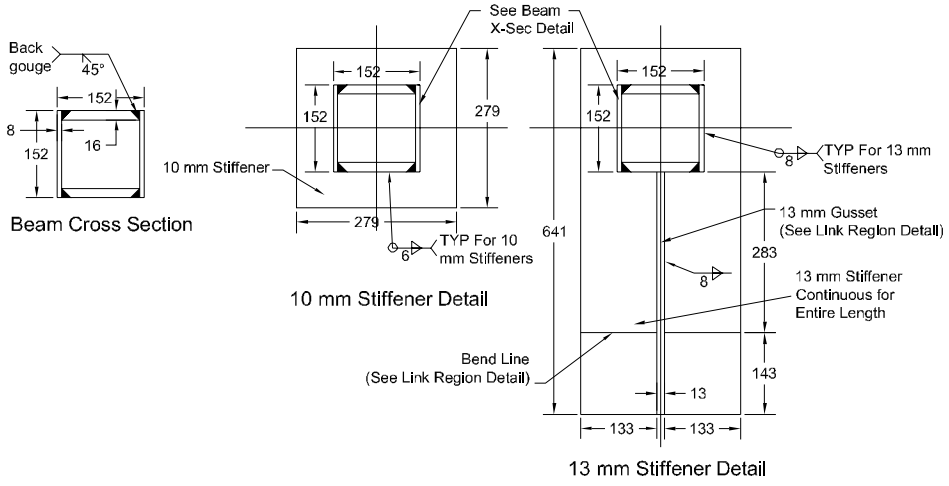

FIGURE 4-5 Link and Stiffener Cross-Sections

4.6 Link Construction

The construction sequence for the link, established in collaboration with the fabricator, is outlined below:

- The flanges were beveled to accommodate the full penetration welds described above.
- As shown in figure 4-6, the two webs and one flange were tack welded to four square internal alignment plates located at various points in the beam outside the link region.
- The webs were then tack welded to much thicker plates along their length to prevent distortion during welding. These thicker plates are shown in figure 4-6 and labelled "distortion prevention plates".
- The two full penetration welds to connect the two web plates to the one flange plate were then made. The beam was then flipped and the second flange was welded on.
- When all four full penetration welds were complete the distortion prevention plates were removed. Final checking of the straightness indicated that the member conformed to American Society of Testing of Material (ASTM) standards (ASTM A6/A6M-04).

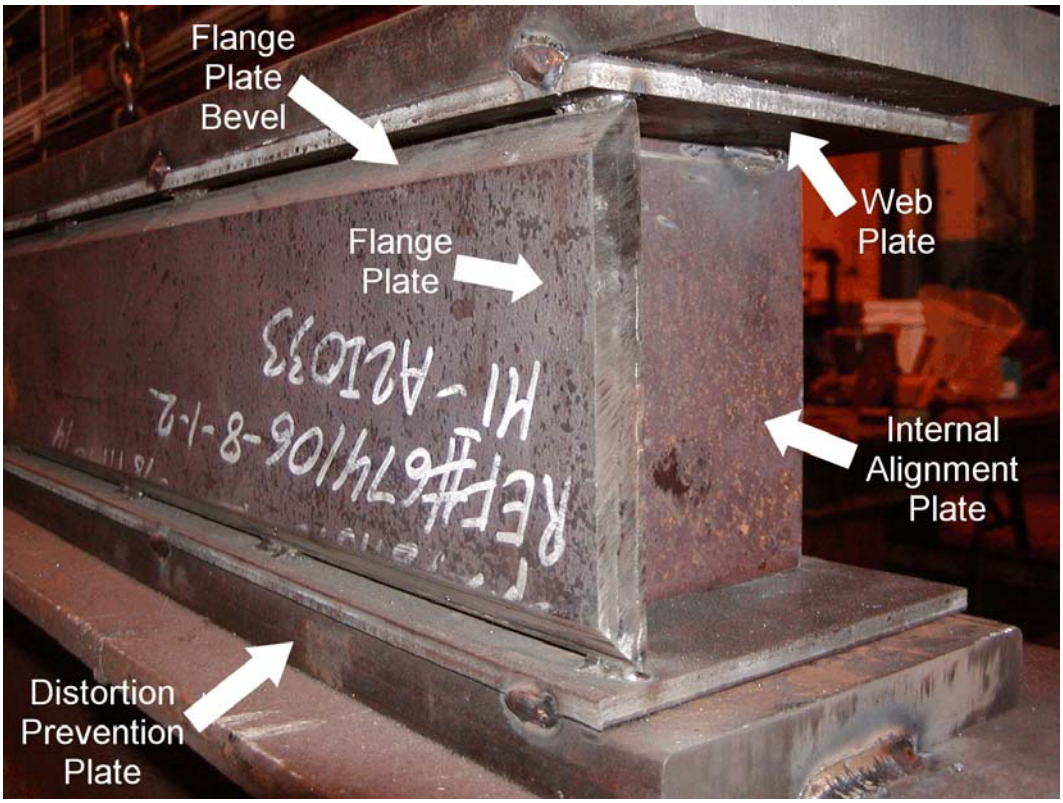

FIGURE 4-6 Construction of Link Beam

4.7 Framing Connections

The connections for the braces were designed to resist a maximum link shear force of 800 kN, 210% of the nominal link shear force using specified material properties. All connection design forces were found from a SAP2000 pushover analysis using the above as the link plastic shear force. Standard procedures for connection design were employed, such as; elastic vector analysis for the welds (Salmon and Johnson, 1996), gusset rupture checks, and gusset buckling and yielding checks using Whitmore sections. The resulting connection details are shown in figures 4-7 and 4-4 for the brace-to-column and brace-to-beam connections respectively.

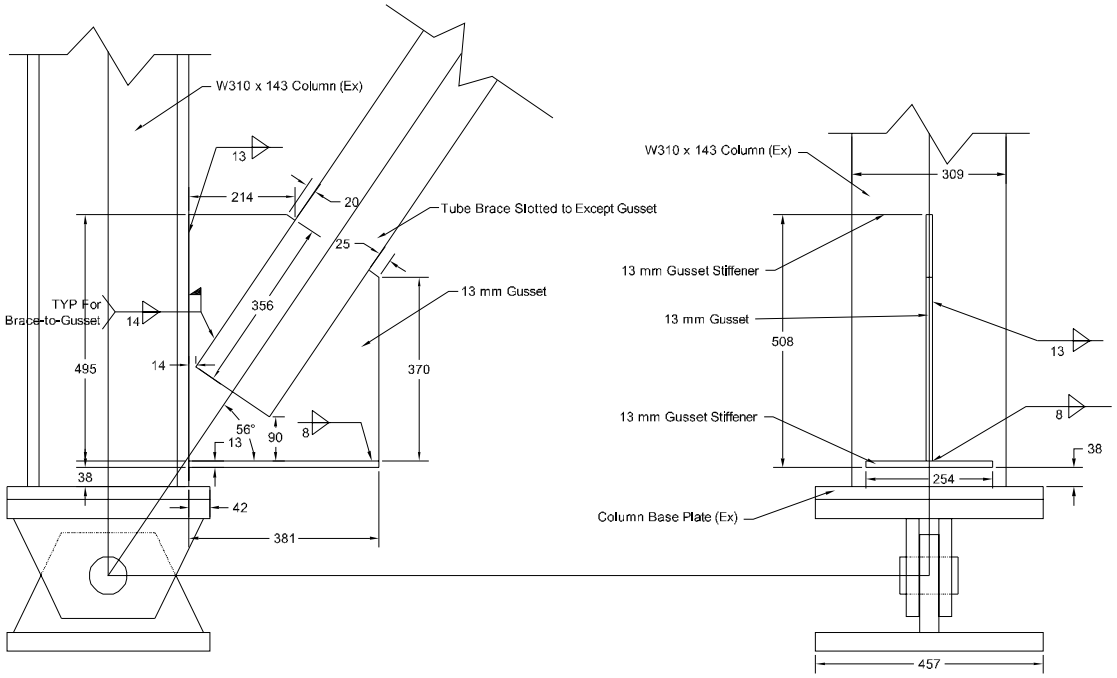

FIGURE 4-7 Brace-to-Column Connection Detail

The beam-to-column connection was designed as moment resisting for the actions corresponding to a link shear force of 800 kN. The HSS beam-to-WF column connection shown in figure 4-8 was selected in consultation with the Steel Tube Institute (private communication, February, 2003). A column web stiffener was necessary to increase the calculated column shear strength at the connection.

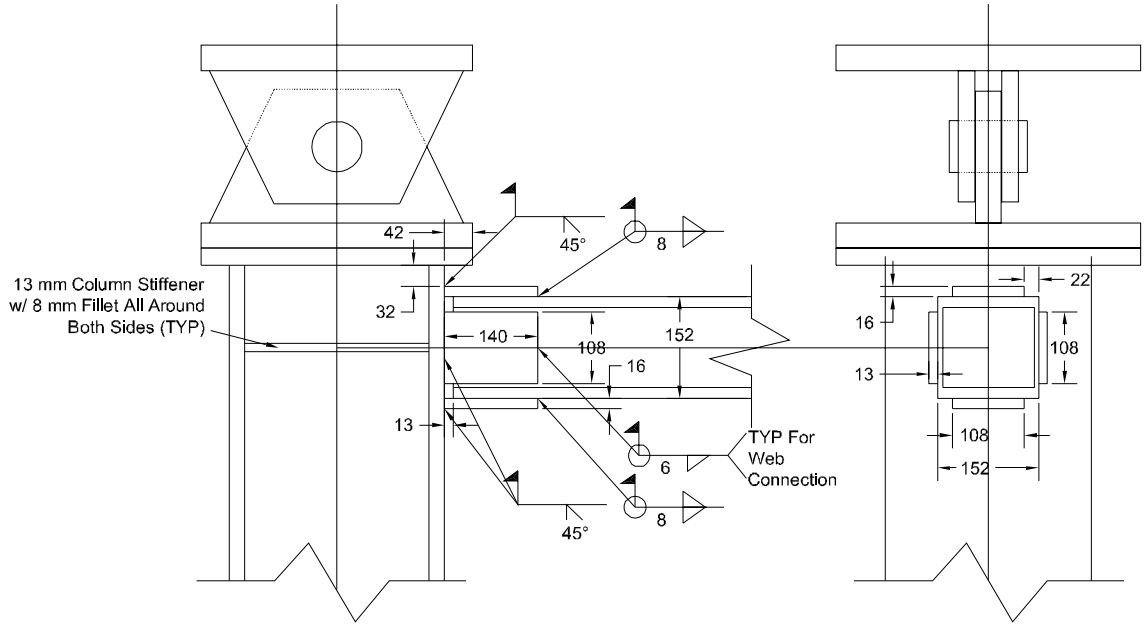

FIGURE 4-8 Beam-to-Column Connection Detail

Column base and top plates were designed for the forces resulting from the same SAP2000 pushover analyses used above. Resulting base and top plates were specified as 25 mm (1 in) thick and the hole pattern was designed to match that of the existing clevises (or rocker bearings) available in the SEESL. The selected column base and top plate detail is shown in figure 4-9a.

The loading beam end plate was designed to accept the bolts for the actuator head and to resist a load of 2225 kN (500 kip) which is twice the capacity of the actuator. The final loading beam end plate detail is shown in figure 4-9b.

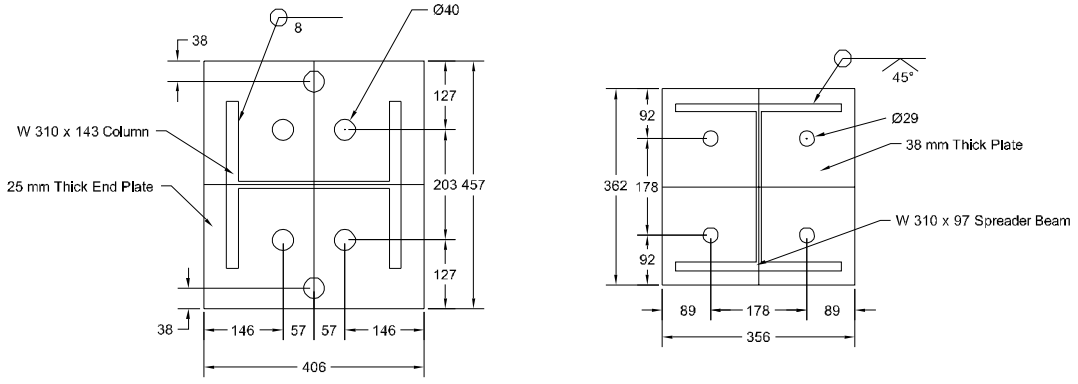

(a) Column Base and Top Plate (b) Loading Beam End Plate

FIGURE 4-9 End Plate Details

4.8 Foundation Beam and Clevises

The foundation beam and clevises (or rocker bearings) used in the experimental setup are described in Berman and Bruneau (2003) and were designed for the support reactions generated by a frame with dimensions of 3660 mm wide by 2440 mm tall and an actuator force of 2225 kN (500 kip). They were found to be adequate considering the support reactions anticipated for this experiment, with a reasonable margin of safety.

4.9 Lateral Bracing

Lateral bracing was provided for safety at points above the columns on the loading beam using large rollers attached to adjacent towers as shown in figure 4-10. In order to observe the lateral stability of the link, no lateral bracing was provided to the link beyond the possible out-of-plane resistance provided by the eccentric braces.

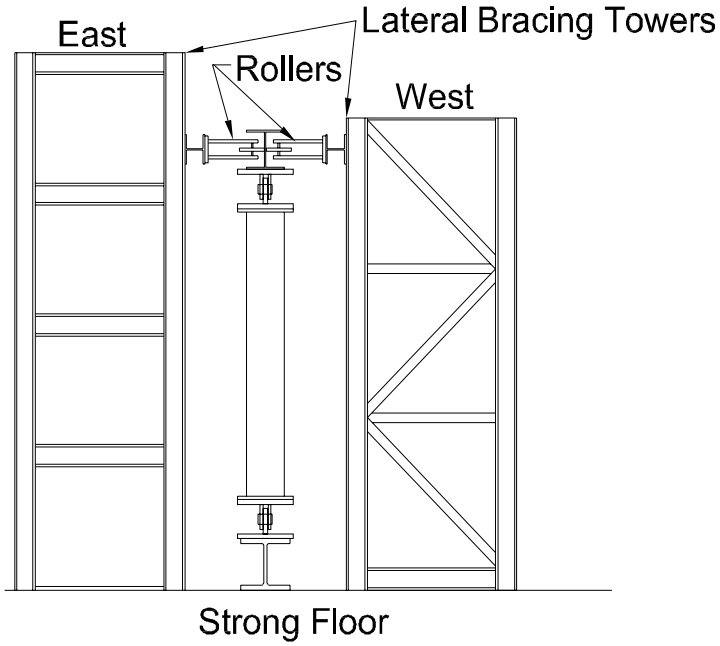

FIGURE 4-10 Lateral Bracing

4.10 Materials

4.10.1 Link Beam

All plates for the hybrid link beam were specified to be ASTM A572 Grade 50 steel and compliance was verified by review of the mill certificates. The two web plates were cut from the same original 16 mm (5/8 in) thick plate; similarly, the two flange plates were cut from

a single 8 mm (5/16 in) thick plate. Coupons for tension testing conforming to ASTM standards (ASTM A370) were fabricated from both the flange and web plate materials. Mean coupon test results are shown in figures 4-11 and 4-12 for the web and flange material respectively. Note that the yield stress for the web material, 448 MPa (65 ksi), is considerably higher than the 345 MPa (50 ksi) specified while the yield stress of the flange material, 393 MPa (57 ksi), is closer to the specified value and slightly exceeding the AISC expected yield strength of 380 MPa (55 ksi) for this steel grade (AISC, 2002). The ramifications of these observations are considered in later sections. Using the results of the coupon tests, the link plastic shear, V_p, and plastic moment, M_p, were determined to be 495 kN (111 kips), and 157.6 kN-m (1395 kip-in) respectively.

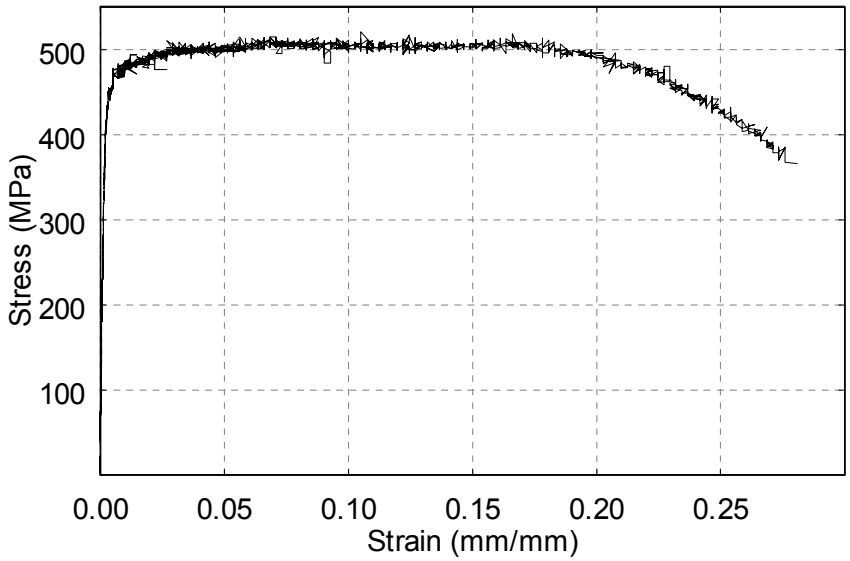

FIGURE 4-11 Web Material Stress-Strain Curve

4.10.2 Frame Members, Connection Plates, Weld Metal, and Bolts

The columns of the test specimen were reused from a previous experiment in which they remained elastic. They were specified to be ASTM A572 Grade 50 steel. Similarly, the connection plates and brace members were specified to be ASTM A572 Grade 50 and ASTM A500 Grade B respectively. No coupon tests were performed on the material of the above components as they were expected to remain elastic during this test. All weld metal was specified as E7018 electrode.

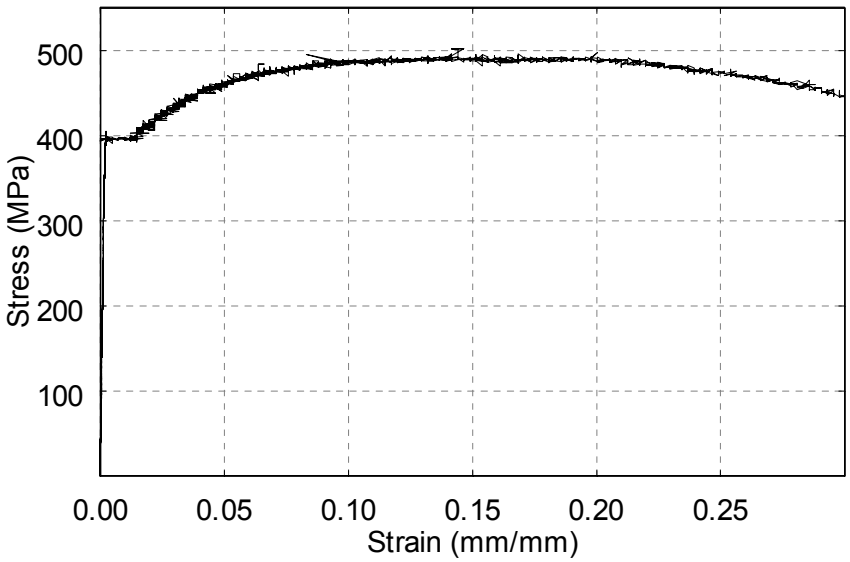

FIGURE 4-12 Flange Material Stress-Strain Curve

Bolts were specified as ASTM A490 structural bolts and were pre-tensioned using a HYTORC Blitz 4-A hydraulic torque wrench. The turn-of-the-nut method described in AISC, 1998 was used for this purpose.

4.11 Instrumentation

The instrumentation layout was chosen such that there would be redundant measurements of key parameters. For instance, the link shear force was determined from (4-1) knowing the lateral force applied by the actuator (provided by the actuator's internally mounted load cell), or from the forces and moments in the braces and beam segments outside the link (calculated using data from strain gauges were placed on those members). Story drift was measured with redundancy by using more than one temposonic at the link-beam level. The following is a complete description of the instrumentation layout used for this test which is shown in figures 4-13 and 4-14.

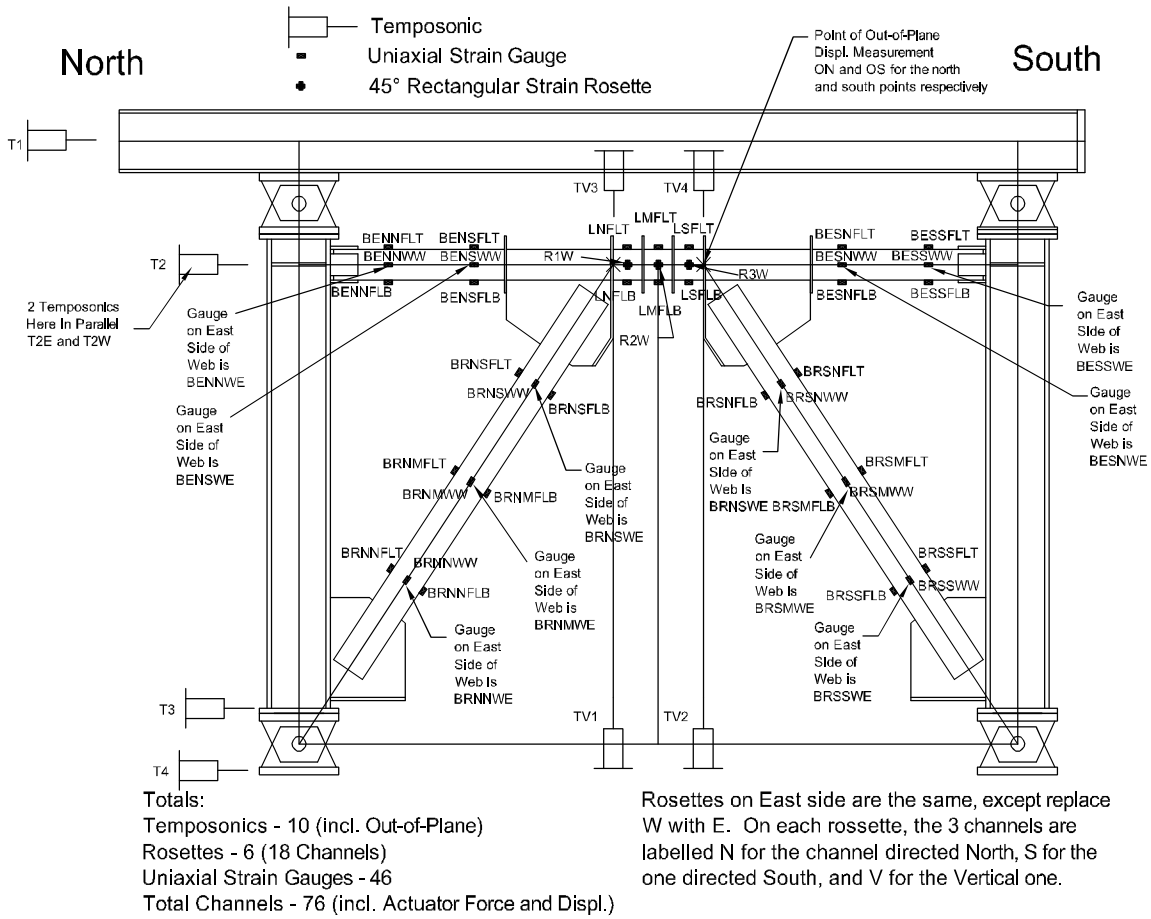

FIGURE 4-13 Instrumentation Layout with Instrument Names

4.11.1 Temposonics

Several Temposonic Magnetic Strictive Transducers (Temposonics) were used to measure displacement at certain locations during testing. T4 was used to measure any slip of the clevises at the base of the experiment, T1 measured the displacement of the loading beam, and T2E and T2W measured the displacement of the specimen at the centerline of the link beam. All of those temposonics were mounted on a frame that was attached to the foundation beam, therefore, any displacement of the foundation beam did not effect their measurements. TV1 and TV2 measured the vertical displacement of the link relative to the foundation beam while TV3 and TV4 measured it relative to the loading beam. Since the loading beam moved horizontally with the specimen TV3 and TV4 directly measured the vertical motion of the link

ends. Therefore, denoting the instrument displacement as δ, with a subscript indicating the instrument name, the link rotation, γ, can be calculated as:

$$\gamma = \frac{\delta_{TV4} - \delta_{TV3}}{e} + \frac{\delta_{T2E}}{h} \tag{4-9}$$

(noting that when the specimen is pushed to the north, the south end of the link moves down so that δ_{TV4} is negative, δ_{TV3} is positive, and δ_{T2E} is negative, resulting in a negative link rotation). Additionally, assuming negligible movement of the foundation beam, the drift angle of the specimen is simply the second term of (4-9). For redundancy, similar results could also be obtained using measurements from TV1 and TV2 provided the displacement component from the horizontal movement of the link beam relative to the foundation beam is corrected using the measurements from T2W or T2E.

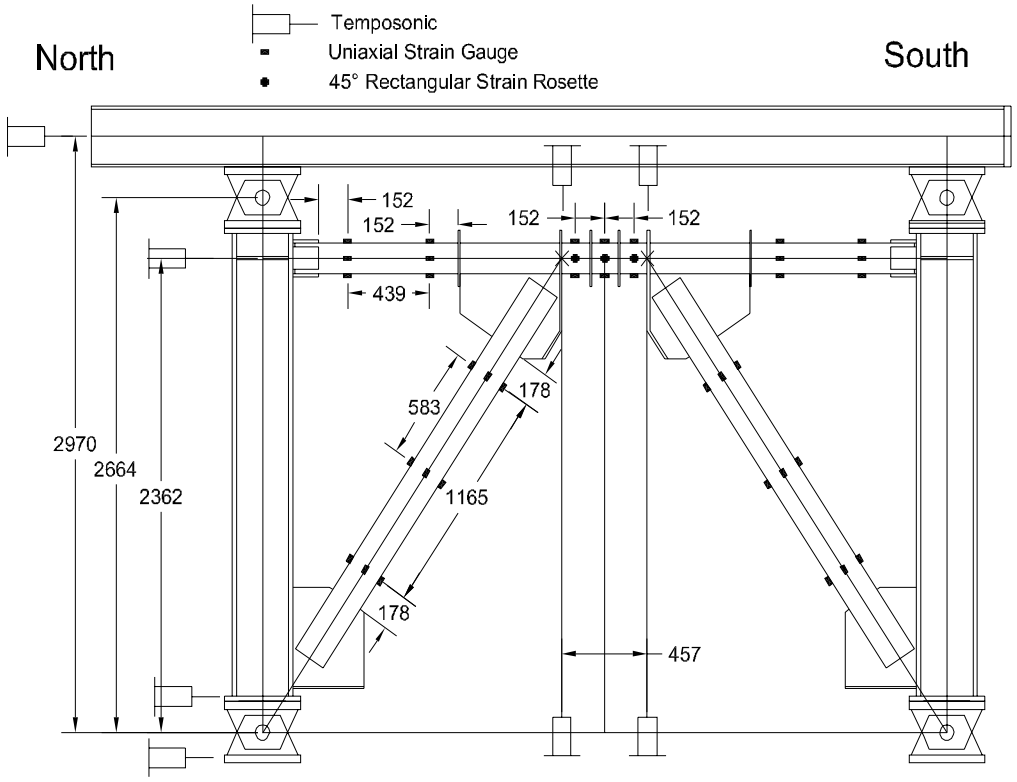

FIGURE 4-14 Instrumentation Layout with Dimensions

4.11.2 Strain Gauges

As noted in figure 4-13, two types of strain gauges were used, namely, uniaxial gauges and 45° rosettes. Both types were manufactured by Vishay Measurements Group and were attached using M-Bond 200 adhesive. Rosettes were type CEA-06-125UR-120 and were placed on the link web as shown in figures 4-13 and 4-14. A typical strain rosette is shown in figure 4-15. Measured strains were used to calculate principal strains and directions using standard plane strain equations. Principal strains can then be compared with the yield strain of the web material obtained from coupon tests, to identify the onset of web yielding during testing.

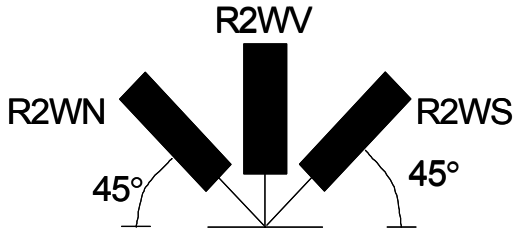

FIGURE 4-15 Example Strain Rosette Layout

The uniaxial strain gauges were type CEA-06-125UW-120. Four gauges were attached (one on each flange and one on each web) at two different locations on each segment of the beam outside the link region. From these gauges, and the assumption that the beam segments outside the link region remains elastic, the beam moment diagram, shear forces, and axial forces can be determined. Furthermore, the gauges on each web allow for the out-of-plane moments and shear to be calculated, which can give insight into the lateral stability of the hybrid link cross-section. This same layout (4 gauges at each location, one on each web and one on each flange) was used at each of three locations on each of the eccentric braces, allowing for calculation of in-plane and out-of-plane moment diagrams and shear forces, as well as axial forces.

Uniaxial gauges were also added to the flanges of the link, midway between the stiffeners to provide an estimate of the link axial force in the early stages of testing. Finally, the gauges

at the middle of the link, LMFLT and LMFLB, can be used to verify the assumption of zero moment at that location.

4.12 General Test Setup

The fabricated specimen was brought into the SEESL and mounted on the clevises which were in-turn mounted on the foundation beam. The loading beam was laterally braced and the actuator was mounted. Following this, the specimen, except for the columns and loading beam, was whitewashed with a lime and water mixture intended to flake off as the steel yields, giving a visual indication of yielding. Finally, the instrumentation was attached. Figures 4-16 through 4-20 show general photographs of the specimen setup, including some close-ups of the link region.

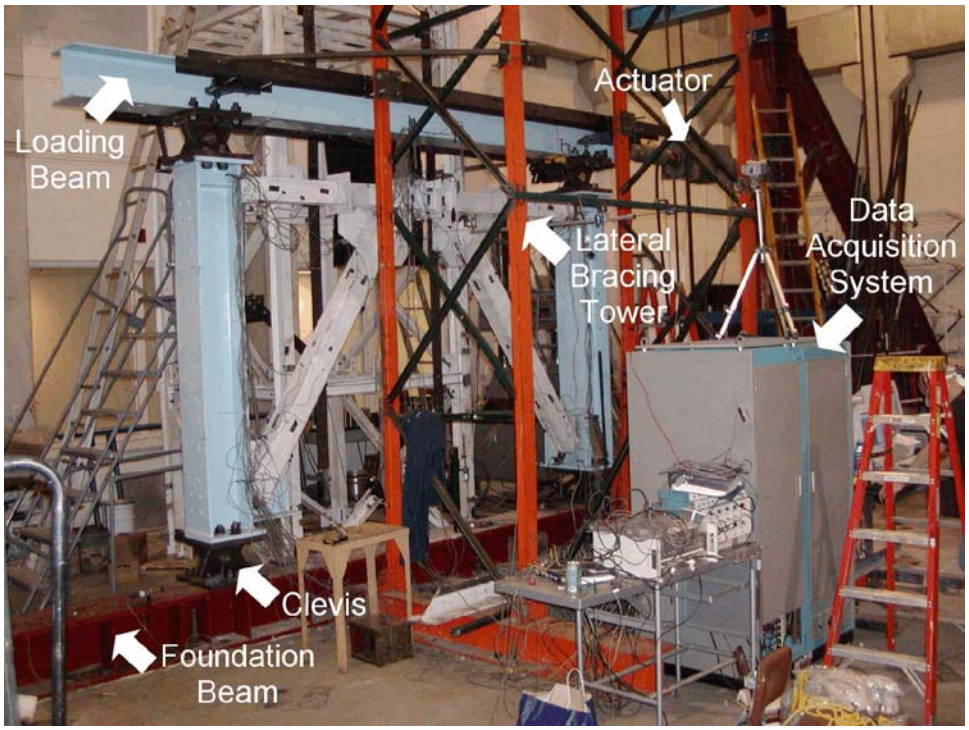

FIGURE 4-16 Completed Test Setup

FIGURE 4-17 Link and Brace Connections

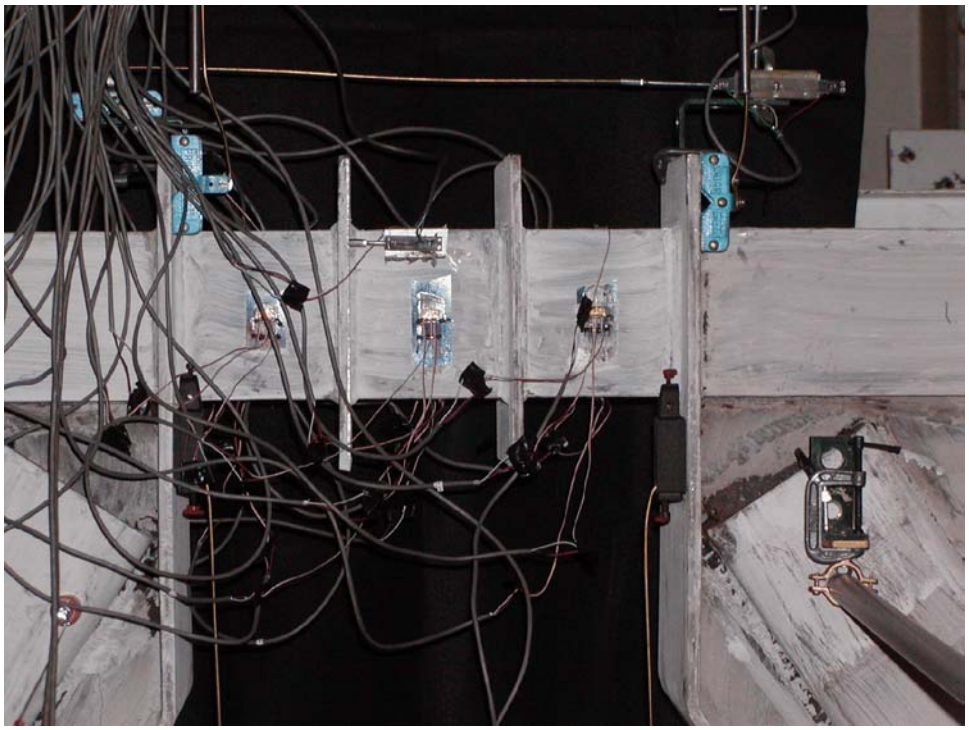

FIGURE 4-18 Instrumented Link Closeup

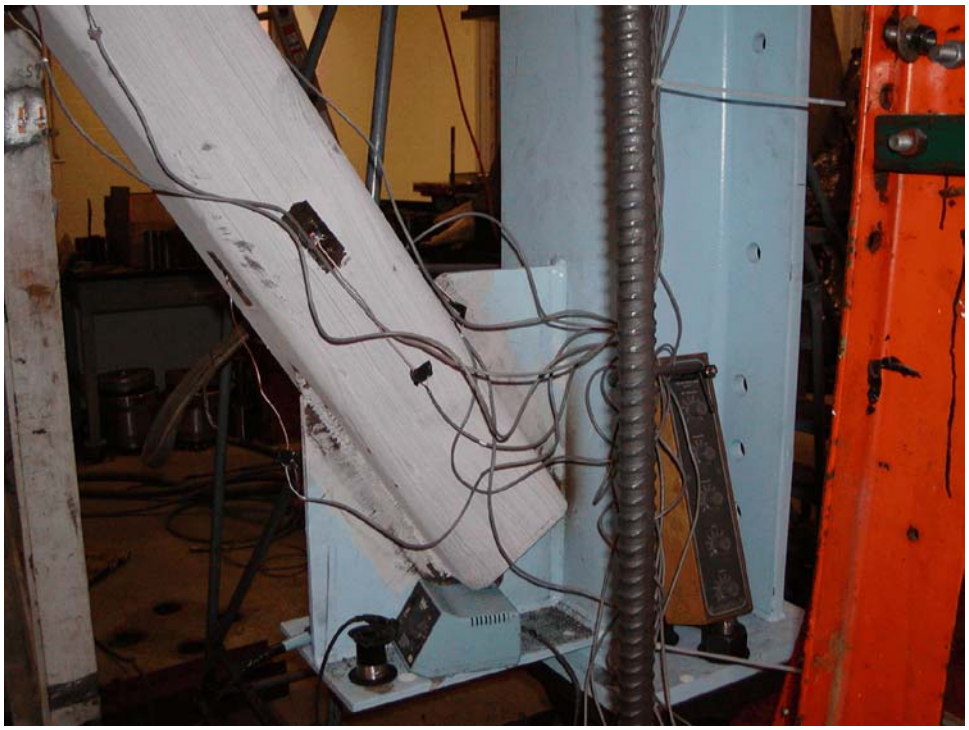

FIGURE 4-19 Brace-to-Column Connection

FIGURE 4-20 Beam-to-Column Connection

SECTION 5

LOADING AND EXPERIMENTAL OBSERVATIONS

5.1 General

This section describes the quasi-static loading protocol established for the experiment, and observations made during and after the cyclic testing of the specimen. The resulting specimen hysteresis curve is presented and referenced for the purpose of these observations. Post-test observations about the type of fracture suffered by the link flange are made by investigating the failure surface using basic fractographic methods.

5.2 Loading Protocol

5.2.1 Estimation of Specimen Yield Force

As described in Section 4, the link in this study is classified as a shear link, therefore, the yield point of the specimen can be assumed to coincide with the development of V_p in the link. Using (4-1), a yield base shear and actuator force of 667 kN (150 kip) was calculated for the expected V_p of 495 kN (111 kips). Note this base shear is larger than the target used for specimen design due to the larger-than-specified yield strength of the web material. This estimated yield base shear for the test specimen was used to determine the loading protocol for the cycles up to and including the first yield cycles as described below.

5.2.2 ATC Loading Protocol

The quasi-static loading protocol used here was developed based on the guidelines presented in ATC-24 (ATC, 1992) and is shown in figure 5-1. The cycles up to and including yield were performed under force control. Verification of the yield force was done by checking the values for principal strains from the rosettes on the web of the link, the displacement of the specimen at the first occurrence of that force was marked as the yield displacement.

After yield had been identified, the subsequent cycles were done using the displacement recorded at temposonic T2E of figure 4-13 to control the displacement imposed to the specimen. Table 5-1 gives the recorded values of maximum base shear (obtained from the actuator load cell output), V_a, the calculated values of percent drift and link rotation, γ, obtained using (4-9), and the corresponding fraction of the yield displacement for each cycle imposed on the specimen. The experimentally obtained hysteresis curve for the specimen is shown figure 5-2.

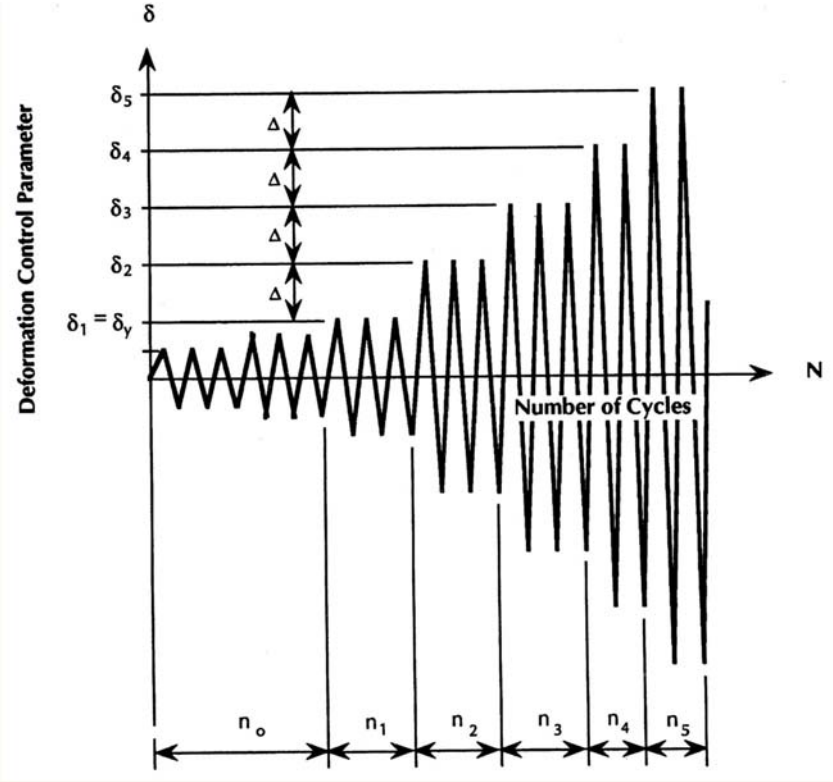

FIGURE 5-1 ATC Loading Protocol (ATC, 1992)

It should be noted that in some previous tests by others on EBF links alone, or on link-brace-column assemblies (Itani, 1997, Arce, 2002, and Duscika et al., 2002), the loading protocol from the AISC seismic provisions (AISC, 1997) for testing of link-to-column connections has been used. It should be noted that the AISC protocol would have resulted in more cycles of rotations in the inelastic range and that future testing on the links alone will use that protocol. However, since an entire EBF was being tested here, and the behavior of the framing outside the link was also of interest, it was decided that the ATC recommendations were appropriate since they are based on frame drift.

TABLE 5-1 Loading History

Cycle No.	Fraction of δ_y	Drift %	γ (rad)	V_a (kN)	V_L (kN)
1	0.33	0.11	0.004	213	157
2	0.33	0.11	0.004	217	159
3	0.33	0.11	0.004	212	156
4	0.67	0.23	0.008	434	319
5	0.67	0.23	0.008	432	318
6	0.67	0.24	0.009	445	327
7	1.0	0.38	0.014	668	491
8	1.0	0.37	0.013	646	475
9	1.0	0.37	0.013	664	488
10	2.0	0.76	0.038	842	619
11	2.0	0.75	0.037	850	625
12	2.0	0.75	0.037	853	627
13	3.0	1.15	0.067	893	656
14	3.0	1.14	0.066	912	671
15	3.0	1.14	0.066	912	670
16	4.0	1.54	0.096	947	696
17	4.0	1.52	0.093	956	703
18	5.0	1.92	0.123	991	728
19	5.0	1.92	0.123	996	733
20	6.0	2.30	0.151	1009	742

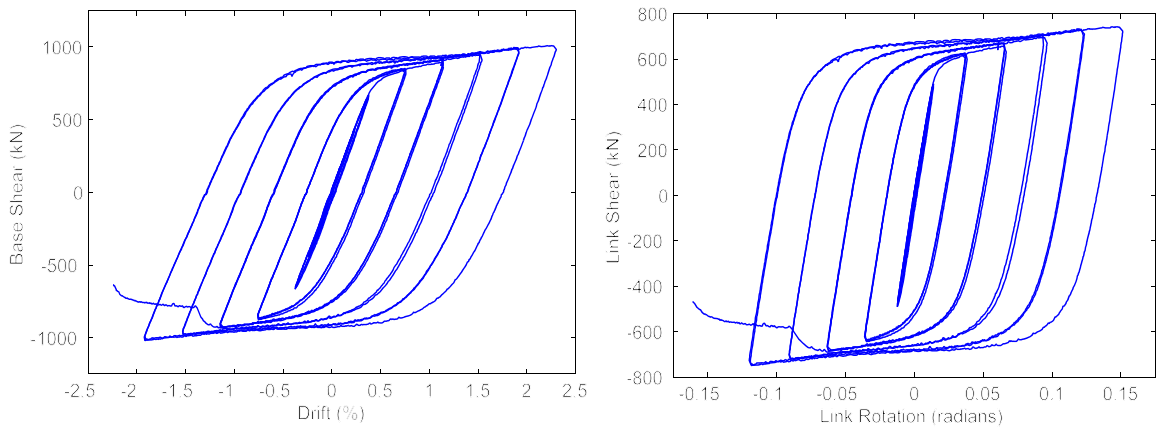

FIGURE 5-2 Base Shear vs. Frame Drift and Link Shear vs. Link Rotation

5.3 Experimental Observations

5.3.1 Elastic Cycles

Behavior during the cycles at 0.11% drift was elastic, as indicated by readings from all link strain gauges. The maximum principal strain of the link web during these first three cycles was 0.0005, which is approximately 25% of the web material's yield strain. From the strain gauges on the link flanges, the maximum flange strain at the gauge locations during the first three cycles of loading was 0.00035, which can be extrapolated to the link endpoint assuming the moment at the link midpoint is zero. After extrapolation, the approximate maximum flange strain at the link endpoint was 0.000525 or 27% of the yield strain for the material. The maximum link shear reached during these cycles was 160 kN (36 kip), found from the actuator force using (4-1), which is 32% of V_p (V_p = 495 kN [111 kip]). Using the link shear-moment equilibrium relationship $M_L = V_L e/2$ (this will be used for the calculation of link end moments throughout this section), the corresponding maximum link moment during these cycles was 37 kN-m (327 kip-in), which is approximately 23% of M_p considering the delivered material properties (M_p = 157.6 kN-m [1394 kip-in]).

Elastic behavior continued during the cycles at 0.23% drift. Maximum web principal strain was 0.001, or 50% of the yield strain. Extrapolating the maximum strain from the link flange gauges to the link endpoint gave a maximum strain there of 0.0012, or 61% of the flange yield strain. A maximum link shear of 320 kN was found during these cycles, from

which a maximum link moment of 73 kN-m was calculated. These correspond to 65% and 46% of V_p and M_p, respectively.

The specimen yield point was determined to be a base shear of 668 kN (150.2 kip) and drift of 0.37% based on principal strains from rosette readings on the link webs, the initial estimates of yield base shear and link plastic shear, and the observation that a slight decrease in stiffness was occurring. Through three cycles at the yield drift, the maximum link shear force and end moment were 491 kN (110 kip) and 112 kN-m (991 kip-in) respectively, which correspond to 99.1% of V_p and 71% of M_p. During Cycles 7, 8, and 9 the maximum principal strain in the link web varied from 0.0028 to 0.0021 or 126% and 95% of the web yield strain, and the maximum flange strain at the link endpoint was approximately 0.00185, or 94% of the flange yield strain. These results indicate that the link web yielded in shear prior to the link flanges yielding from flexure.

5.3.2 Inelastic Cycles

Following the three cycles at the yield drift, the specimen was subjected to increasing multiples of that drift, following the protocol outlined in Table 5-1.

During the cycles at $2\delta_y$, the maximum base shear and link shear force increased approximately 30% compared to the values obtained during the cycles at $1\delta_y$, to 853 kN (192 kips) and 627 kN (141 kips) respectively. The maximum link end moment reached during these cycles was determined to be 143.4 kN-m (1269 kip-in) or 91% of M_p. Shear deformations of the link became visible during these cycles, as shown in figure 5-3 at the point of maximum positive drift during Cycle 11. Also observed during Cycles 10-12 was the onset of whitewash flaking, as shown in figure 5-4 at the maximum negative drift of Cycle 12. The strain rosettes on the web of the link failed during the cycles at $2\delta_y$. Extrapolation of the strain gauge readings on the link flanges showed the maximum flange strain at the link end was estimated to be 0.00465 (mm/mm) or 233% of the flange yield strain. This indicates that the end moment had exceeded the yield moment of the link, M_y, 129 kN-m (1140 kip-in), but as noted above was still below the plastic moment. The maximum link rotation during these cycles at $2\delta_y$ was 0.038 radians, or almost three times

the yield rotation of link. The difference between the relative increases in drift and link rotation can be attributed to the flexibility of the framing outside the link. Since the link and the framing outside the link can be thought of as two springs in series, once the link reaches its plastic shear capacity it absorbs most of the additional displacement, whereas prior to that both the link and the framing outside the link deform. Therefore, the difference in link rotation between drifts of $1.0\delta_y$ and $2.0\delta_y$ is larger than the difference between in link rotations at $0.0\delta_y$ and $1.0\delta_y$.

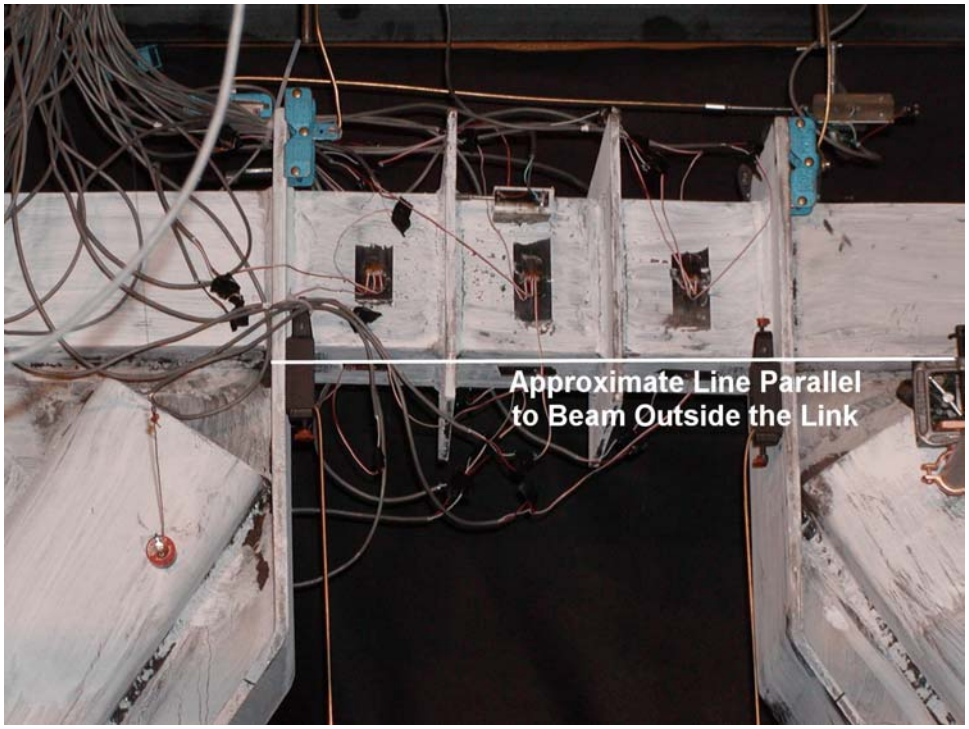

FIGURE 5-3 Deformed Link at $2\delta_y$, 0.76% Drift, 0.038 rads Rotation, Cycle 11

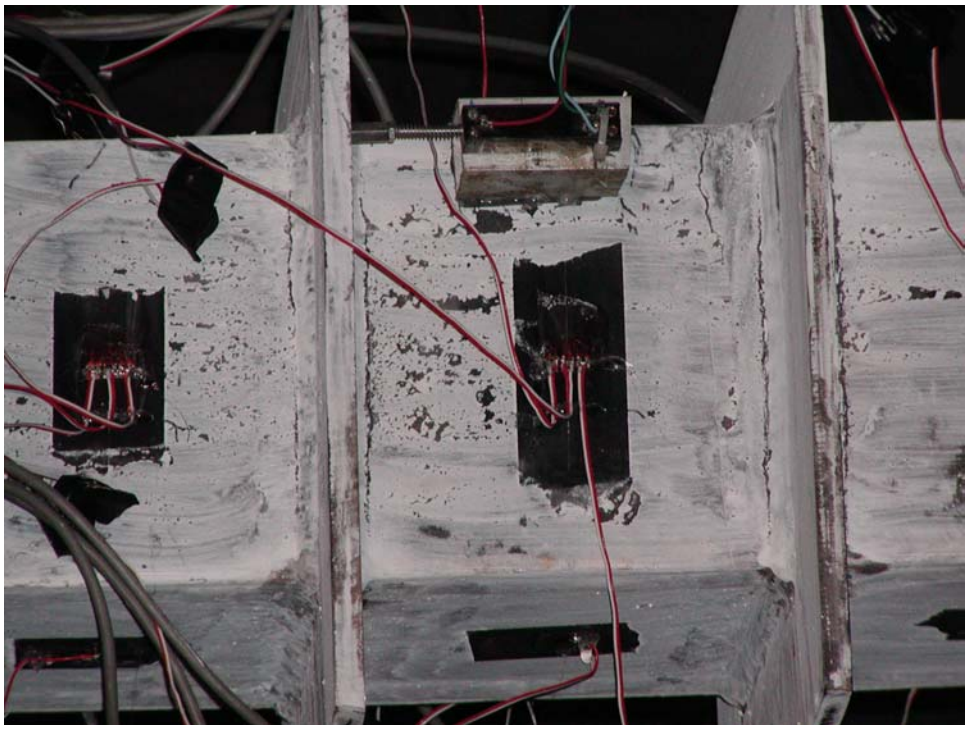

FIGURE 5-4 Whitewash Flaking off Link Web at -2δ_y, -0.75% Drift, -0.037 rads Rotation, Cycle 12

During the cycles at $3\delta_y$, the maximum base shear and link shear were approximately 1.4 times the yield base shear and plastic link shear forces respectively. The maximum link end moment during these cycles was found to be 154 kN-m (1357 kip-in) or approximately 97% of M_p. At this point the strain gauges on the link flanges also failed (with the exception of the ones at the link midpoint), and no strain gauge data could be recorded for either the link webs or flanges beyond $2\delta_y$. Figure 5-5 shows the deformed link at 1.15% drift during Cycle 13, corresponding to a link rotation of 0.066 rads. At this stage there was no evidence of any flange, web, or lateral buckling of the link. A slight curl of the link stiffeners, where the stiffener sections above and below the flanges rotated with respect to stiffener sections on the webs, was observed during Cycle 13 at $3\delta_y$ and became more pronounced during the final cycle at this displacement (Cycle 15). This phenomena is shown in figure 5-6. Also evident in figure 5-6 is the flaking of whitewash off the bottom flange of the link, near the link ends. This flaking started at the end of the cycles at $2\delta_y$ and was also observed on the top flange. The maximum link rotation during the cycles at $3\delta_y$ was 0.067 rads or about 5 times the link rotation at yield.

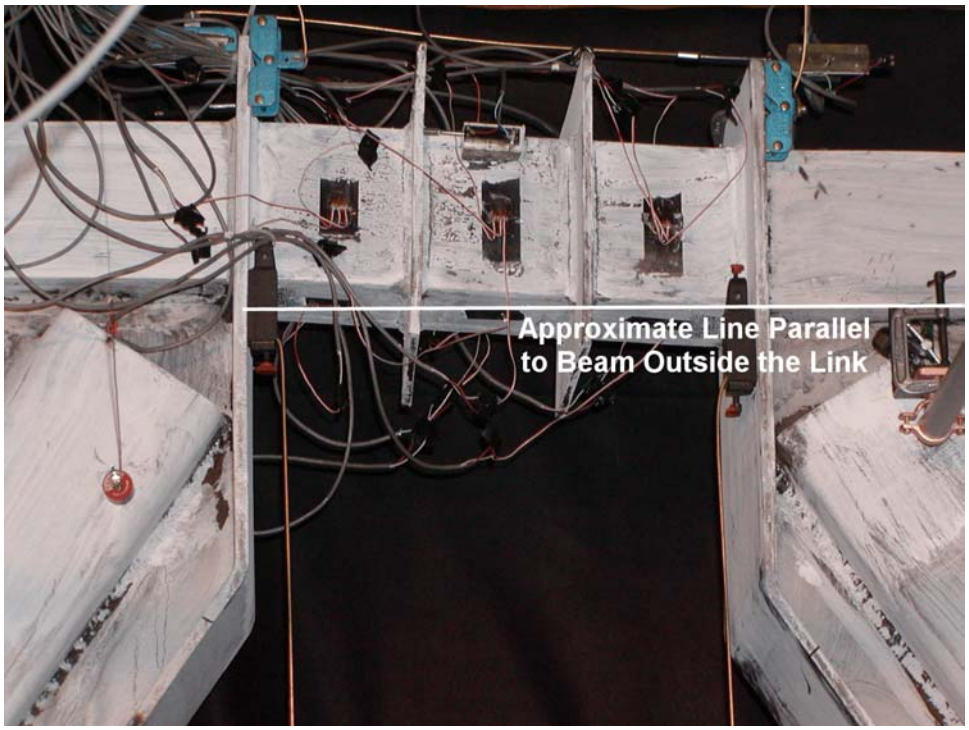

FIGURE 5-5 Deformed Link at $3\delta_y$, 1.15% Drift, 0.066 rads Rotation, Cycle 13

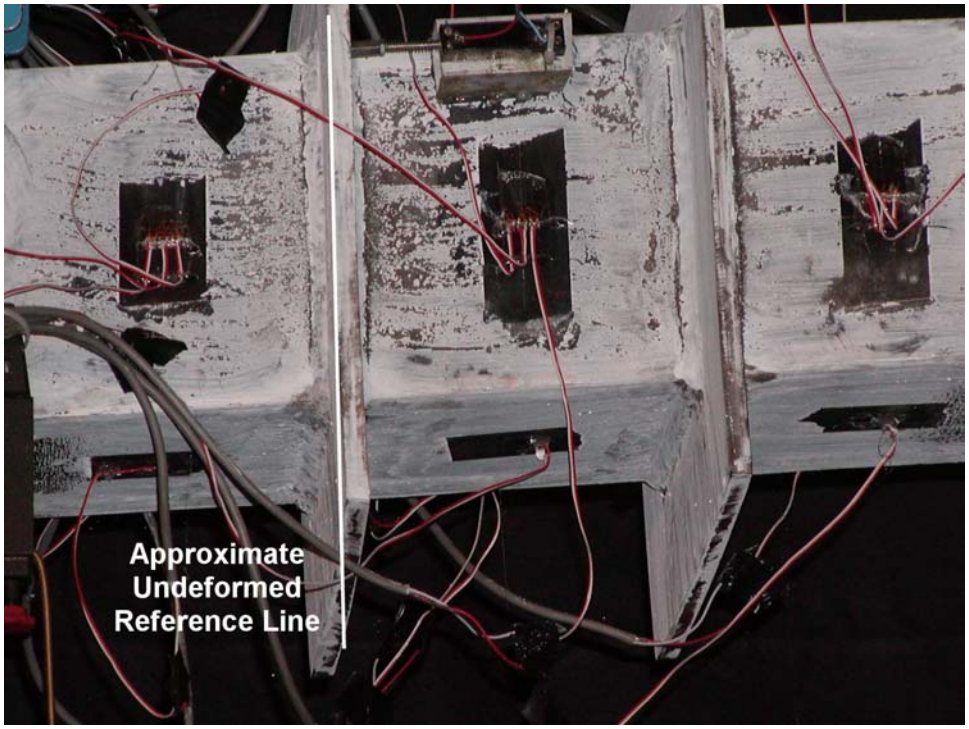

FIGURE 5-6 Curl of Link Stiffeners at $-3\delta_y$, -1.15% Drift, -0.067 rads Rotation, Cycle 15

As specified by ATC-24, only two cycles were performed at $4\delta_y$, or 1.52% drift. During these cycles the maximum end moment for the link was determined to be 161 kN-m (1423 kip-in) or 102% of M_p. It is important to note that the link was subjected to an end moment slightly larger than M_p and a shear force of 1.45 times V_p, or 700 kN (158 kips) during these cycles, indicating that there may be negligible shear-moment interaction in this hybrid link with a hollow rectangular cross-section. The link rotation of 0.096 rads (plastic rotation of 0.083 and elastic rotation of 0.013) for these cycles exceeded the maximum link plastic rotation of 0.08 rads allowed by the AISC seismic provisions (AISC, 1997). The deformed link at a total rotation of 0.096 rads during Cycle 17 is shown in figure 5-7. An increase in the amplitude of the stiffener curling noted above was evident during these cycles. Figure 5-8 shows the deformation of the left link stiffener at a link rotation of 0.096 rads during Cycle 17.

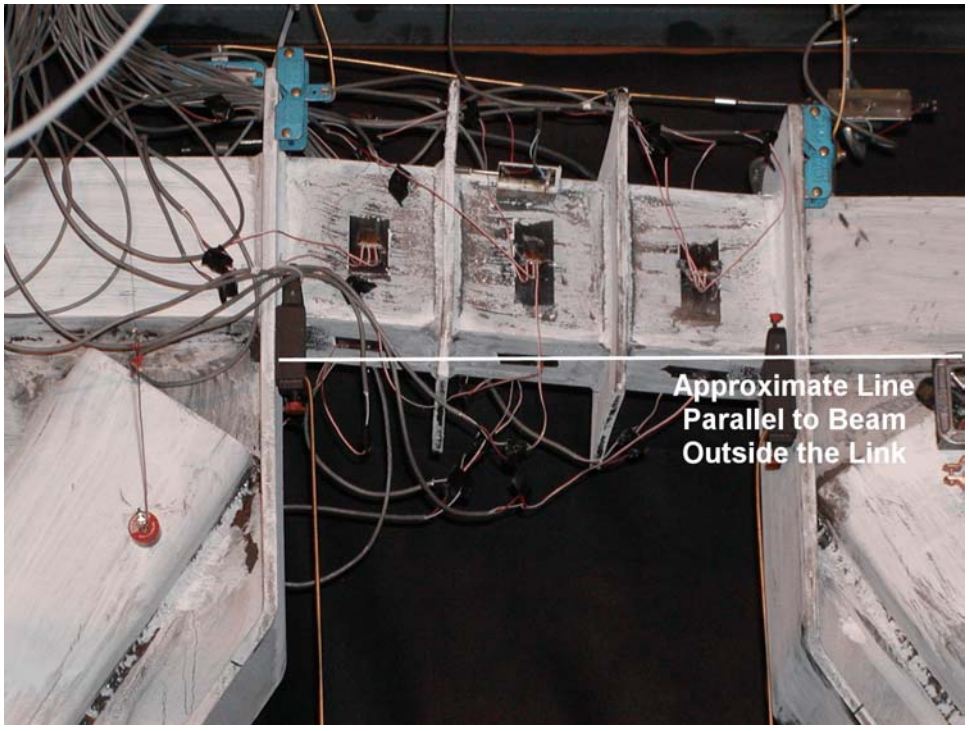

FIGURE 5-7 Deformed Link at $4\delta_y$, 1.52% Drift, 0.096 rads Rotation, Cycle 17

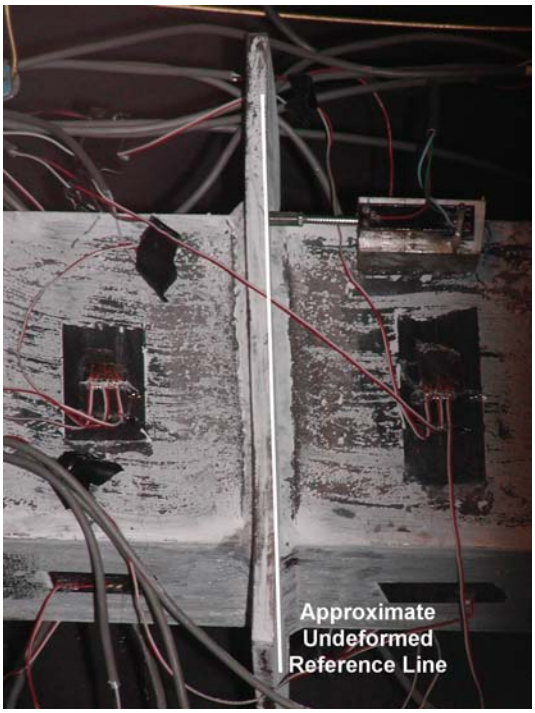

FIGURE 5-8 Curl of Link Stiffener at $4\delta_y$, 1.52% Drift, 0.096 rads Rotation, Cycle 17

The final full cycles of loading were at $5\delta_y$, or 1.92% drift, and corresponded to link rotations of 0.123 rads (0.11 rads plastic rotation and 0.013 rads elastic rotation), which is over 1.3 times the AISC target rotation 0.08 rads. The maximum end moment reached during these cycles was 168 kN-m (1482 kip-in), which corresponds to 106% of M_p. Again, this coincided with a link shear 730 kN or 1.48 times V_p. Figures 5-9, and 5-10 show the link deformation at +1.92% drift and -1.92% drift of Cycle 19 respectively and figure 5-11 shows the curl of the link stiffeners at the latter point.

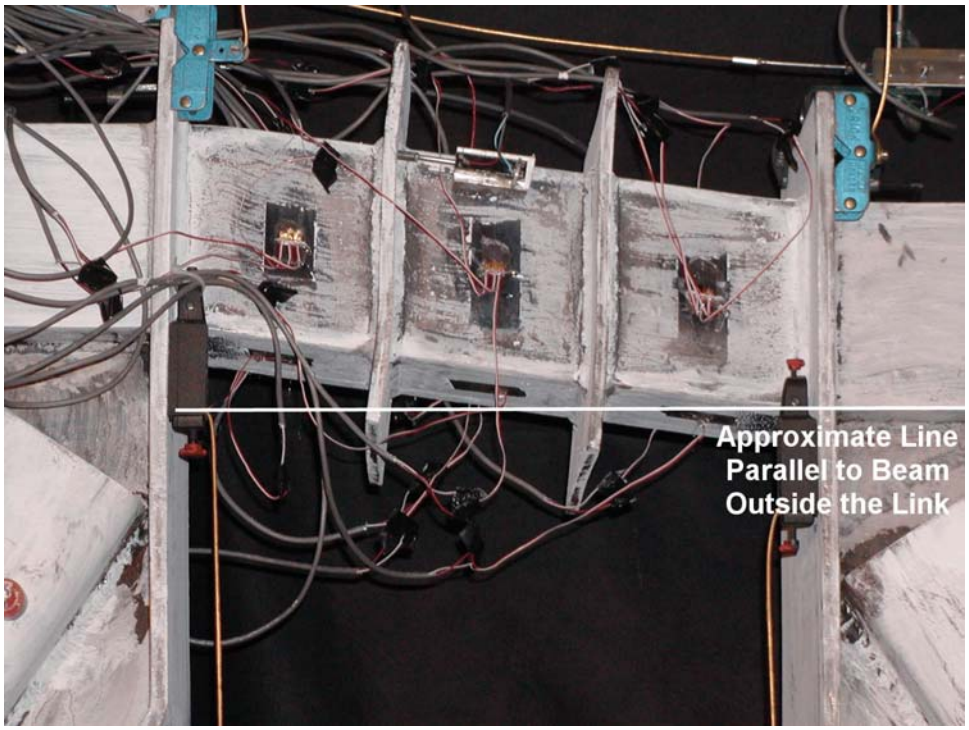

FIGURE 5-9 Deformed Link at $5\delta_y$, 1.92% Drift, 0.123 rads Rotation, Cycle 19

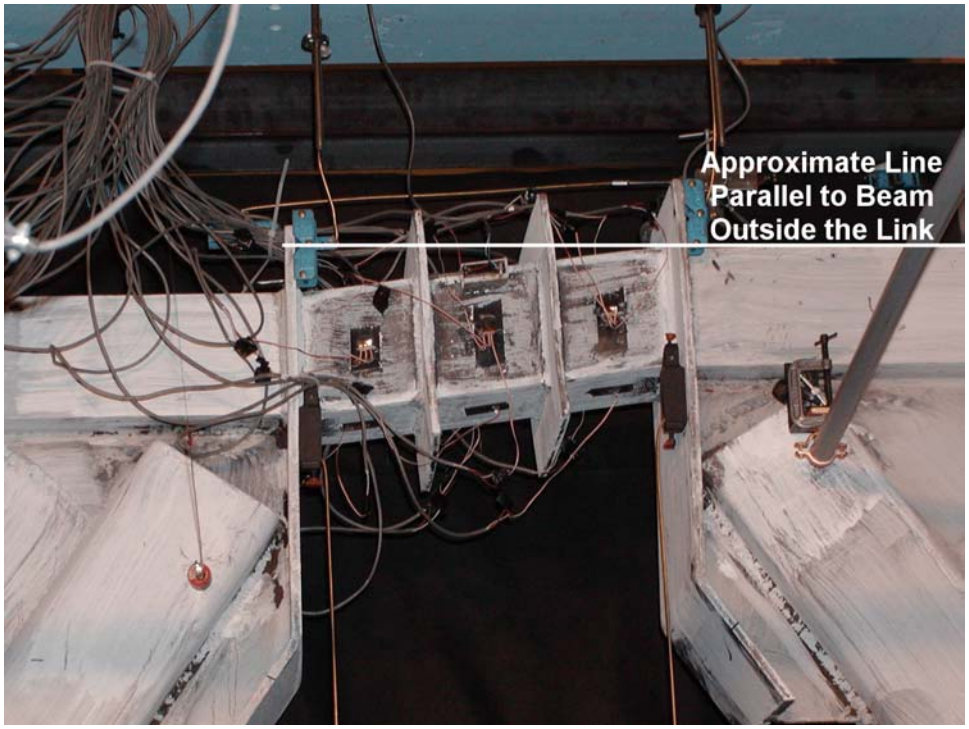

FIGURE 5-10 Deformed Link at $-5\delta_y$, -1.92% Drift, -0.123 rads Rotation, Cycle 19

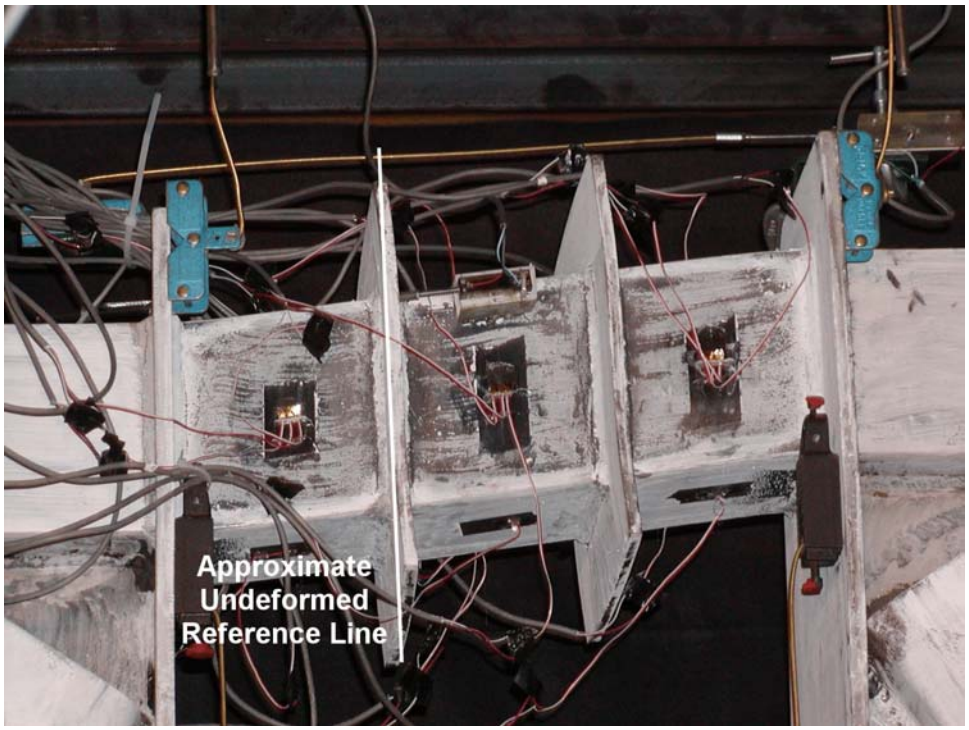

FIGURE 5-11 Curl of Link Stiffeners at -5δ_y, -1.92% Drift, -0.123 rads Rotation, Cycle 19

FIGURE 5-12 Deformed Link at 6δ_y, 2.3% Drift, 0.151 rads Rotation, Cycle 20

Fracture occurred during loading into the negative drift portion of Cycle 20. During the positive drift region of Cycle 20 the maximum link end moment was 170 kN-m (1500 kip-in) or 108% of M_p, and was accompanied by a link shear of 742 kN (167 kip) or 1.5 times V_p. Figure 5-12 shows the link at 2.3% drift, corresponding to a rotation of 0.151 rads. Figure 5-13 shows the curl of the stiffeners at the same point. Upon unloading from the maximum positive drift and reloading into the negative drift region the bottom flange of the north end of the link fractured near the heat-affected-zone adjacent to the weld of the stiffener for the brace-to-beam connection as shown in figure 5-14. This occurred at approximately -1.2% drift. At about -1.4% drift the top flange at the south end of the link fractured, again near the heat-affected-zone of the weld for the stiffener at the brace-to-beam connection as shown in figure 5-15.

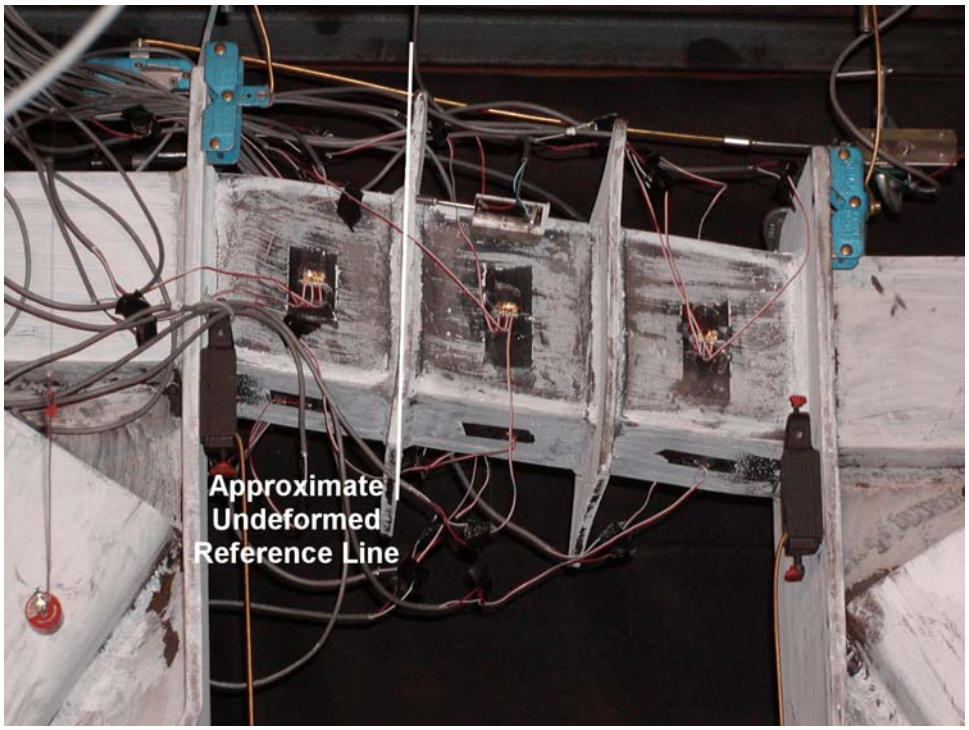

FIGURE 5-13 Deformed Link and Stiffener Curl at $6\delta_y$, 2.3% Drift, 0.151 rads Rotation, Cycle 20

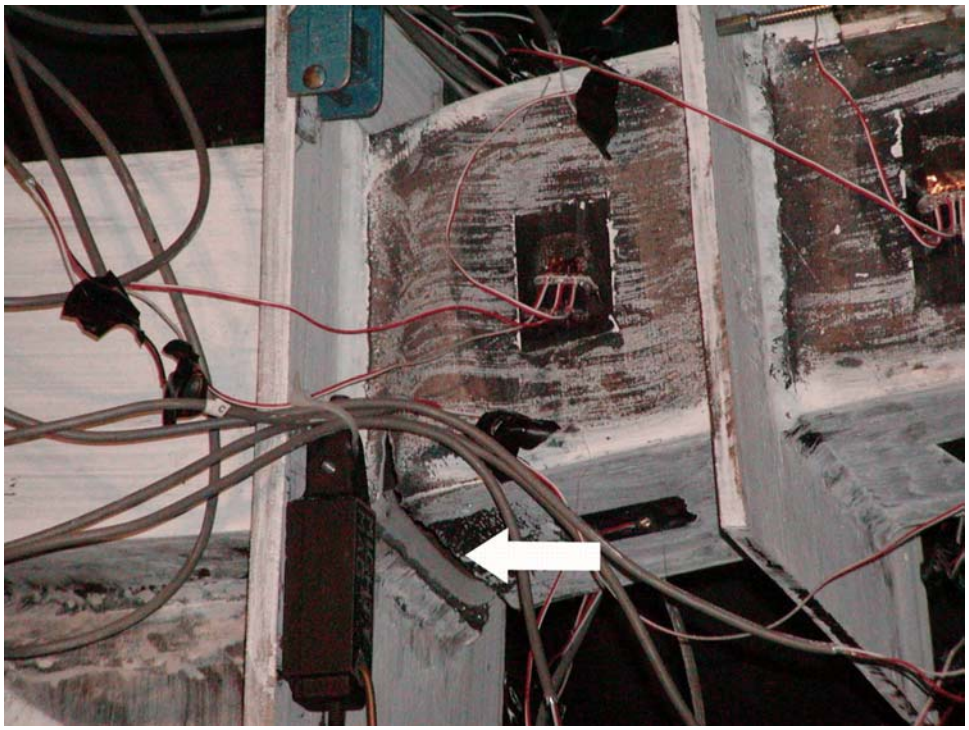

FIGURE 5-14 Fracture of Bottom Flange at North End of Link at -1.2%Drift of Cycle 20

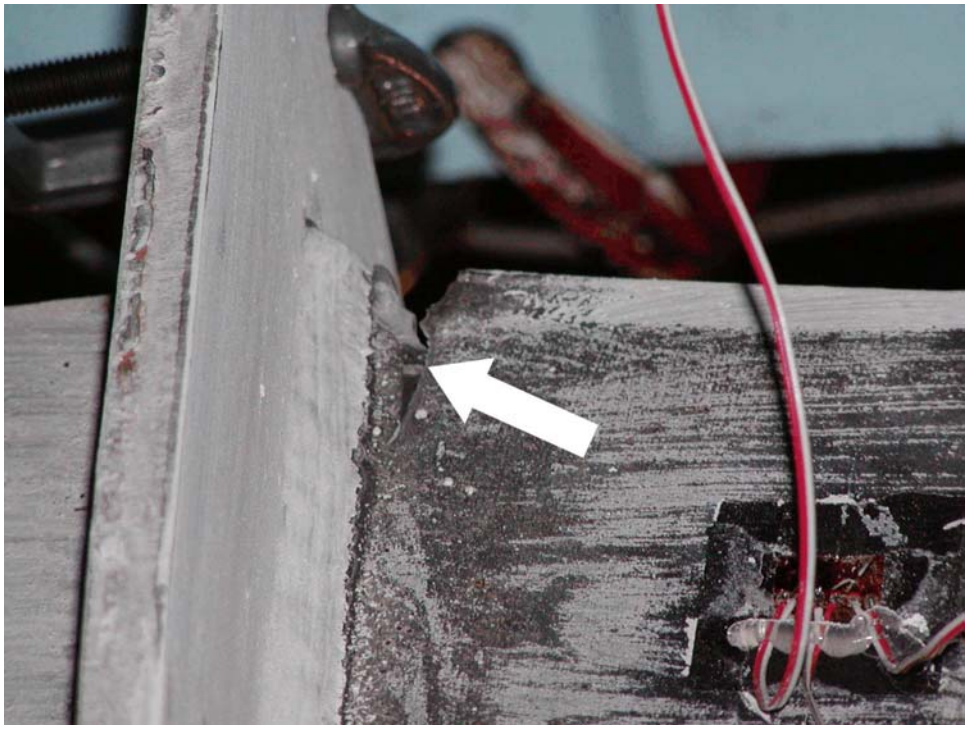

FIGURE 5-15 Fracture of Top Flange at South End of Link at -1.4% Drift of Cycle 20

5.4 Examination and Basic Fractography of Failure Surface

Following the completion of testing the link was removed, taking care to avoid damaging the fracture surface. Then the failure surface was exposed using a bandsaw to cut away the portions of the link web that were still intact. Figures 5-16, 5-17, and 5-18 show the fracture surface on the link side and figures 5-19, 5-20, and 5-21 show the fracture surface on the brace-to-beam connection side (note that in both sets of figures, the link has been turned upside down from its position during testing and it is the first fracture surface that is shown, (i.e., the fracture that occurred in the bottom flange on the North end of the link). Fractographic analysis of these surfaces was performed using a magnifying glass and light microscope with 30x magnification by Mark Lukowski (a technician and metallurgist in the Department of Mechanical and Aerospace Engineering at the University at Buffalo) and verified by Dr. Robert C. Wetherhold (a faculty of the same department) following the procedures outlined in Volume 12 of the American Society of Materials (ASM) Handbook (ASM International, 1987). It was judged that the fracture initiated in the heat affected zone adjacent to the stiffener weld, with cracking from the pitted areas identified by arrows in figures 5-22 and 5-23 propagating as fatigue cracks for approximately six load reversals (i.e., three cycles), as shown by the fatigue striations pointed out in figure 5-24 (indicating that low-cycle fatigue of the heat affected zone triggered the cracking). However, there was no drop in strength during these cycles. Finally, the through thickness fracture occurred as a fast-fracture, identified by the coarse surface visible as the majority of the fracture surface in all the previously mentioned figures. There was no evidence of fracture starting from the full-penetration groove welds used to assemble the rectangular link cross-section. Changes in the link details to avoid such a fracture could be a topic requiring further research.

FIGURE 5-16 Fracture Surface on Link Side-1

FIGURE 5-17 Fracture Surface on Link Side-2

FIGURE 5-18 Fracture Surface on Link Side-3

FIGURE 5-19 Fracture Surface on Brace-to-Beam Connection Side-1

FIGURE 5-20 Fracture Surface on Brace-to-Beam Connection Side-2

FIGURE 5-21 Fracture Surface on Brace-to-Beam Connection Side-3

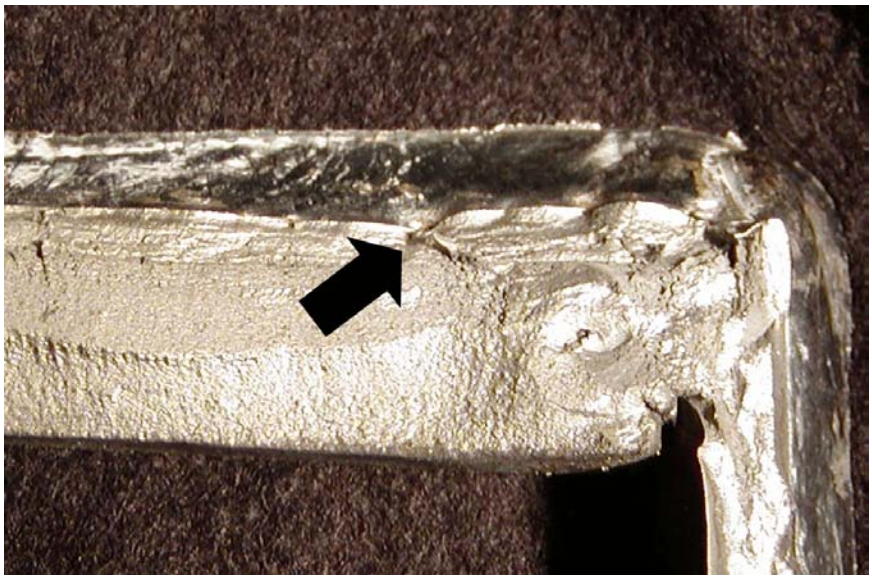

FIGURE 5-22 Pitted Region and Likely Location of Crack Initiation

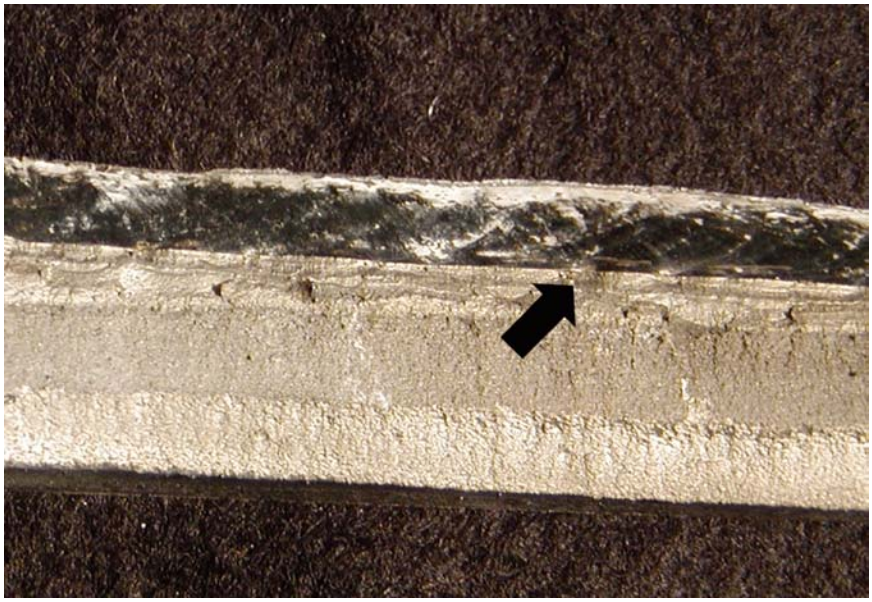

FIGURE 5-23 Second Pitted Region and Another Likely Location of Crack Initiation

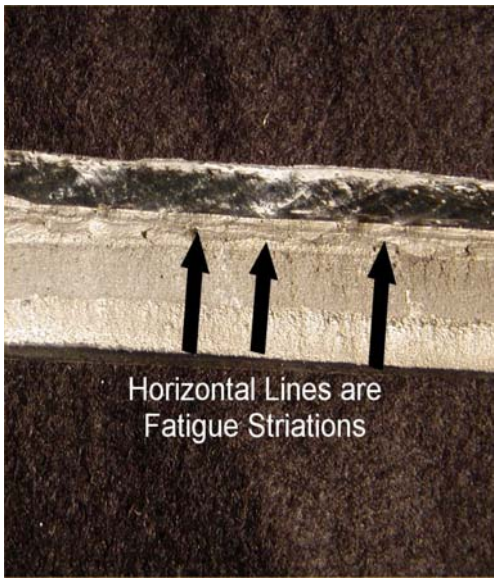

FIGURE 5-24 Fatigue Striations

SECTION 6

EXPERIMENTAL RESULTS AND ANALYSIS

6.1 General

This section quantitatively describes the results of proof-of-concept testing of an EBF utilizing a hybrid rectangular link. First, the general specimen behavior is discussed with emphasis on behavior of the link. Then, experimentally obtained values for link plastic shear, plastic moment, balanced link length, and link overstrength are compared with those calculated from Section 3 equations. Next, the effects of complying with the web and flange compactness limits specified by AISC for conventional EBFs, as well as the maximum stiffener spacing derived in Section 3, are examined. Finally, cumulative energy dissipation of the link is investigated and possible methods for estimating and improving the fracture life of the link flange are discussed.

6.2 General Specimen Behavior

6.2.1 Frame Hysteresis

Figure 6-1 shows the full and stable base shear vs. frame drift hysteresis obtained for the specimen, similar to what is expected for an EBF. The initial stiffness of the specimen was determined to be 80 kN/mm (457 kip/in) from the elastic cycles of figure 6-1. The yield drift was identified as 0.37% and corresponded to a base shear of 668 kN (150 kip), while the maximum base shear and drift were 1009 kN (227 kip) and 2.3%, respectively.

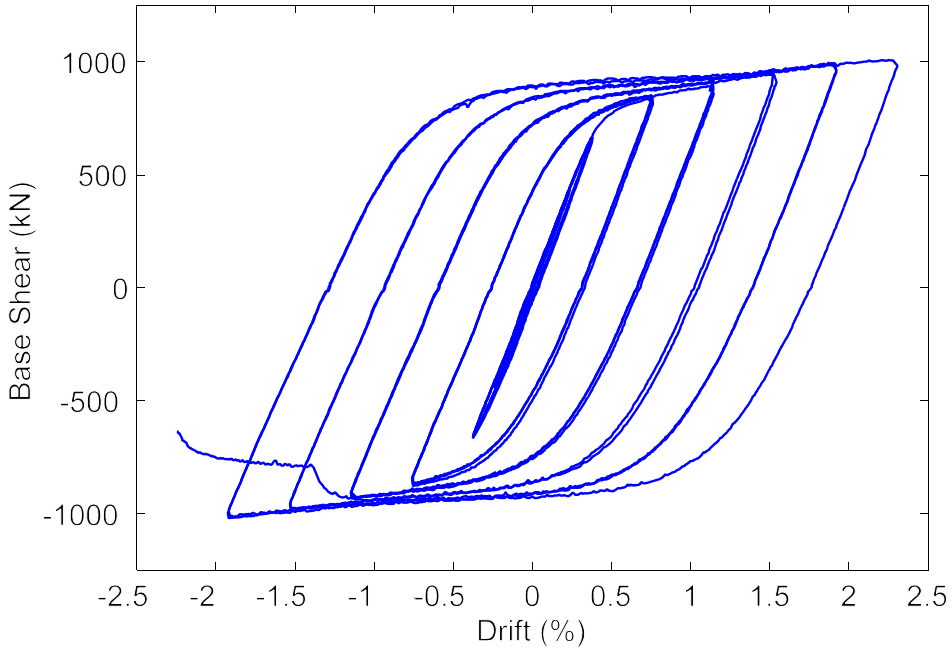

FIGURE 6-1 Base Shear vs. Frame Drift

6.2.2 Link Hysteresis

Figure 6-2 shows the corresponding link shear force vs. link rotation hysteresis. The link shear and rotation at yield were 490 kN (110 kip) and 0.014 radians, while the maximum link shear and rotation were 742 kN (167 kip) and 0.151 radians, respectively. Considering projections of the elastic and inelastic slopes of figure 6-2, the plastic shear force was approximately 520 kN. The link shear force at a link rotation of 0.08 radians (the current limit for EBFs in buildings), was 689 kN (155 kip). Figure 6-3 shows the end moment vs. rotation, where the end moment is calculated from the link shear using $M_L = V_L e/2$. The end moments at specimen yield, development of V_p, and 0.08 radians of link rotation, were 112 kN-m (991 kip-in), 119 kN-m, and 158 kN-m (1400 kip-in), respectively, while the maximum end moment reached during the test was 170 kN-m (1504 kip-in).

As discussed in Section 5, the failure mode of the link was fracture of the bottom flange. Factors that likely contributed to this are the large plastic strain demands at that location and the high degree of constraint due to the presence of gussets, stiffeners, and welds used for the link-to-brace connection. Methods to estimate and extend the low cycle fatigue life of shear of shear links subject to this failure mode will be considered briefly in later sections.

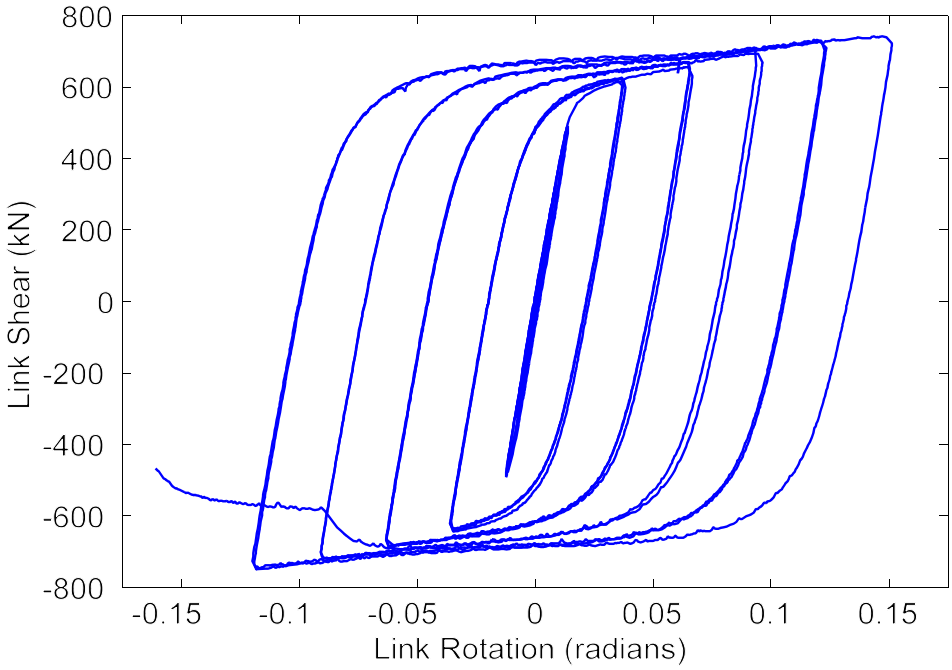

FIGURE 6-2 Link Shear vs. Link Rotation

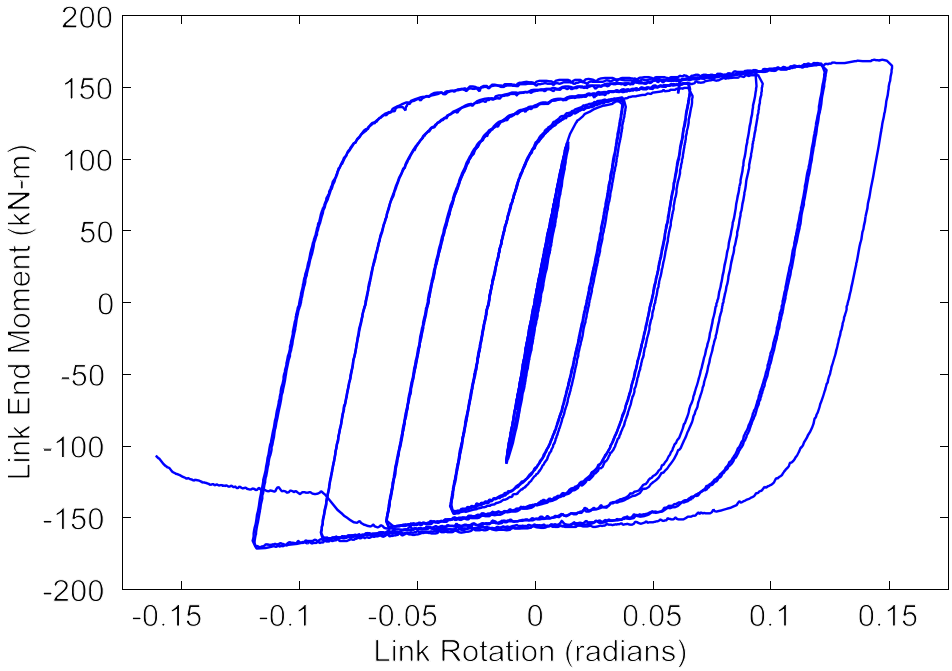

FIGURE 6-3 Link End Moment vs. Link Rotation

6.2.3 Behavior of Framing Outside the Link

The in plane moments and axial forces in the braces and beam segments outside the link were calculated at the strain gauge locations and then projected to the member endpoints. It was found that those members remained elastic. Maximum axial forces reached in the braces and beam segments outside the link were approximately 45% and 50% of the respective yield axial forces. The largest moments (occurring at the member ends nearest the link) were 50% and 45% of the respective members yield moment.

Shown in figures 6-4 and 6-5 are the out-of-plane moments of the braces and beam-outside-the-link projected to the working point of the connection with the link and normalized by the calculated link plastic moment. As shown, the largest out-of-plane moment is on the order of 2.5% of the link plastic moment, which can be taken out through connections to the columns without the need for lateral bracing. These moments may also exist in this case because of minor fabrication and assembly misalignments that were present at the start of testing. Therefore, results confirm that in the absence of lateral torsional buckling of the link beam, the out-of-plane moments of the braces need not be considered in the design of EBF utilizing hybrid rectangular cross-sections.

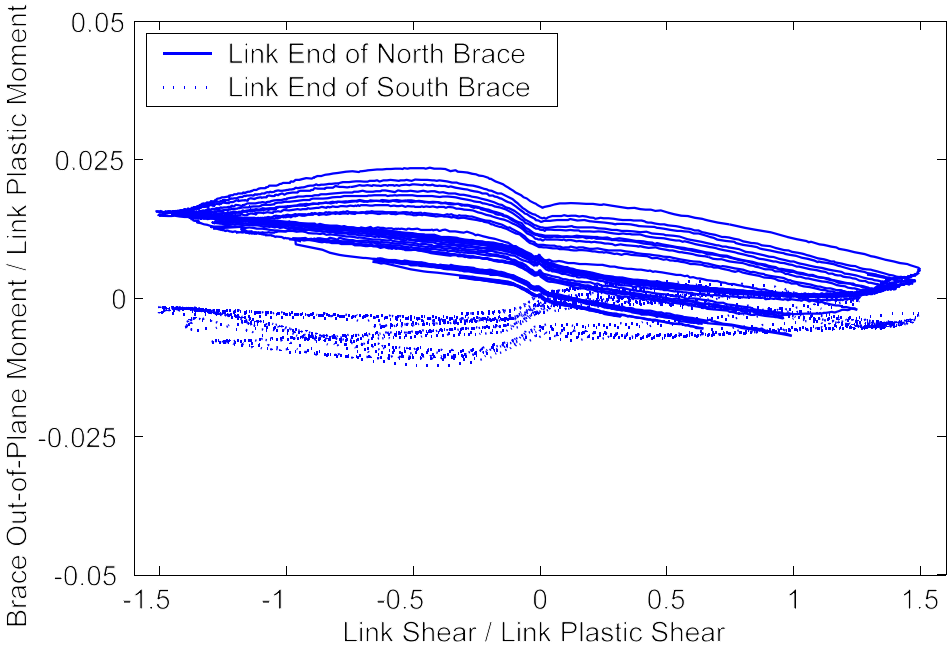

FIGURE 6-4 Normalized Out-of-Plane Brace Moments Projected to the Link Centerline vs. Normalized Link Shear

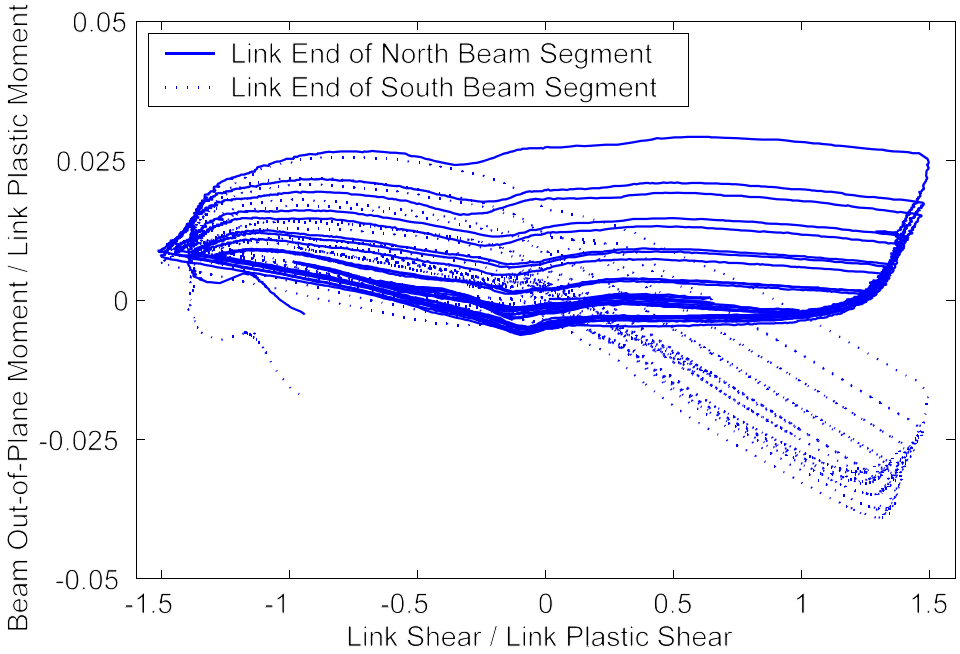

FIGURE 6-5 Normalized Out-of-Plane Beam Moments Projected to the Link End Point vs. Normalized Link Shear

6.3 Comparison with Anticipated Behavior

6.3.1 Strength

Table 6-1 gives values from calculations using the equations of Section 3 and actual material properties (both yield and ultimate stresses) for link plastic shear, maximum link shear, and reduced and unreduced plastic moment. The table also includes the ratios of calculated link shear to the experimentally obtained values for the link plastic shear, V_{pe} (520 kN), the link shear at 0.08 radians of rotation, V_{8e} (689 kN), and the maximum link shear, V_{maxe} (742 kN). Additionally, the ratios of calculated plastic moments (reduced and unreduced) to the moment at development of V_{pe}, M_{Vpe} (119 kN-m), the moment at 0.08 radians of rotation, M_{8e} (158 kN-m), and the maximum moment M_{maxe} (170 kN-m) are given in Table 6-1. Ratios that are less than 1.0 indicate that the equation is conservative for link design and unconservative for capacity design of surrounding framing (i.e., it under predicts the shear or moment), while ratios greater than 1.0 indicate the equation is unconservative for link design and conservative for capacity design (i.e., it over predicts the shear or moment). Recall that the yield and ultimate stresses of the web material, F_{yw} and F_{uw}, were found to be 448 MPa (65 ksi) and 510 MPa (74 ksi) respectively, and that the yield and ultimate stresses

of the flange material, F_{yf} and F_{uf}, were found to be 393 MPa (57 ksi) and 490 MPa (71 ksi) respectively.

TABLE 6-1 Comparison of Calculated and Observed Link Shear Forces and Moments

	For F_{yw} and F_{yf}				For F_{uw} and F_{uf}			
V_p (Eq. #)	V_p Value (kN)	V_p Value / V_{pe}	V_p Value / V_{8e}	V_p Value / V_{maxe}	V_p Value (kN)	V_p Value / V_{pe}	V_p Value / V_{8e}	V_p Value / V_{maxe}
V_p (3-3)	495	0.96	0.72	0.67	564.2	1.09	0.82	0.76
V_p (3-61)	626.0	1.20	0.91	0.84	712.7	1.37	1.03	0.96
V_p (3-62)	547.2	1.05	0.79	0.73	628.5	1.21	0.91	0.85
V_p (3-75)	667.8	1.28	0.97	0.90	760.2	1.46	1.10	1.02
M_p (Eq. #)	M_p Value (kN-m)	M_p Value / M_{Vpe}	M_p Value / M_{8e}	M_p Value / M_{maxe}	M_p Value (kN-m)	M_p Value / M_{Vpe}	M_p Value / M_{8e}	M_p Value / M_{maxe}
M_{pr} (3-2)	131.7	1.11	0.83	0.78	162.4	1.36	1.03	0.96
M_p (3-1)	157.6	1.32	1.00	0.93	191.9	1.61	1.21	1.13

From table 6-1, which examines the results of the single test to date of a hybrid rectangular link, the plastic shear capacity is adequately predicted by (3-3), to be 0.96 of the experimentally observed link plastic shear force. In terms of predicting the overstrength of a hybrid rectangular link, i.e. the maximum shear strength, table 6-1 indicates that (3-75), the panel zone equation for moment connections adapted to EBF links, is the most accurate

and is somewhat conservative for use in capacity design when F_{uw} is used and slightly unconservative when F_{yw} is used..

It is evident that both M_{pr} and M_p as calculated by (3-2) and (3-1), respectively, were exceeded during the test. Strain hardening seems the likely cause since coupon test results in (3-1) and (3-2). This suggests that shear-moment interaction can be neglected and a rectangular interaction curve can be used to adequately represent the shear and moment interaction in shear links subjected to large inelastic deformations. In other words, as Kasai and Popov found for WF shear links, both V_p and M_p can simultaneously develop in hybrid rectangular shear links, provided for which buckling failure modes are not present.

6.3.2 Link Length

The normalized link length, $\rho = e/(M_p/V_p)$, can also be examined in terms of experimental versus calculated values. This link was designed to have a normalized link length of 1.30 when the specified material yield stress of 345 MPa (50 ksi) is used for both the webs and flanges. Using the actual material properties, the normalized link length is calculated to be 1.43. The normalized link length when using the experimentally determined value of V_{pe} and the calculated value of M_p from (3-1) with actual material properties, becomes 1.51. All those values indicate that the inelastic response of the link is expected to be dominated by shear yielding, as the normalized lengths are less than 1.6 (AISC, 2002). However, it was experimentally observed that the link end moment exceeded both M_{pr} and M_p (calculated using actual material properties), indicating that while shear dominated, some of the inelastic response of the link was due to flexural yielding (some of which is expected as strain hardening occurs as a result of shear yielding). Note that when a rectangular interaction curve can be assumed, as discussed in Section 6.3.1, the maximum link length to obtain a shear link is $2M_p/V_p$. Kasai and Popov derived the 1.6 factor that appears in the AISC Seismic Provisions by assuming a maximum link shear of $1.5V_p$ and a maximum moment of $1.2M_p$. Here the maximum link shear was $1.5V_p$ (with V_p from [3-3]) and the maximum moment was $1.1M_p$ (with M_p from [3-1]).

6.3.3 Web and Flange Compactness

As explained in Section 5, the failure mode of the proof-of-concept EBF with a hybrid rectangular link was fracture of the bottom flange at the north end of the link during the negative excursion of Cycle 20 without visible evidence of local buckling. The lack of local buckling indicates this failure mode resulted from localized strain demand and a high degree of constraint, and may not depend on web or flange compactness. In that sense, and noting that a rotation of 0.15 radians was reached prior to failure, the values for web and flange compactness ratios used for the case seem to be adequate. Table 6-2 shows the link web and flange compactness ratios for the specimen, the limits for these from the AISC seismic provisions for rectangular HSS shapes in axial or flexural compression for both the specified (345 MPa) and actual yield stresses, and the limits for flange compactness derived in Section 3 and given in (3-38) for both the specified and actual flange yield stresses. Note that the AISC limits are based on test results of braces in concentrically braced frames and not rectangular beams subjected to large simultaneous plastic shear and flexure.

TABLE 6-2 Web and Flange Compactness Ratios and Limits

	$(d - 2t_f) / t_w$	$(b - 2t_w) / t_f$	AISC Seismic Limits		Flange Limits (3-38)	
			Specified F_y	Actual F_y	Specified F_y	Actual F_y
Web	15.2	-	15.6	13.6	-	-
Flange	-	8.6	15.6	14.6	24.6	23.0

As shown by table 6-2, the AISC limits were satisfied for the specified material properties for both the flanges and the webs, however, using the actual material properties, the web compactness limit was exceeded by 12%. Nonetheless, the specimen showed no signs of web buckling, even when deformed past the rotation limit specified in the AISC seismic provisions. It may be possible to relax the limit on web compactness, especially if there is no axial load on the link, since the webs in a shear link are subject to shear rather than compression, but this would have to be substantiated by further research, considering simultaneously the contribution of web stiffeners as they are also added to serve the same purpose.

6.3.4 Stiffener Spacing and the Web Compactness Limit

In Section 3, a proposed design equation for maximum web stiffener spacing was derived. The design equation (3-49) represents an approximation of the theoretical equation (3-48). As mentioned in Section 3 and shown in the Appendix, the average factor of safety between the proposed design equation and theoretical equation was chosen to be similar to the average factor of safety between the design equation in the AISC seismic provisions and the theoretical equation derived by Kasai and Popov (1986a) for WF links. In both the theoretical and code equations (for WF and rectangular cross-sections), as the web compactness, β in this case, goes to zero the maximum stiffener spacing goes to infinity as shown in figure 6-6. Note that the generation of the theoretical curves of figure 6-6 included the transition from equations derived for $\alpha \leq 1.0$ to equations derived for $\alpha \geq 1.0$, while as shown in the Appendix, the code equations are still valid for $\alpha \geq 1.0$ without modification.

Note the typical web compactness limit for a WF EBF link with zero axial load and a 345 MPa yield stress is 76, for which stiffeners are required by both the code equation and the theoretical equation. However, for rectangular cross-section links, the theoretical equation indicates that at a web compactness corresponding to the 15.6 limit noted above, no stiffeners are required, while the proposed code equation would require stiffeners at a spacing of approximately the web depth.

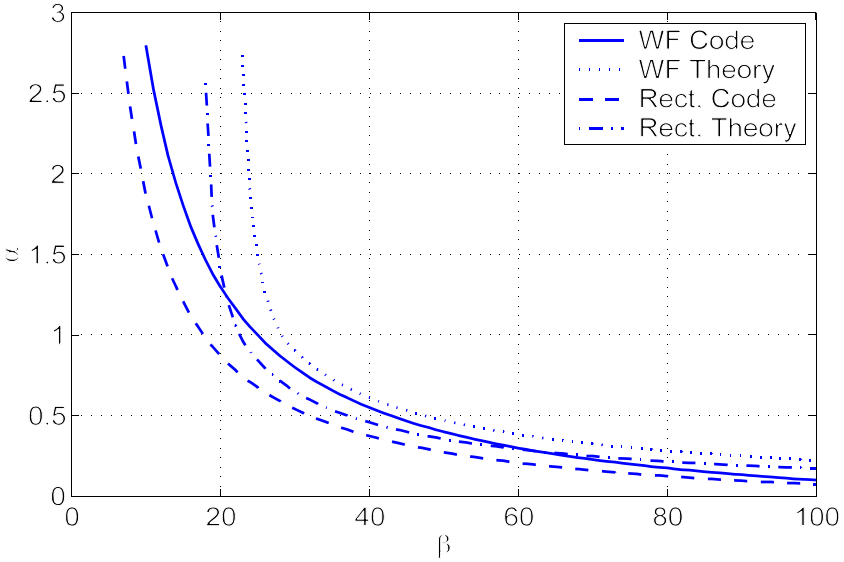

FIGURE 6-6 Comparison of Theoretical and Code Equations for Maximum Stiffener Spacing for WF and Rectangular Links

It appears that while the proposed code equation for links with rectangular cross-sections shows generally the same conservatism as that for WF links over a web compactness range of 25 to 85, it becomes progressively more conservative for web compactness of less than 25. To demonstrate this, consider (3-48) rewritten for panel aspect ratios of greater than one as:

$$\alpha = \sqrt{\frac{4}{\left(\frac{\gamma_u \beta^2}{4.35}\right) - 5.34}} \tag{6-1}$$

One can show that for $\beta \leq 17$, α is undefined. Note that β, the web compactness, and α, the panel aspect ratio (stiffener spacing divided by clear web depth), have been taken as as d/t_w and a/d, respectively in figure 6-6. The AISC limit for web compactness for $F_{yw} = 345$ MPa (50 ksi) is 15.6. Therefore, the theoretical equation implies that no stiffeners are required, while the proposed code equation requires stiffeners at a spacing of approximately $18t_w$. Since the derivation of both the theoretical and proposed code equations for stiffener spacing in links of rectangular cross-section are based on preventing web buckling, satisfying both the web compactness limit and the stiffener spacing requirement appears to be redundant. Therefore, further investigation to ascertain whether both of these must be satisfied is warranted.

6.4 Energy Dissipation

As shown in figure 6-7, the cumulative energy input to the system, taken as the sum over the entire test of energy dissipated by each hysteretic loop (i.e. summing the areas of the actuator force vs. actuator displacement hysteresis curves), was for the most part dissipated through inelastic action of the link. The cumulative link energy dissipation has been calculated as the sum over the duration of testing of the area under the link shear vs. link end relative deformation hysteresis, the latter of which is simply the link rotation times the link length. Differences between the input energy and the energy dissipated by the link are due to several factors, including the friction in the system, which stems from the clevises and bolted connections, assumptions used to find the link shear force and rotation, and measurement error. The total energy dissipated by the link was 770 kN-m. Figure 6-8 shows the energy

dissipated by the link per cycle. As expected, the energy dissipated per cycle increases with increasing deformation amplitude. Furthermore, there was no strength degradation, or degradation in the link's ability to dissipate energy in subsequent cycles at a constant deformation amplitude (i.e., the energy dissipated during the second cycle at $2\delta_y$ is essentially the same as the first cycle at $2\delta_y$).

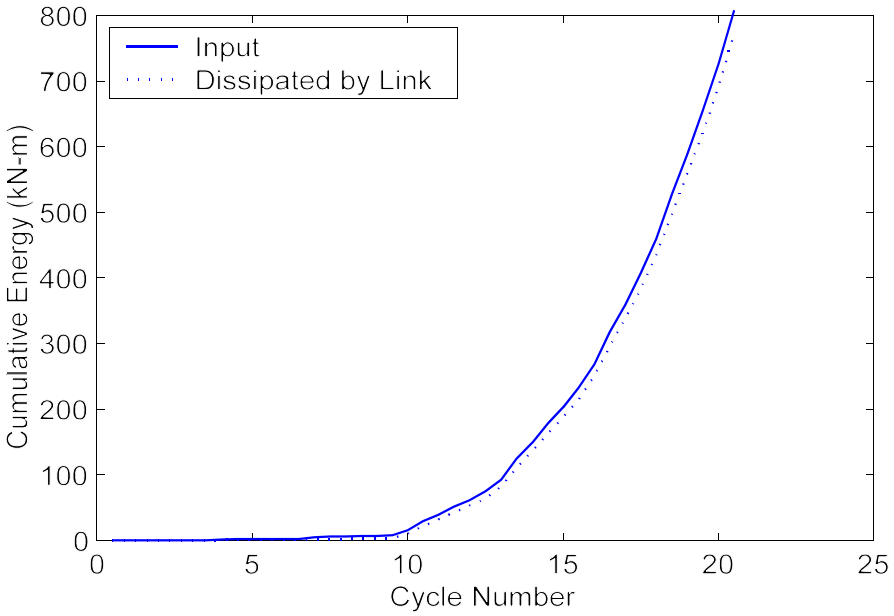

FIGURE 6-7 Cumulative Input Energy and Energy Dissipated by the Link vs. Cycle Number

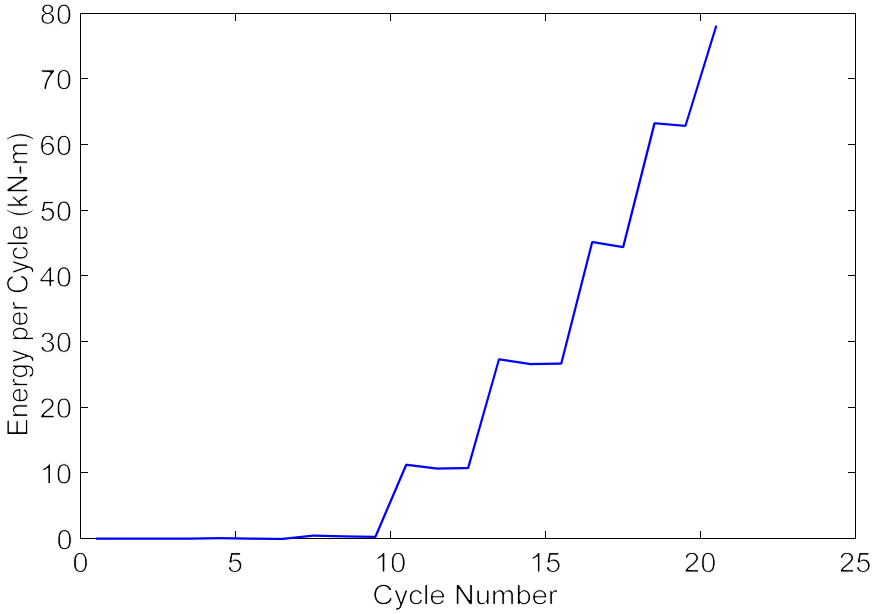

FIGURE 6-8 Energy Dissipated by the Link per Cycle

6.5 Summary

This section quantitatively described the results of proof-of-concept testing of an EBF utilizing a link with a hybrid rectangular cross-section. Specimen hysteretic behavior was reported and comparisons were made with key Section 3 equations. It was found that (3-3) adequately predicted the plastic shear strength of the link and (3-75) adequately predicted the link overstrength. It was shown that this link behaved dominantly as a shear link in that plastic shear developed prior to the reduced plastic moment. However, both the reduced and total plastic moments were exceeded in the late stages of testing. It was also shown that the current seismic AISC provisions would have limited the link rotation to 0.08 radians, whereas the actual specimen performed adequately up to 0.15 radians. All framing members outside of the link remained elastic and out-of-plane moments at the link ends were found to be insignificant. The web and flange compactness ratios used were found to provide the necessary resistance to buckling, although it was shown that the stiffener spacing limits and web compactness limits may be redundant in this particular case. The energy dissipated by the link corresponded to the energy input to the system. Some methods for predicting the low-cycle fatigue life of a link subject to the failure mode observed here (flange fracture at the connection with the eccentric brace) were suggested for possible use in collaboration with finite element analysis results in future research.

SECTION 7
CONCLUSIONS AND RECOMMENDATIONS FOR FURTHER RESEARCH

7.1 Conclusions

This report has identified, categorized, and qualitatively compared several options for the seismic retrofit of truss braced steel bridge piers. Through these comparisons, strategies which were promising in terms of performance, but lacked fundamental research in areas necessary for their implementation were identified as follows:

- Laterally stable links for eccentrically braced frames.
- Design of supplemental retrofit systems for protection of existing elements.

This report presented an initial theoretical and experimental investigation on the first topic listed above, utilizing links with hybrid rectangular cross-sections as a proposed solution to achieve the desired performance. Equations for plastic shear, plastic moment, link length, stiffener spacing, minimum flange compactness, and link overstrength were derived in manners consistent with the development of the existing codified design equations for WF links in EBFs. A proof-of-concept test specimen was designed and tested under cyclic, quasi-static conditions in the SEESL at UB. The proof-of-concept specimen met and exceeded performance objectives in terms of both link rotation and ductility. It reached a link rotation of 0.15 radians and a ductility of 6 in terms of frame drift (in terms of link rotation the ductility reached was over 10). No signs of lateral torsional buckling of the link and link beam were observed. The specimen eventually failed with a fracture of the bottom link flange, adjacent to the connection with the north eccentric brace. From fractographic

analysis with a light microscope, the failure was found to be due to a combination of overload and low cycle fatigue.

Comparison of the results of this single test specimen with the equations derived for design showed reasonable agreement in terms of strength calculations. It was then determined that the stiffener spacing equation derived here and web compactness limits from the AISC seismic provisions for webs of HSS sections are likely redundant (i.e. both may not need to be satisfied). Finally, methods for calculating and enhancing the low cycle fatigue life of EBF links subject to flange fracture were briefly described, as this failure mode was also observed in some past tests on EBF with WF links.

7.2 Recommendations for Further Research

7.2.1 Design Considerations for Supplemental Systems

As mentioned in Section 2 of this report, supplemental retrofit systems may be effective retrofit options for braced steel bridge piers. However, the effects of overturing on the performance of tall bridge piers is a subject where there is little literature available. It is clear that these taller bridge piers may have significant displacements from global overturing. Supplemental retrofit options considered in this project dissipate energy and provide ductility through the global shear deformations of the pier, and, although others are working on systems based on the global overturning (Pollino and Bruneau, 2005), the effect of overturning on the performance of shear deformation dependent elements is unknown. Therefore, a study that evaluates the effects of global overturning deformations on the performance of piers with supplemental system retrofit strategies would be beneficial. This could include comparing what is assumed when the ductility portion, R_μ, of the seismic force modification factor, R, is specified in design codes and the results of numerical simulation of several piers in terms of local (element level) ductility and global ductility. Literature searches on the effects of overturing deformations on the ductility of systems which rely on shear deformations to activate structural fuse elements have shown that there have not been previous studies on this issue.

7.2.2 Development of Laterally Stable Links for EBFs

While the single experiment performed thus far has certainly shown that links with hybrid rectangular cross-sections can perform as well as WF links in EBFs, there is still considerable development to be done. First, verification of the proposed design equations for likely ranges of parameters is necessary before this system will be considered for implementation in industry. This includes a rigorous experimental and finite element based validation of the new stiffener spacing and flange compactness limits derived for this system. Next, the link rotation limits for various link lengths need to be revisited. Since the 0.02 radian rotation limit for WF flexural links in the AISC seismic provision is partly related to lateral torsional buckling, research to develop appropriate rotation limit for shear and flexural links of rectangular cross-section would be beneficial. In all those instances, experimental results would provide data for calibration of finite element models, using ABAQUS for instance, and those models could then be used to generate other data points so that reasonable design limits can be determined.

Additionally, the limit state of flange fracture as a result of low cycle fatigue needs to be investigated, to estimate the low cycle fatigue life of links in EBFs, and develop details for EBF links to prevent or delay flange fracture due to low cycle fatigue. Development of link details to prevent or delay flange fracture due to low cycle fatigue would also require both an experimental and numerical component.

SECTION 8

REFERENCES

AISC (1980). *Manual of Steel Construction, 8th Ed*. American Institute of Steel Construction, Chicago, IL.

AISC (1997). *Specification for the Design of Hollow Structural Sections*. American Institute of Steel Construction, Chicago, IL.

AISC (1998). *Manual of Steel Construction: Load and Resistance Factor Design, 3rd Ed*. American Institute of Steel Construction, Chicago, IL.

AISC (2002). *Seismic Provisions for Structural Steel Buildings*. American Institute of Steel Construction, Chicago, IL.

ASM International (1987). *ASM Handbook Volume 12 - Fractography.* ASM International, Materials Park, OH.

ASTM A6/A6M-04. "Standard Specification for General Requirements for Rolled Structural Steel Bars, Plates, Shapes, and Sheet Piling." ASTM International.

ASTM A370-03a. "Standard Test Methods and Definitions for Mechanical Testing of Steel Products." ASTM International.

ATC (1992). *Guidelines for Seismic Testing of Components of Steel Structures Report-24*, Applied Technology Council, Redwood City, CA.

Astaneh, A., Bolt, B., Fenves, G., Lysmer, J., and Powell, G. (1993) "Seismic Condition Assessment of the San Francisco-Oakland Bay Bridge." *Proceedings of the Symposium on Structural Engineering in Natural Hazards Mitigation*, ASCE, Irvine, Ca.

Astaneh, A., and Cho, S.W. (1994) "Compression Behavior of Critical Members of the Golden Gate Bridge." *Proceedings of the Fifth US National Conference on Earthquake Engineering*, EERI, Vol. 2, p 713-722, Chicago, IL, July 10-14.

Astaneh, A., Shea, J.H., and Cho, S.W. (1995) "Seismic Behavior and Retrofit Design of Steel Long Span Bridges." *Proceedings of the National Seismic Conference on Bridges and Highways: Progress in Research and Practice*, San Diego, CA, Dec. 10-13.

Astaneh, A. (1998) "Proof-Testing of Latticed Members and their Connections on the San Francisco-Oakland Bay Bridge." *Technical Report UCB/CEE-STEEL-98/03*, Department of Civil and Environmental Engineering, University of California Berkeley, Berkeley, CA.

Arce, G. (2002). "Impact of Higher Strength Steels on Local Buckling and Overstrength of Links in Eccentrically Braced Frames." M.S. Thesis, Department of Civil Engineering, University of Texas at Austin, Austin, TX.

Balendra, T., Lim, E.L., and Liaw, C.W. (1997). "Large-Scale Seismic Testing of Knee-Brace-Frame." *Journal of Structural Engineering*, ASCE, 123(1), 11-19.

Berman, J.W., and Bruneau, M. (2003). "Experimental Investigation of Light-Gauge Steel Plate Shear Walls for the Seismic Retrofit of Buildings." *Technical Report MCEER-03-0001*, Multidisciplinary Center for Earthquake Engineering Research, State University of New York at Buffalo, Buffalo, NY.

Bruneau, M., Uang, C.M., and Whittaker, A. (1998) *Ductile Design of Steel Structures*. McGraw-Hill, New York, NY.

CSI (1997). *Sap2000 User's Manual*, Computers and Structures, Inc., Berkeley, CA.

Dietrich, A.M., and Itani, A.M. (1999). "Cyclic Behavior of Laced and Perforated Steel Members on the San Francisco-Oakland Bay Bridge." *Technical Report CCEER 99-9*, Center for Civil Engineering Earthquake Research, University of Nevada Reno, Reno, NV.

Dusicka, P., Itani, A.M., and Buckle, I.G. (2002). "Cyclic Behavior of Shear Links and Tower Shaft Assembly of San Francisco-Oakland Bay Bridge Tower." *Technical Report CCEER 02-06*, Center for Civil Engineering Earthquake Research, University of Nevada Reno, Reno, NV.

Ely, A.L., and Birdy, J. (1997). "Vincent Thomas Bridge: Seismic Retrofit Design Details." *Proceedings of the Second National Seismic Conference on Bridges and Highways: Progress in Research and Practice,* 8-11 July 1997, Sacremento, CA.

Engelhardt, M.D., and Popov, E.P. (1989). "Behavior of Long Links in Eccentrically Braced Frames." *Report No. UCB/EERC-89-01*, Earthquake Engineering Research Center, College of Engineering, University of California Berkeley, Berkeley, CA.

Galambos, T.V. (1998) *Guide to Stability Design Criteria for Metal Structures*. John Wiley and Sons, New York, NY.

Garud, Y.S. (1981) "A new Approach fo the Evaluation of Fatigue Under Multiaxial Loadings." *Journal of Engineering Materials and Technology*, ASME, Vol. 103, April 1981, 118-125.

Haaijer, G. (1957). "Plate Buckling in the Strain-Hardening Range." *Journal of the Engineering Mechanics Division*, ASCE, 83(2), 1212-1 - 1212-47.

Hassan, O.F., and Goel, S.C. (1991). "Modeling of Bracing Members and Seismic Behavior of Concentrically Braced Steel Structures." *Technical Report UMCE 91-1*, University of Michigan Department of Civil Engineering, Ann Arbor, MI.

Hjelmstad, K.D., and Popov, E.P. (1983). "Cyclic Behavior and Design of Link Beams." *Journal of Structural Engingeering*, ASCE, 109(10), 2387-2403.

Hodge, P.G. (1959). *Plastic Analysis of Structures*. McGraw Hill, Inc., New York, NY.

Ingham, T., Rodriguez, S., Nadar, M., Taucer, F. and Seim, C. (1995). "Seismic Retrofit of the Golden Gate Bridge", *Proceedings of the National Seismic Conference on Bridges and Highways: Progress in Research and Practice*, December 10-13, San Diego, CA.

Itani, A.M. (1997). "Cyclic Behavior of Richmond-San Rafael Tower Links." *Technical Report CCEER 97-4*, Center for Civil Engineering Earthquake Research, University of Nevada Reno, Reno, NV.

Itani, A., Vesco, T., and Dietrich, A. (1998) "Cyclic Behavior of "As-Built" Laced Members with End Gusset Plates on the San Francisco-Oakland Bay Bridge." *Technical Report CCEER 98-01*, Center for Civil Engineering Earthquake Research, University of Nevada, Reno.

Kasai, K., and Popov, E.P. (1986a). "Study of Seismically Resistant Eccentrically Braced Steel Frame Systes." *Report No. UCB/EERC-86/01*, Earthquake Engineering Research Center, College of Engineering, University of California Berkeley, Berkeley, CA.

Kasai, K., and Popov, E.P. (1986b). "General Behavior of WF Steel Shear Link Beams." *Journal of Structural Engineering*, ASCE, 112(2), 362-382.

Klesnil, M., and Lukas, P. (1992). *Fatigue of Metallic Materials. 2nd Ed.* Elsevier Science Publishers, New York, NY.

Krawinkler, H., Bertero, V.V., and Popov, E.P. (1971). "Inelastic Behavior of Steel Beam-to-Column Subassemblages." *Report No. UCB/EERC-71/07*, Earthquake Engineering Research Center, College of Engineering, University of California Berkeley, Berkeley, CA.

Lee, K., and Bruneau, M. (2004). "Seismic Vulnerability Evaluation of Axially Loaded Steel Built-Up Laced Members." *Technical Report MCEER-04-0007*, Multidisciplinary Center for Earthquake Engineering Research, State University of New York at Buffalo, Buffalo, NY.

Lee, S., and Goel, S.C. (1987). "Seismic Behavior of Hollow and Concrete-Filled Square Tubular Members." *Technical Report UMCE 87-11*, University of Michigan Department of Civil Engineering, Ann Arbor, M.I.

Mander, J.B., and Kasalanati, A. (1994). "Low-Cycle Fatigue Behavior of Reinforcing Steel." *Journal of Structural Engineering*, ASCE, 6(4), 453-468.

Mattos, R.J., and Lawrence, F.V. (1977). *Estimation of the Fatigue Crack Initiation Life in Welds Using Low Cycle Fatigue Concepts.* Society of Automotive Engineers, Warrendale, PA.

Morrow, J. (1965). "Cyclic Plastic Energy and Fatigue of Metals." *ASTM STP 378, Internal Friction, Damping, and Cyclic Plasticity*, ASTM International, July 1965, 45-87.

Mrazik, A., Skaloud, M., and Tochacek, M. (1987). *Plastic Design of Steel Structures*. Halsted Press, New York, NY.

Naiem, F. (2001) *The Seismic Design Handbook, 2nd Ed.* Kluwar Academic Publishers, Boston, MA.

Neal, B.G. (1961). "Effect of Shear Force on the Fully Plastic Moment of an I-Beam.." *Journal of Mechanical Engineering Science*, 3(3).

Pollino, M., and Bruneau, M. (2005) "Seismic Retrofit of Bridge Steel Truss Piers Using a Controlled Rocking Approach." *Technical Report MCEER-04-0011*,

Multidisciplinary Center for Earthquake Engineering Research, State University of New York at Buffalo, Buffalo, NY.

Popov, E.P., and Malley, J.O. (1983) "Design of Links and Beam-to-Column Connections for Eccentrically Braced Steel Frames." *Report No. UCB/EERC-83/03*, Earthquake Engineering Research Center, College of Engineering, University of California Berkeley, Berkeley, CA.

Rezai, M., Prion, H.G.L., and Timler, P. (1999). "Pilot Testing of Ductile Fuses in HSS Concentrically Braced Steel Frames - Phase II Brace Fuse Detail Testing." Department of Civil Engineering, University of British Columbia, Vancouver, Canada.

Rezai, M., Prion, H.G.L., Tremblay, R., Bouatay, N., and Timler, P. (2000). "Seismic Performance of Brace Fuse Elements for Concentrically Braced Steel Frames." *Behavior of Steel Structures in Seismic Areas: Proceedings of the Third International Conference: STESSA 2000*, 21-24 Aug. 2000, Montreal, Canada.

Richards, P., and Uang, C.M. (2002) "Evaluation of Rotation Capacity and Overstrength of Links in Eccentrically Braced Frames." *Report No. SSRP-2002/18*, Structural Systems Research Project, Department of Structural Engineering, University of California San Diego, La Jolla, CA.

Ricles, J.M., and Popov E.P. (1989). "Composite Action in Eccentrically Braced Frames." *Journal of Structural Engineering*, ASCE, 115(8), 2046-2066.

Ritchie, P., Kauhl, N., and Kulicki, J. (1999). "Critical Seismic Issues for Existing Steel Bridges." *Technical Report MCEER-99-0013*, Multidisciplinary Center for Earthquake Engineering Research, State University of New York at Buffalo, Buffalo, NY.

Roeder, C.W., and Popov, E.P. (1977) "Inelastic Behavior of Eccentrically Braced Steel Frames Under Cyclic Loadings." *Report No. UCB/EERC-77/18*, Earthquake Engineering Research Center, College of Engineering, University of California Berkeley, Berkeley, CA.

Salmon, C.G., and Johnson, J.E. (1996). *Steel Structures - Design and Behavior.* 4th Edition, HarperCollins College Publishers, New York, NY.

Sugiura, K., Chang, K.C., and Lee, G.C. (1991). "Evaluation of Low-Cycle Fatigue Strength of Structural Metals." *Journal of Engineering Mechanics*, ASCE, 117(10), 2373-2383.

Timoshenko, S.P., and Gere, J.M. (1961).*Theory of Elastic Stability.* 2nd Edition, McGraw-Hill, New York, NY.

Tremblay, R., and Bouatay, N. (1999a). "Pilot Testing of Ductile Yield Plate Fuses for HSS Braces Intended for Low-Rise Buildings - Phase I Full Scale Testing of Prototype Brace Fuse Detail." *Report CDT/ST99-05*, Department of Civil Engineering, Structural Division, Ecole Polytechnique, Montreal, Canada.

Tremblay, R., and Bouatay, N. (1999b). "Pilot Testing of Ductile Yield Plate Fuses for HSS Braces Intended for Low-Rise Buildings - Phase III Full Scale Testing of Prototype Brace Fuse Detail." *Report CDT/ST99-16*, Department of Civil Engineering, Structural Division, Ecole Polytechnique, Montreal, Canada.

Uang, C.M., and Kleiser, M. (1997) "Cyclic Performance of As-Built Latticed Members for the San Francisco-Oakland Bay Bridge." *Report No. SSRP-97-01*, Department of Structural Engineering, University of California, San Diego.

APPENDIX

STIFFENER SPACING DERIVATION

General: This is a summary of the work done by Kasai and Popov (1986a) who studied the web buckling of WF EBF links. The results of this work will be extended EBFs using built-up rectangular tubes as the links.

Plastic Plate Shear Buckling:

Assumed form of equation: $\tau = \eta(\tau)\cdot\tau_E$ **(1)**

Where τ_E is the elastic plate shear buckling stress and $\eta(\tau)$ is the plastic reduction factor.

Define: $\alpha = \frac{a}{b}$ $\beta = \frac{b}{t_w}$ Where a is the stiffener spacing, *b* is the clear web depth and t_w is the web thickness.

Elastic shear buckling stress: $\tau_E = \frac{\pi^2\cdot E}{12\cdot\left(1-\nu^2\right)}\cdot K_s(\alpha)\cdot\left(\frac{1}{\beta}\right)^2$ **(2)**

Where *E* is Young's Modulus, ν is Poisson's Ratio, and $K_s(\alpha)$ is a factor reflecting the boundary conditions.

Kasai and Popov used a $Ks(\alpha)$ value for a plate fully fixed on four sides. They stated that the lateral bracing at the link ends, the relative shortness of the links, as well as the effect of flange restraint made this a valid assumption

Therefore: $K_s(\alpha) = \begin{cases} \left(8.98 + \frac{5.6}{\alpha^2}\right) & \text{if } \alpha \geq 1 \\ \left(5.6 + \frac{8.98}{\alpha^2}\right) & \text{otherwise} \end{cases}$ **(3)**

Plastic Reduction Factor:

Using the results of 30 test specimens which had a wide range of cyclic displacement histories, yield strengths, strain hardening modulii, α's, and β's a linear relationship between η and the secant shear modulus was found (with a high degree of correlation).

Secant shear modulus: $$G_S = \frac{\tau}{\gamma'} = \frac{\tau_B}{\gamma'_B} \quad \textbf{(4)}$$

Where γ' is the deformation angle from the current point to the previous poin of zero shear (for cyclic loading). γ'_B is the γ' at which point web buckling occurs (typically, the largest excursion from zero shear). τ_B is the shear stress at buckling.

Plastic Reduction Factor (cont.):

From the test data it was found that: $$\eta = 3.7\left(\frac{G_S}{G}\right) \quad \textbf{(5)}$$

Where η <= 0.3.

Substituting (5) and (4) into (1) gives: $$\gamma'_B = 3.7 \cdot \frac{\tau_E}{G} \quad \textbf{(6)}$$

Substituting (2) and: $$G = \frac{E}{2 \cdot (1 - \nu)} \quad \textbf{(7)}$$

into (6) gives: $$\gamma'_B = 8.7 \cdot K_s(\alpha) \cdot \left(\frac{1}{\beta}\right)^2 \quad \textbf{(8)}$$

Therefore, this equation directly relates the maximum deformation angle from the last point of zero shear to only α, and β, which are the design parameters

Using $\gamma'_B = 2\gamma_u$, $\beta = d/t_w$, and $\alpha = a/d$ with the maximum value of α equal to 1.0, (8) can be rewritten as:

$$\gamma_u = 4.35 \cdot \left(5.6 + \frac{8.98}{\alpha^2}\right) \cdot \left(\frac{1}{\beta}\right)^2 \quad \textbf{(9)}$$

Stiffener Design Equation:

Kasai and Popov then propose the following as a conservative approximation of (9) for the design of the link stiffener spacing (which is the AISC code equation):

$$\frac{a}{t_w} + \frac{1}{5}\cdot\frac{d}{t_w} = C_B$$

Where C_B = 56, 38, and 29 for γ_u = 0.03, 0.06, and 0.08 respectively. **(10)**

Written in terms of α and β (10) becomes:

$$\alpha = \frac{C_B}{\beta} - \frac{1}{5} \qquad \textbf{(11)}$$

and (9) solved for a becomes:

$$\alpha = \sqrt{\frac{8.98}{\frac{\gamma_u\cdot\beta^2}{4.35} - 5.6}} \qquad \textbf{(12)}$$

Comparison of (11) and (12):

Using γ_u = 0.08 and C_B = 29 equations (11) and (12) are compared below by plotting α vs. β:

$j := 0..85$ $\quad \beta_j := j + 18$ $\quad \gamma_u := 0.08$ $\quad C_B := 29$

$$\alpha_{code_j} := \frac{C_B}{\beta_j} - \frac{1}{5} \qquad \alpha_{actual_j} := \sqrt{\frac{8.98}{\frac{\gamma_u\cdot(\beta_j)^2}{4.35} - 5.6}}$$

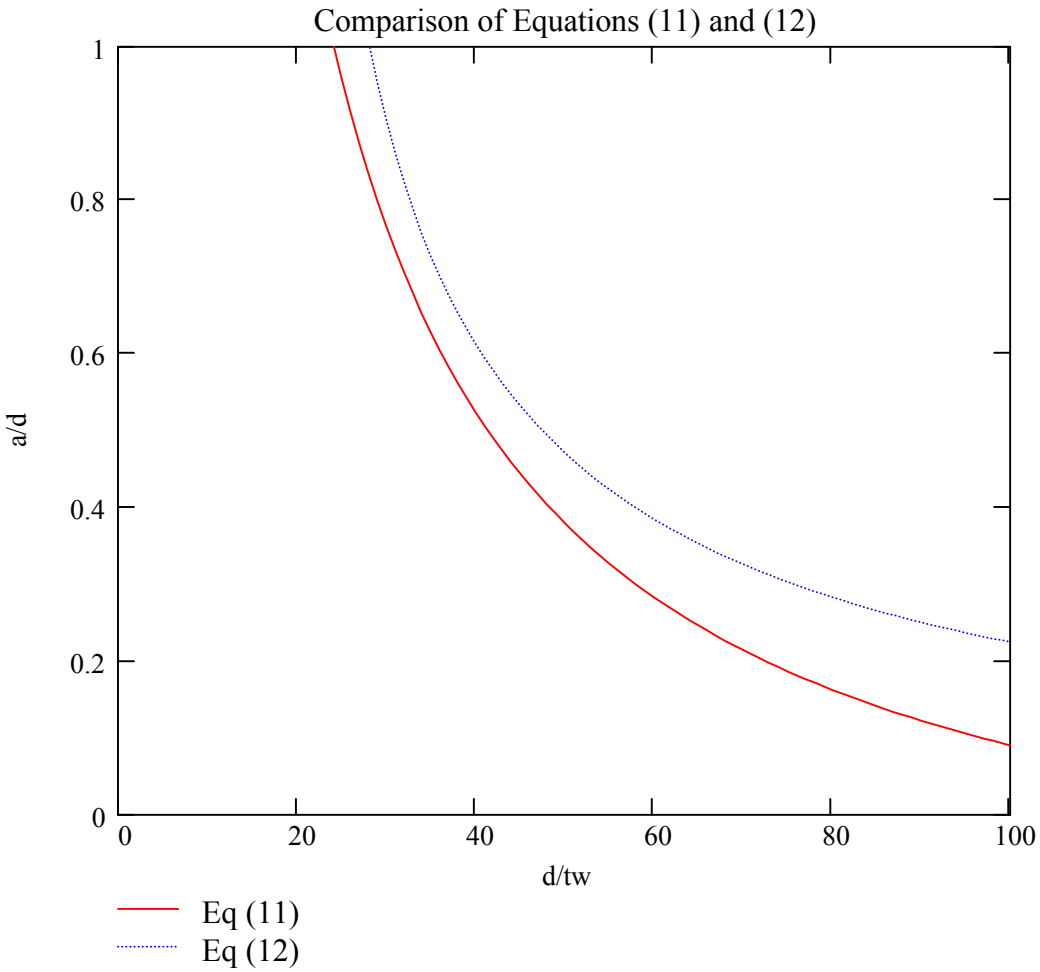

The average factor is:

$$SF := \frac{\sum_{i=0}^{85} \frac{\alpha_{actual_i}}{\alpha_{code_i}}}{86} \qquad SF = 1.603$$

Application to Hybrid Rectangular Cross-Section

General: The procedure used by Kasai and Popov (1986a) to find a conservative design equation for the spacing for EBF WF links can be applied to hybrid rectangular cross-sections as follows:

Revised Boundary Conditions:

Because we are dealing now with an link that is not laterally braced, and the web is somewhat less restrained by the flanges of the rectangular section, a Ks(α) for a plate simply supported on 4 sides will be used (this is conservative):

From Galambos (1998):

$$K_s(\alpha) = \begin{cases} 5.34 + \dfrac{4}{\alpha^2} & \text{if } \alpha \geq 1.0 \\ \left(4 + \dfrac{5.34}{\alpha^2}\right) & \text{otherwise} \end{cases} \qquad \textbf{(13)}$$

WF Results:

For links made of WF sections with different α's, β's, yield stresses, strain hardening modulii, and subjected to various displacement histories, Kasai and Popov found:

$$2\cdot\gamma_u = 8.7\cdot K_s(\alpha)\cdot\left(\frac{1}{\beta}\right)^2 \qquad \textbf{(14)}$$

Where γ_u is the ultimate link rotation, $\alpha = a/d$, $\beta = d/t_w$, d = section depth, a = stiffener spacing, and t_w = web thickness.

This equation should be applicable to links using built-up tubes due to the large variatioin of paratemers which were studied and the high degree of correlation obtained by Kasai and Popov.

Built-up Tubes:

Setting the maximum value of α to 1.0 and substituting (13) into (14) give

$$2\cdot\gamma_u = 8.7\cdot\left(4 + \frac{5.34}{\alpha^2}\right)\cdot\left(\frac{1}{\beta}\right)^2 \qquad \textbf{(15)}$$

Solving for α gives:

$$\alpha = \sqrt{\frac{5.34}{\left(\dfrac{\gamma_u\cdot\beta^2}{4.35}\right) - 4}} \qquad \textbf{(16)}$$

a **vs** b **for Built-up Tube Sections:**

For $\gamma_u = 0.08$ rad. the following plot can be developed using (16):

$$\gamma_u := 0.08 \qquad i := 0..85 \qquad \beta_i := i + 15 \qquad \alpha_i := \sqrt{\frac{5.34}{\left[\frac{\gamma_u \cdot (\beta_i)^2}{4.35}\right]} - 4}$$

Also, using a similar form of the design equation for stiffener spacing that Kasai and Popov used, the necessary values for the constants C_B and C_2 can be found by plotting the design equation with (16) and comparing:

$$C_B := 20 \qquad C_2 := \frac{1}{8}$$

$$\alpha_{code_i} := \frac{C_B}{\beta_i} - C_2 \qquad \textbf{(17)}$$

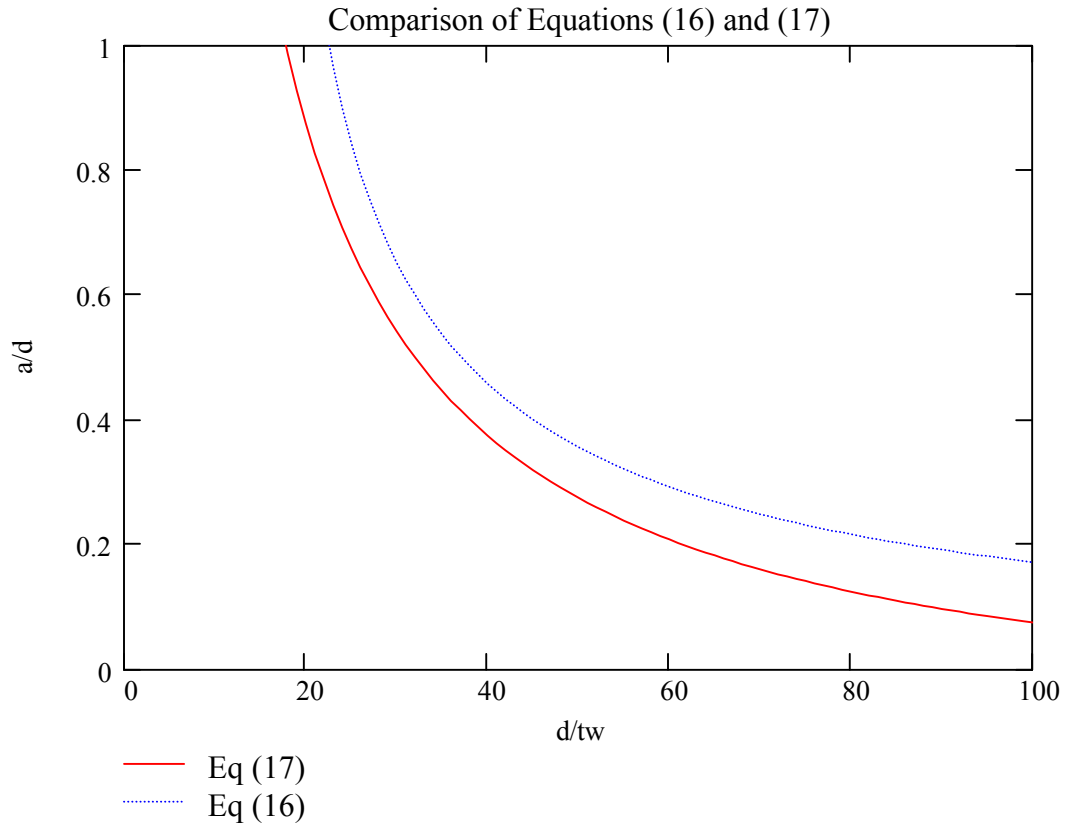

Average Safety Factor for Proposed Design Equation for $\gamma_u = 0.08$ rad:

$$SF := \frac{\sum_{i=0}^{85} \frac{\alpha_i}{\alpha_{code_i}}}{86} \qquad SF = 1.585$$

For γ_u = 0.08 rad. the following plot can be developed using (16):

$$\gamma_u := .02 \qquad i := 0..85 \qquad \beta_i := i + 15 \qquad \alpha_i := \sqrt{\frac{5.34}{\left[\frac{\gamma_u \cdot (\beta_i)^2}{4.35}\right]} - 4}$$

Also, using a similar form of the design equation for stiffener spacing that Kasai and Popov used, the necessary values for the constants C_B and C_2 can be found by plotting the design equation with (16) and comparing:

$$C_B := 37 \qquad C_2 := \frac{1}{8}$$

$$\alpha_{code_i} := \frac{C_B}{\beta_i} - C_2$$

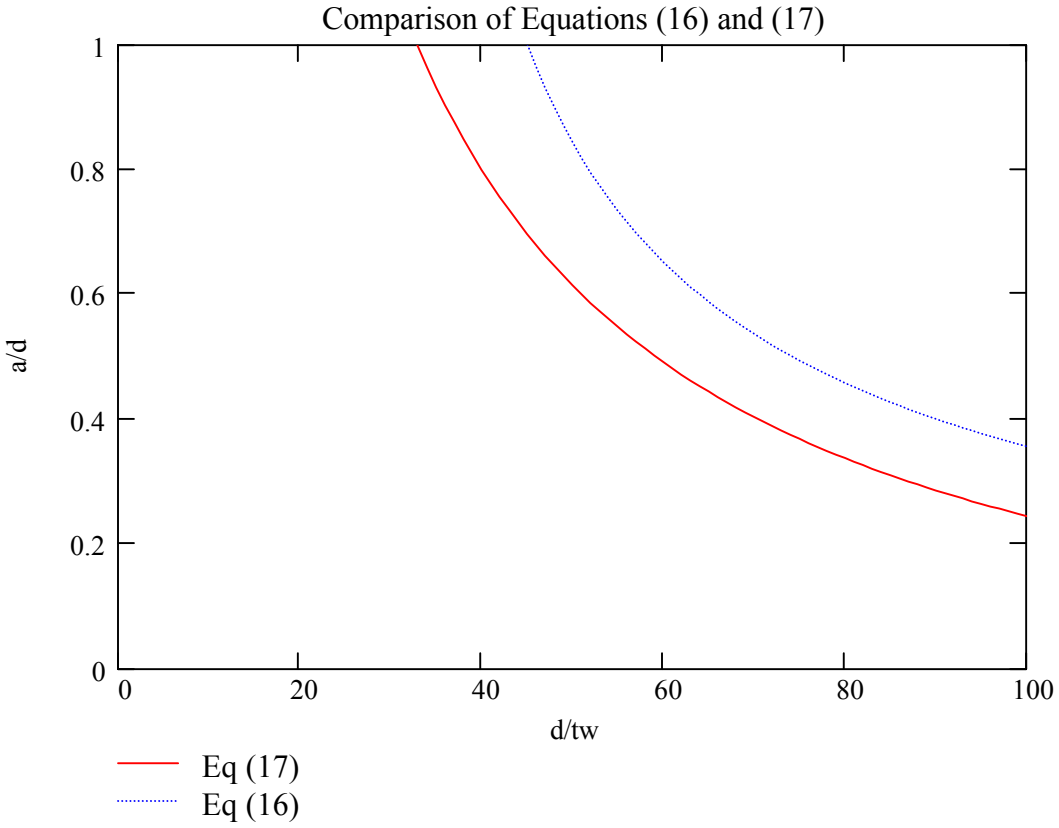

Average Safety Factor for Proposed Design Equation for γ_u = 0.02 rad:

$$SF := \frac{\sum_{i=31}^{85} \frac{\alpha_i}{\alpha_{code_i}}}{86 - 31} \qquad SF = 1.367$$

Reformulated for $\alpha>1.0$:

$$\gamma_u := 0.02 \qquad i := 0..400 \qquad \alpha_i := \frac{i}{25} + 0.001 \qquad \beta_i := \sqrt{\frac{8.7\cdot\left[5.34 + \frac{4}{(\alpha_i)^2}\right]}{2\cdot\gamma_u}}$$

$$C_B := 37 \qquad C_2 := \frac{1}{8}$$

$$\beta_{code_i} := \frac{i}{4} + 0.001 \qquad \alpha_{code_i} := \frac{C_B}{\beta_{code_i}} - C_2$$

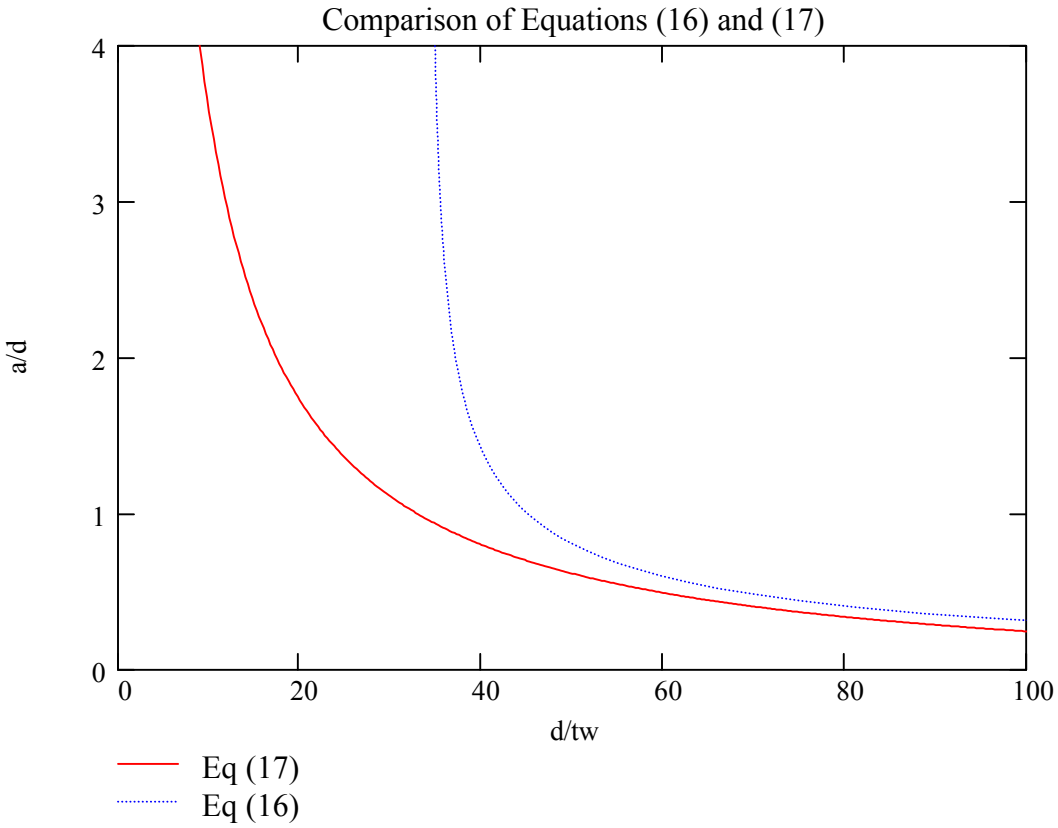

The proposed stiffener equations agree well with theory and have similar margins of safety as those developed by Kasai for $\alpha<1.0$. However, for $\alpha>1.0$ the are overly conservative relative to theory. In fact, for $\gamma = 0.08$ and 0.02 the theory indicates that web stiffeners are not necessary for web slenderness ratios of less than 17 and 34 respectively. This is significant since the current web slenderness limits for HSS in the AISC Seismic Specifications are 15.6 for $F_y = 50$ ksi.

Multidisciplinary Center for Earthquake Engineering Research
List of Technical Reports

The Multidisciplinary Center for Earthquake Engineering Research (MCEER) publishes technical reports on a variety of subjects related to earthquake engineering written by authors funded through MCEER. These reports are available from both MCEER Publications and the National Technical Information Service (NTIS). Requests for reports should be directed to MCEER Publications, Multidisciplinary Center for Earthquake Engineering Research, State University of New York at Buffalo, Red Jacket Quadrangle, Buffalo, New York 14261. Reports can also be requested through NTIS, 5285 Port Royal Road, Springfield, Virginia 22161. NTIS accession numbers are shown in parenthesis, if available.

NCEER-87-0001 "First-Year Program in Research, Education and Technology Transfer," 3/5/87, (PB88-134275, A04, MF-A01).

NCEER-87-0002 "Experimental Evaluation of Instantaneous Optimal Algorithms for Structural Control," by R.C. Lin, T.T. Soong and A.M. Reinhorn, 4/20/87, (PB88-134341, A04, MF-A01).

NCEER-87-0003 "Experimentation Using the Earthquake Simulation Facilities at University at Buffalo," by A.M. Reinhorn and R.L. Ketter, to be published.

NCEER-87-0004 "The System Characteristics and Performance of a Shaking Table," by J.S. Hwang, K.C. Chang and G.C. Lee, 6/1/87, (PB88-134259, A03, MF-A01). This report is available only through NTIS (see address given above).

NCEER-87-0005 "A Finite Element Formulation for Nonlinear Viscoplastic Material Using a Q Model," by O. Gyebi and G. Dasgupta, 11/2/87, (PB88-213764, A08, MF-A01).

NCEER-87-0006 "Symbolic Manipulation Program (SMP) - Algebraic Codes for Two and Three Dimensional Finite Element Formulations," by X. Lee and G. Dasgupta, 11/9/87, (PB88-218522, A05, MF-A01).

NCEER-87-0007 "Instantaneous Optimal Control Laws for Tall Buildings Under Seismic Excitations," by J.N. Yang, A. Akbarpour and P. Ghaemmaghami, 6/10/87, (PB88-134333, A06, MF-A01). This report is only available through NTIS (see address given above).

NCEER-87-0008 "IDARC: Inelastic Damage Analysis of Reinforced Concrete Frame - Shear-Wall Structures," by Y.J. Park, A.M. Reinhorn and S.K. Kunnath, 7/20/87, (PB88-134325, A09, MF-A01). This report is only available through NTIS (see address given above).

NCEER-87-0009 "Liquefaction Potential for New York State: A Preliminary Report on Sites in Manhattan and Buffalo," by M. Budhu, V. Vijayakumar, R.F. Giese and L. Baumgras, 8/31/87, (PB88-163704, A03, MF-A01). This report is available only through NTIS (see address given above).

NCEER-87-0010 "Vertical and Torsional Vibration of Foundations in Inhomogeneous Media," by A.S. Veletsos and K.W. Dotson, 6/1/87, (PB88-134291, A03, MF-A01). This report is only available through NTIS (see address given above).

NCEER-87-0011 "Seismic Probabilistic Risk Assessment and Seismic Margins Studies for Nuclear Power Plants," by Howard H.M. Hwang, 6/15/87, (PB88-134267, A03, MF-A01). This report is only available through NTIS (see address given above).

NCEER-87-0012 "Parametric Studies of Frequency Response of Secondary Systems Under Ground-Acceleration Excitations," by Y. Yong and Y.K. Lin, 6/10/87, (PB88-134309, A03, MF-A01). This report is only available through NTIS (see address given above).

NCEER-87-0013 "Frequency Response of Secondary Systems Under Seismic Excitation," by J.A. HoLung, J. Cai and Y.K. Lin, 7/31/87, (PB88-134317, A05, MF-A01). This report is only available through NTIS (see address given above).

NCEER-87-0014 "Modelling Earthquake Ground Motions in Seismically Active Regions Using Parametric Time Series Methods," by G.W. Ellis and A.S. Cakmak, 8/25/87, (PB88-134283, A08, MF-A01). This report is only available through NTIS (see address given above).

NCEER-87-0015 "Detection and Assessment of Seismic Structural Damage," by E. DiPasquale and A.S. Cakmak, 8/25/87, (PB88-163712, A05, MF-A01). This report is only available through NTIS (see address given above).

NCEER-87-0016 "Pipeline Experiment at Parkfield, California," by J. Isenberg and E. Richardson, 9/15/87, (PB88-163720, A03, MF-A01). This report is available only through NTIS (see address given above).

NCEER-87-0017 "Digital Simulation of Seismic Ground Motion," by M. Shinozuka, G. Deodatis and T. Harada, 8/31/87, (PB88-155197, A04, MF-A01). This report is available only through NTIS (see address given above).

NCEER-87-0018 "Practical Considerations for Structural Control: System Uncertainty, System Time Delay and Truncation of Small Control Forces," J.N. Yang and A. Akbarpour, 8/10/87, (PB88-163738, A08, MF-A01). This report is only available through NTIS (see address given above).

NCEER-87-0019 "Modal Analysis of Nonclassically Damped Structural Systems Using Canonical Transformation," by J.N. Yang, S. Sarkani and F.X. Long, 9/27/87, (PB88-187851, A04, MF-A01).

NCEER-87-0020 "A Nonstationary Solution in Random Vibration Theory," by J.R. Red-Horse and P.D. Spanos, 11/3/87, (PB88-163746, A03, MF-A01).

NCEER-87-0021 "Horizontal Impedances for Radially Inhomogeneous Viscoelastic Soil Layers," by A.S. Veletsos and K.W. Dotson, 10/15/87, (PB88-150859, A04, MF-A01).

NCEER-87-0022 "Seismic Damage Assessment of Reinforced Concrete Members," by Y.S. Chung, C. Meyer and M. Shinozuka, 10/9/87, (PB88-150867, A05, MF-A01). This report is available only through NTIS (see address given above).

NCEER-87-0023 "Active Structural Control in Civil Engineering," by T.T. Soong, 11/11/87, (PB88-187778, A03, MF-A01).

NCEER-87-0024 "Vertical and Torsional Impedances for Radially Inhomogeneous Viscoelastic Soil Layers," by K.W. Dotson and A.S. Veletsos, 12/87, (PB88-187786, A03, MF-A01).

NCEER-87-0025 "Proceedings from the Symposium on Seismic Hazards, Ground Motions, Soil-Liquefaction and Engineering Practice in Eastern North America," October 20-22, 1987, edited by K.H. Jacob, 12/87, (PB88-188115, A23, MF-A01). This report is available only through NTIS (see address given above).

NCEER-87-0026 "Report on the Whittier-Narrows, California, Earthquake of October 1, 1987," by J. Pantelic and A. Reinhorn, 11/87, (PB88-187752, A03, MF-A01). This report is available only through NTIS (see address given above).

NCEER-87-0027 "Design of a Modular Program for Transient Nonlinear Analysis of Large 3-D Building Structures," by S. Srivastav and J.F. Abel, 12/30/87, (PB88-187950, A05, MF-A01). This report is only available through NTIS (see address given above).

NCEER-87-0028 "Second-Year Program in Research, Education and Technology Transfer," 3/8/88, (PB88-219480, A04, MF-A01).

NCEER-88-0001 "Workshop on Seismic Computer Analysis and Design of Buildings With Interactive Graphics," by W. McGuire, J.F. Abel and C.H. Conley, 1/18/88, (PB88-187760, A03, MF-A01). This report is only available through NTIS (see address given above).

NCEER-88-0002 "Optimal Control of Nonlinear Flexible Structures," by J.N. Yang, F.X. Long and D. Wong, 1/22/88, (PB88-213772, A06, MF-A01).

NCEER-88-0003 "Substructuring Techniques in the Time Domain for Primary-Secondary Structural Systems," by G.D. Manolis and G. Juhn, 2/10/88, (PB88-213780, A04, MF-A01).

NCEER-88-0004 "Iterative Seismic Analysis of Primary-Secondary Systems," by A. Singhal, L.D. Lutes and P.D. Spanos, 2/23/88, (PB88-213798, A04, MF-A01).

NCEER-88-0005 "Stochastic Finite Element Expansion for Random Media," by P.D. Spanos and R. Ghanem, 3/14/88, (PB88-213806, A03, MF-A01).

NCEER-88-0006 "Combining Structural Optimization and Structural Control," by F.Y. Cheng and C.P. Pantelides, 1/10/88, (PB88-213814, A05, MF-A01).

NCEER-88-0007 "Seismic Performance Assessment of Code-Designed Structures," by H.H-M. Hwang, J-W. Jaw and H-J. Shau, 3/20/88, (PB88-219423, A04, MF-A01). This report is only available through NTIS (see address given above).

NCEER-88-0008 "Reliability Analysis of Code-Designed Structures Under Natural Hazards," by H.H-M. Hwang, H. Ushiba and M. Shinozuka, 2/29/88, (PB88-229471, A07, MF-A01). This report is only available through NTIS (see address given above).

NCEER-88-0009 "Seismic Fragility Analysis of Shear Wall Structures," by J-W Jaw and H.H-M. Hwang, 4/30/88, (PB89-102867, A04, MF-A01).

NCEER-88-0010 "Base Isolation of a Multi-Story Building Under a Harmonic Ground Motion - A Comparison of Performances of Various Systems," by F-G Fan, G. Ahmadi and I.G. Tadjbakhsh, 5/18/88, (PB89-122238, A06, MF-A01). This report is only available through NTIS (see address given above).

NCEER-88-0011 "Seismic Floor Response Spectra for a Combined System by Green's Functions," by F.M. Lavelle, L.A. Bergman and P.D. Spanos, 5/1/88, (PB89-102875, A03, MF-A01).

NCEER-88-0012 "A New Solution Technique for Randomly Excited Hysteretic Structures," by G.Q. Cai and Y.K. Lin, 5/16/88, (PB89-102883, A03, MF-A01).

NCEER-88-0013 "A Study of Radiation Damping and Soil-Structure Interaction Effects in the Centrifuge," by K. Weissman, supervised by J.H. Prevost, 5/24/88, (PB89-144703, A06, MF-A01).

NCEER-88-0014 "Parameter Identification and Implementation of a Kinematic Plasticity Model for Frictional Soils," by J.H. Prevost and D.V. Griffiths, to be published.

NCEER-88-0015 "Two- and Three- Dimensional Dynamic Finite Element Analyses of the Long Valley Dam," by D.V. Griffiths and J.H. Prevost, 6/17/88, (PB89-144711, A04, MF-A01).

NCEER-88-0016 "Damage Assessment of Reinforced Concrete Structures in Eastern United States," by A.M. Reinhorn, M.J. Seidel, S.K. Kunnath and Y.J. Park, 6/15/88, (PB89-122220, A04, MF-A01). This report is only available through NTIS (see address given above).

NCEER-88-0017 "Dynamic Compliance of Vertically Loaded Strip Foundations in Multilayered Viscoelastic Soils," by S. Ahmad and A.S.M. Israil, 6/17/88, (PB89-102891, A04, MF-A01).

NCEER-88-0018 "An Experimental Study of Seismic Structural Response With Added Viscoelastic Dampers," by R.C. Lin, Z. Liang, T.T. Soong and R.H. Zhang, 6/30/88, (PB89-122212, A05, MF-A01). This report is available only through NTIS (see address given above).

NCEER-88-0019 "Experimental Investigation of Primary - Secondary System Interaction," by G.D. Manolis, G. Juhn and A.M. Reinhorn, 5/27/88, (PB89-122204, A04, MF-A01).

NCEER-88-0020 "A Response Spectrum Approach For Analysis of Nonclassically Damped Structures," by J.N. Yang, S. Sarkani and F.X. Long, 4/22/88, (PB89-102909, A04, MF-A01).

NCEER-88-0021 "Seismic Interaction of Structures and Soils: Stochastic Approach," by A.S. Veletsos and A.M. Prasad, 7/21/88, (PB89-122196, A04, MF-A01). This report is only available through NTIS (see address given above).

NCEER-88-0022 "Identification of the Serviceability Limit State and Detection of Seismic Structural Damage," by E. DiPasquale and A.S. Cakmak, 6/15/88, (PB89-122188, A05, MF-A01). This report is available only through NTIS (see address given above).

NCEER-88-0023 "Multi-Hazard Risk Analysis: Case of a Simple Offshore Structure," by B.K. Bhartia and E.H. Vanmarcke, 7/21/88, (PB89-145213, A05, MF-A01).

NCEER-88-0024 "Automated Seismic Design of Reinforced Concrete Buildings," by Y.S. Chung, C. Meyer and M. Shinozuka, 7/5/88, (PB89-122170, A06, MF-A01). This report is available only through NTIS (see address given above).

NCEER-88-0025 "Experimental Study of Active Control of MDOF Structures Under Seismic Excitations," by L.L. Chung, R.C. Lin, T.T. Soong and A.M. Reinhorn, 7/10/88, (PB89-122600, A04, MF-A01).

NCEER-88-0026 "Earthquake Simulation Tests of a Low-Rise Metal Structure," by J.S. Hwang, K.C. Chang, G.C. Lee and R.L. Ketter, 8/1/88, (PB89-102917, A04, MF-A01).

NCEER-88-0027 "Systems Study of Urban Response and Reconstruction Due to Catastrophic Earthquakes," by F. Kozin and H.K. Zhou, 9/22/88, (PB90-162348, A04, MF-A01).

NCEER-88-0028 "Seismic Fragility Analysis of Plane Frame Structures," by H.H-M. Hwang and Y.K. Low, 7/31/88, (PB89-131445, A06, MF-A01).

NCEER-88-0029 "Response Analysis of Stochastic Structures," by A. Kardara, C. Bucher and M. Shinozuka, 9/22/88, (PB89-174429, A04, MF-A01).

NCEER-88-0030 "Nonnormal Accelerations Due to Yielding in a Primary Structure," by D.C.K. Chen and L.D. Lutes, 9/19/88, (PB89-131437, A04, MF-A01).

NCEER-88-0031 "Design Approaches for Soil-Structure Interaction," by A.S. Veletsos, A.M. Prasad and Y. Tang, 12/30/88, (PB89-174437, A03, MF-A01). This report is available only through NTIS (see address given above).

NCEER-88-0032 "A Re-evaluation of Design Spectra for Seismic Damage Control," by C.J. Turkstra and A.G. Tallin, 11/7/88, (PB89-145221, A05, MF-A01).

NCEER-88-0033 "The Behavior and Design of Noncontact Lap Splices Subjected to Repeated Inelastic Tensile Loading," by V.E. Sagan, P. Gergely and R.N. White, 12/8/88, (PB89-163737, A08, MF-A01).

NCEER-88-0034 "Seismic Response of Pile Foundations," by S.M. Mamoon, P.K. Banerjee and S. Ahmad, 11/1/88, (PB89-145239, A04, MF-A01).

NCEER-88-0035 "Modeling of R/C Building Structures With Flexible Floor Diaphragms (IDARC2)," by A.M. Reinhorn, S.K. Kunnath and N. Panahshahi, 9/7/88, (PB89-207153, A07, MF-A01).

NCEER-88-0036 "Solution of the Dam-Reservoir Interaction Problem Using a Combination of FEM, BEM with Particular Integrals, Modal Analysis, and Substructuring," by C-S. Tsai, G.C. Lee and R.L. Ketter, 12/31/88, (PB89-207146, A04, MF-A01).

NCEER-88-0037 "Optimal Placement of Actuators for Structural Control," by F.Y. Cheng and C.P. Pantelides, 8/15/88, (PB89-162846, A05, MF-A01).

NCEER-88-0038 "Teflon Bearings in Aseismic Base Isolation: Experimental Studies and Mathematical Modeling," by A. Mokha, M.C. Constantinou and A.M. Reinhorn, 12/5/88, (PB89-218457, A10, MF-A01). This report is available only through NTIS (see address given above).

NCEER-88-0039 "Seismic Behavior of Flat Slab High-Rise Buildings in the New York City Area," by P. Weidlinger and M. Ettouney, 10/15/88, (PB90-145681, A04, MF-A01).

NCEER-88-0040 "Evaluation of the Earthquake Resistance of Existing Buildings in New York City," by P. Weidlinger and M. Ettouney, 10/15/88, to be published.

NCEER-88-0041 "Small-Scale Modeling Techniques for Reinforced Concrete Structures Subjected to Seismic Loads," by W. Kim, A. El-Attar and R.N. White, 11/22/88, (PB89-189625, A05, MF-A01).

NCEER-88-0042 "Modeling Strong Ground Motion from Multiple Event Earthquakes," by G.W. Ellis and A.S. Cakmak, 10/15/88, (PB89-174445, A03, MF-A01).

NCEER-88-0043 "Nonstationary Models of Seismic Ground Acceleration," by M. Grigoriu, S.E. Ruiz and E. Rosenblueth, 7/15/88, (PB89-189617, A04, MF-A01).

NCEER-88-0044 "SARCF User's Guide: Seismic Analysis of Reinforced Concrete Frames," by Y.S. Chung, C. Meyer and M. Shinozuka, 11/9/88, (PB89-174452, A08, MF-A01).

NCEER-88-0045 "First Expert Panel Meeting on Disaster Research and Planning," edited by J. Pantelic and J. Stoyle, 9/15/88, (PB89-174460, A05, MF-A01).

NCEER-88-0046 "Preliminary Studies of the Effect of Degrading Infill Walls on the Nonlinear Seismic Response of Steel Frames," by C.Z. Chrysostomou, P. Gergely and J.F. Abel, 12/19/88, (PB89-208383, A05, MF-A01).

NCEER-88-0047 "Reinforced Concrete Frame Component Testing Facility - Design, Construction, Instrumentation and Operation," by S.P. Pessiki, C. Conley, T. Bond, P. Gergely and R.N. White, 12/16/88, (PB89-174478, A04, MF-A01).

NCEER-89-0001 "Effects of Protective Cushion and Soil Compliancy on the Response of Equipment Within a Seismically Excited Building," by J.A. HoLung, 2/16/89, (PB89-207179, A04, MF-A01).

NCEER-89-0002 "Statistical Evaluation of Response Modification Factors for Reinforced Concrete Structures," by H.H-M. Hwang and J-W. Jaw, 2/17/89, (PB89-207187, A05, MF-A01).

NCEER-89-0003 "Hysteretic Columns Under Random Excitation," by G-Q. Cai and Y.K. Lin, 1/9/89, (PB89-196513, A03, MF-A01).

NCEER-89-0004 "Experimental Study of `Elephant Foot Bulge' Instability of Thin-Walled Metal Tanks," by Z-H. Jia and R.L. Ketter, 2/22/89, (PB89-207195, A03, MF-A01).

NCEER-89-0005 "Experiment on Performance of Buried Pipelines Across San Andreas Fault," by J. Isenberg, E. Richardson and T.D. O'Rourke, 3/10/89, (PB89-218440, A04, MF-A01). This report is available only through NTIS (see address given above).

NCEER-89-0006 "A Knowledge-Based Approach to Structural Design of Earthquake-Resistant Buildings," by M. Subramani, P. Gergely, C.H. Conley, J.F. Abel and A.H. Zaghw, 1/15/89, (PB89-218465, A06, MF-A01).

NCEER-89-0007 "Liquefaction Hazards and Their Effects on Buried Pipelines," by T.D. O'Rourke and P.A. Lane, 2/1/89, (PB89-218481, A09, MF-A01).

NCEER-89-0008 "Fundamentals of System Identification in Structural Dynamics," by H. Imai, C-B. Yun, O. Maruyama and M. Shinozuka, 1/26/89, (PB89-207211, A04, MF-A01).

NCEER-89-0009 "Effects of the 1985 Michoacan Earthquake on Water Systems and Other Buried Lifelines in Mexico," by A.G. Ayala and M.J. O'Rourke, 3/8/89, (PB89-207229, A06, MF-A01).

NCEER-89-R010 "NCEER Bibliography of Earthquake Education Materials," by K.E.K. Ross, Second Revision, 9/1/89, (PB90-125352, A05, MF-A01). This report is replaced by NCEER-92-0018.

NCEER-89-0011 "Inelastic Three-Dimensional Response Analysis of Reinforced Concrete Building Structures (IDARC-3D), Part I - Modeling," by S.K. Kunnath and A.M. Reinhorn, 4/17/89, (PB90-114612, A07, MF-A01). This report is available only through NTIS (see address given above).

NCEER-89-0012 "Recommended Modifications to ATC-14," by C.D. Poland and J.O. Malley, 4/12/89, (PB90-108648, A15, MF-A01).

NCEER-89-0013 "Repair and Strengthening of Beam-to-Column Connections Subjected to Earthquake Loading," by M. Corazao and A.J. Durrani, 2/28/89, (PB90-109885, A06, MF-A01).

NCEER-89-0014 "Program EXKAL2 for Identification of Structural Dynamic Systems," by O. Maruyama, C-B. Yun, M. Hoshiya and M. Shinozuka, 5/19/89, (PB90-109877, A09, MF-A01).

NCEER-89-0015 "Response of Frames With Bolted Semi-Rigid Connections, Part I - Experimental Study and Analytical Predictions," by P.J. DiCorso, A.M. Reinhorn, J.R. Dickerson, J.B. Radziminski and W.L. Harper, 6/1/89, to be published.

NCEER-89-0016 "ARMA Monte Carlo Simulation in Probabilistic Structural Analysis," by P.D. Spanos and M.P. Mignolet, 7/10/89, (PB90-109893, A03, MF-A01).

NCEER-89-P017 "Preliminary Proceedings from the Conference on Disaster Preparedness - The Place of Earthquake Education in Our Schools," Edited by K.E.K. Ross, 6/23/89, (PB90-108606, A03, MF-A01).

NCEER-89-0017 "Proceedings from the Conference on Disaster Preparedness - The Place of Earthquake Education in Our Schools," Edited by K.E.K. Ross, 12/31/89, (PB90-207895, A012, MF-A02). This report is available only through NTIS (see address given above).

NCEER-89-0018 "Multidimensional Models of Hysteretic Material Behavior for Vibration Analysis of Shape Memory Energy Absorbing Devices, by E.J. Graesser and F.A. Cozzarelli, 6/7/89, (PB90-164146, A04, MF-A01).

NCEER-89-0019 "Nonlinear Dynamic Analysis of Three-Dimensional Base Isolated Structures (3D-BASIS)," by S. Nagarajaiah, A.M. Reinhorn and M.C. Constantinou, 8/3/89, (PB90-161936, A06, MF-A01). This report has been replaced by NCEER-93-0011.

NCEER-89-0020 "Structural Control Considering Time-Rate of Control Forces and Control Rate Constraints," by F.Y. Cheng and C.P. Pantelides, 8/3/89, (PB90-120445, A04, MF-A01).

NCEER-89-0021 "Subsurface Conditions of Memphis and Shelby County," by K.W. Ng, T-S. Chang and H-H.M. Hwang, 7/26/89, (PB90-120437, A03, MF-A01).

NCEER-89-0022 "Seismic Wave Propagation Effects on Straight Jointed Buried Pipelines," by K. Elhmadi and M.J. O'Rourke, 8/24/89, (PB90-162322, A10, MF-A02).

NCEER-89-0023 "Workshop on Serviceability Analysis of Water Delivery Systems," edited by M. Grigoriu, 3/6/89, (PB90-127424, A03, MF-A01).

NCEER-89-0024 "Shaking Table Study of a 1/5 Scale Steel Frame Composed of Tapered Members," by K.C. Chang, J.S. Hwang and G.C. Lee, 9/18/89, (PB90-160169, A04, MF-A01).

NCEER-89-0025 "DYNA1D: A Computer Program for Nonlinear Seismic Site Response Analysis - Technical Documentation," by Jean H. Prevost, 9/14/89, (PB90-161944, A07, MF-A01). This report is available only through NTIS (see address given above).

NCEER-89-0026 "1:4 Scale Model Studies of Active Tendon Systems and Active Mass Dampers for Aseismic Protection," by A.M. Reinhorn, T.T. Soong, R.C. Lin, Y.P. Yang, Y. Fukao, H. Abe and M. Nakai, 9/15/89, (PB90-173246, A10, MF-A02). This report is available only through NTIS (see address given above).

NCEER-89-0027 "Scattering of Waves by Inclusions in a Nonhomogeneous Elastic Half Space Solved by Boundary Element Methods," by P.K. Hadley, A. Askar and A.S. Cakmak, 6/15/89, (PB90-145699, A07, MF-A01).

NCEER-89-0028 "Statistical Evaluation of Deflection Amplification Factors for Reinforced Concrete Structures," by H.H.M. Hwang, J-W. Jaw and A.L. Ch'ng, 8/31/89, (PB90-164633, A05, MF-A01).

NCEER-89-0029 "Bedrock Accelerations in Memphis Area Due to Large New Madrid Earthquakes," by H.H.M. Hwang, C.H.S. Chen and G. Yu, 11/7/89, (PB90-162330, A04, MF-A01).

NCEER-89-0030 "Seismic Behavior and Response Sensitivity of Secondary Structural Systems," by Y.Q. Chen and T.T. Soong, 10/23/89, (PB90-164658, A08, MF-A01).

NCEER-89-0031 "Random Vibration and Reliability Analysis of Primary-Secondary Structural Systems," by Y. Ibrahim, M. Grigoriu and T.T. Soong, 11/10/89, (PB90-161951, A04, MF-A01).

NCEER-89-0032 "Proceedings from the Second U.S. - Japan Workshop on Liquefaction, Large Ground Deformation and Their Effects on Lifelines, September 26-29, 1989," Edited by T.D. O'Rourke and M. Hamada, 12/1/89, (PB90-209388, A22, MF-A03).

NCEER-89-0033 "Deterministic Model for Seismic Damage Evaluation of Reinforced Concrete Structures," by J.M. Bracci, A.M. Reinhorn, J.B. Mander and S.K. Kunnath, 9/27/89, (PB91-108803, A06, MF-A01).

NCEER-89-0034 "On the Relation Between Local and Global Damage Indices," by E. DiPasquale and A.S. Cakmak, 8/15/89, (PB90-173865, A05, MF-A01).

NCEER-89-0035 "Cyclic Undrained Behavior of Nonplastic and Low Plasticity Silts," by A.J. Walker and H.E. Stewart, 7/26/89, (PB90-183518, A10, MF-A01).

NCEER-89-0036 "Liquefaction Potential of Surficial Deposits in the City of Buffalo, New York," by M. Budhu, R. Giese and L. Baumgrass, 1/17/89, (PB90-208455, A04, MF-A01).

NCEER-89-0037 "A Deterministic Assessment of Effects of Ground Motion Incoherence," by A.S. Veletsos and Y. Tang, 7/15/89, (PB90-164294, A03, MF-A01).

NCEER-89-0038 "Workshop on Ground Motion Parameters for Seismic Hazard Mapping," July 17-18, 1989, edited by R.V. Whitman, 12/1/89, (PB90-173923, A04, MF-A01).

NCEER-89-0039 "Seismic Effects on Elevated Transit Lines of the New York City Transit Authority," by C.J. Costantino, C.A. Miller and E. Heymsfield, 12/26/89, (PB90-207887, A06, MF-A01).

NCEER-89-0040 "Centrifugal Modeling of Dynamic Soil-Structure Interaction," by K. Weissman, Supervised by J.H. Prevost, 5/10/89, (PB90-207879, A07, MF-A01).

NCEER-89-0041 "Linearized Identification of Buildings With Cores for Seismic Vulnerability Assessment," by I-K. Ho and A.E. Aktan, 11/1/89, (PB90-251943, A07, MF-A01).

NCEER-90-0001 "Geotechnical and Lifeline Aspects of the October 17, 1989 Loma Prieta Earthquake in San Francisco," by T.D. O'Rourke, H.E. Stewart, F.T. Blackburn and T.S. Dickerman, 1/90, (PB90-208596, A05, MF-A01).

NCEER-90-0002 "Nonnormal Secondary Response Due to Yielding in a Primary Structure," by D.C.K. Chen and L.D. Lutes, 2/28/90, (PB90-251976, A07, MF-A01).

NCEER-90-0003 "Earthquake Education Materials for Grades K-12," by K.E.K. Ross, 4/16/90, (PB91-251984, A05, MF-A05). This report has been replaced by NCEER-92-0018.

NCEER-90-0004 "Catalog of Strong Motion Stations in Eastern North America," by R.W. Busby, 4/3/90, (PB90-251984, A05, MF-A01).

NCEER-90-0005 "NCEER Strong-Motion Data Base: A User Manual for the GeoBase Release (Version 1.0 for the Sun3)," by P. Friberg and K. Jacob, 3/31/90 (PB90-258062, A04, MF-A01).

NCEER-90-0006 "Seismic Hazard Along a Crude Oil Pipeline in the Event of an 1811-1812 Type New Madrid Earthquake," by H.H.M. Hwang and C-H.S. Chen, 4/16/90, (PB90-258054, A04, MF-A01).

NCEER-90-0007 "Site-Specific Response Spectra for Memphis Sheahan Pumping Station," by H.H.M. Hwang and C.S. Lee, 5/15/90, (PB91-108811, A05, MF-A01).

NCEER-90-0008 "Pilot Study on Seismic Vulnerability of Crude Oil Transmission Systems," by T. Ariman, R. Dobry, M. Grigoriu, F. Kozin, M. O'Rourke, T. O'Rourke and M. Shinozuka, 5/25/90, (PB91-108837, A06, MF-A01).

NCEER-90-0009 "A Program to Generate Site Dependent Time Histories: EQGEN," by G.W. Ellis, M. Srinivasan and A.S. Cakmak, 1/30/90, (PB91-108829, A04, MF-A01).

NCEER-90-0010 "Active Isolation for Seismic Protection of Operating Rooms," by M.E. Talbott, Supervised by M. Shinozuka, 6/8/9, (PB91-110205, A05, MF-A01).

NCEER-90-0011 "Program LINEARID for Identification of Linear Structural Dynamic Systems," by C-B. Yun and M. Shinozuka, 6/25/90, (PB91-110312, A08, MF-A01).

NCEER-90-0012 "Two-Dimensional Two-Phase Elasto-Plastic Seismic Response of Earth Dams," by A.N. Yiagos, Supervised by J.H. Prevost, 6/20/90, (PB91-110197, A13, MF-A02).

NCEER-90-0013 "Secondary Systems in Base-Isolated Structures: Experimental Investigation, Stochastic Response and Stochastic Sensitivity," by G.D. Manolis, G. Juhn, M.C. Constantinou and A.M. Reinhorn, 7/1/90, (PB91-110320, A08, MF-A01).

NCEER-90-0014 "Seismic Behavior of Lightly-Reinforced Concrete Column and Beam-Column Joint Details," by S.P. Pessiki, C.H. Conley, P. Gergely and R.N. White, 8/22/90, (PB91-108795, A11, MF-A02).

NCEER-90-0015 "Two Hybrid Control Systems for Building Structures Under Strong Earthquakes," by J.N. Yang and A. Danielians, 6/29/90, (PB91-125393, A04, MF-A01).

NCEER-90-0016 "Instantaneous Optimal Control with Acceleration and Velocity Feedback," by J.N. Yang and Z. Li, 6/29/90, (PB91-125401, A03, MF-A01).

NCEER-90-0017 "Reconnaissance Report on the Northern Iran Earthquake of June 21, 1990," by M. Mehrain, 10/4/90, (PB91-125377, A03, MF-A01).

NCEER-90-0018 "Evaluation of Liquefaction Potential in Memphis and Shelby County," by T.S. Chang, P.S. Tang, C.S. Lee and H. Hwang, 8/10/90, (PB91-125427, A09, MF-A01).

NCEER-90-0019 "Experimental and Analytical Study of a Combined Sliding Disc Bearing and Helical Steel Spring Isolation System," by M.C. Constantinou, A.S. Mokha and A.M. Reinhorn, 10/4/90, (PB91-125385, A06, MF-A01). This report is available only through NTIS (see address given above).

NCEER-90-0020 "Experimental Study and Analytical Prediction of Earthquake Response of a Sliding Isolation System with a Spherical Surface," by A.S. Mokha, M.C. Constantinou and A.M. Reinhorn, 10/11/90, (PB91-125419, A05, MF-A01).

NCEER-90-0021 "Dynamic Interaction Factors for Floating Pile Groups," by G. Gazetas, K. Fan, A. Kaynia and E. Kausel, 9/10/90, (PB91-170381, A05, MF-A01).

NCEER-90-0022 "Evaluation of Seismic Damage Indices for Reinforced Concrete Structures," by S. Rodriguez-Gomez and A.S. Cakmak, 9/30/90, PB91-171322, A06, MF-A01).

NCEER-90-0023 "Study of Site Response at a Selected Memphis Site," by H. Desai, S. Ahmad, E.S. Gazetas and M.R. Oh, 10/11/90, (PB91-196857, A03, MF-A01).

NCEER-90-0024 "A User's Guide to Strongmo: Version 1.0 of NCEER's Strong-Motion Data Access Tool for PCs and Terminals," by P.A. Friberg and C.A.T. Susch, 11/15/90, (PB91-171272, A03, MF-A01).

NCEER-90-0025 "A Three-Dimensional Analytical Study of Spatial Variability of Seismic Ground Motions," by L-L. Hong and A.H.-S. Ang, 10/30/90, (PB91-170399, A09, MF-A01).

NCEER-90-0026 "MUMOID User's Guide - A Program for the Identification of Modal Parameters," by S. Rodriguez-Gomez and E. DiPasquale, 9/30/90, (PB91-171298, A04, MF-A01).

NCEER-90-0027 "SARCF-II User's Guide - Seismic Analysis of Reinforced Concrete Frames," by S. Rodriguez-Gomez, Y.S. Chung and C. Meyer, 9/30/90, (PB91-171280, A05, MF-A01).

NCEER-90-0028 "Viscous Dampers: Testing, Modeling and Application in Vibration and Seismic Isolation," by N. Makris and M.C. Constantinou, 12/20/90 (PB91-190561, A06, MF-A01).

NCEER-90-0029 "Soil Effects on Earthquake Ground Motions in the Memphis Area," by H. Hwang, C.S. Lee, K.W. Ng and T.S. Chang, 8/2/90, (PB91-190751, A05, MF-A01).

NCEER-91-0001 "Proceedings from the Third Japan-U.S. Workshop on Earthquake Resistant Design of Lifeline Facilities and Countermeasures for Soil Liquefaction, December 17-19, 1990," edited by T.D. O'Rourke and M. Hamada, 2/1/91, (PB91-179259, A99, MF-A04).

NCEER-91-0002 "Physical Space Solutions of Non-Proportionally Damped Systems," by M. Tong, Z. Liang and G.C. Lee, 1/15/91, (PB91-179242, A04, MF-A01).

NCEER-91-0003 "Seismic Response of Single Piles and Pile Groups," by K. Fan and G. Gazetas, 1/10/91, (PB92-174994, A04, MF-A01).

NCEER-91-0004 "Damping of Structures: Part 1 - Theory of Complex Damping," by Z. Liang and G. Lee, 10/10/91, (PB92-197235, A12, MF-A03).

NCEER-91-0005 "3D-BASIS - Nonlinear Dynamic Analysis of Three Dimensional Base Isolated Structures: Part II," by S. Nagarajaiah, A.M. Reinhorn and M.C. Constantinou, 2/28/91, (PB91-190553, A07, MF-A01). This report has been replaced by NCEER-93-0011.

NCEER-91-0006 "A Multidimensional Hysteretic Model for Plasticity Deforming Metals in Energy Absorbing Devices," by E.J. Graesser and F.A. Cozzarelli, 4/9/91, (PB92-108364, A04, MF-A01).

NCEER-91-0007 "A Framework for Customizable Knowledge-Based Expert Systems with an Application to a KBES for Evaluating the Seismic Resistance of Existing Buildings," by E.G. Ibarra-Anaya and S.J. Fenves, 4/9/91, (PB91-210930, A08, MF-A01).

NCEER-91-0008 "Nonlinear Analysis of Steel Frames with Semi-Rigid Connections Using the Capacity Spectrum Method," by G.G. Deierlein, S-H. Hsieh, Y-J. Shen and J.F. Abel, 7/2/91, (PB92-113828, A05, MF-A01).

NCEER-91-0009 "Earthquake Education Materials for Grades K-12," by K.E.K. Ross, 4/30/91, (PB91-212142, A06, MF-A01). This report has been replaced by NCEER-92-0018.

NCEER-91-0010 "Phase Wave Velocities and Displacement Phase Differences in a Harmonically Oscillating Pile," by N. Makris and G. Gazetas, 7/8/91, (PB92-108356, A04, MF-A01).

NCEER-91-0011 "Dynamic Characteristics of a Full-Size Five-Story Steel Structure and a 2/5 Scale Model," by K.C. Chang, G.C. Yao, G.C. Lee, D.S. Hao and Y.C. Yeh," 7/2/91, (PB93-116648, A06, MF-A02).

NCEER-91-0012 "Seismic Response of a 2/5 Scale Steel Structure with Added Viscoelastic Dampers," by K.C. Chang, T.T. Soong, S-T. Oh and M.L. Lai, 5/17/91, (PB92-110816, A05, MF-A01).

NCEER-91-0013 "Earthquake Response of Retaining Walls; Full-Scale Testing and Computational Modeling," by S. Alampalli and A-W.M. Elgamal, 6/20/91, to be published.

NCEER-91-0014 "3D-BASIS-M: Nonlinear Dynamic Analysis of Multiple Building Base Isolated Structures," by P.C. Tsopelas, S. Nagarajaiah, M.C. Constantinou and A.M. Reinhorn, 5/28/91, (PB92-113885, A09, MF-A02).

NCEER-91-0015 "Evaluation of SEAOC Design Requirements for Sliding Isolated Structures," by D. Theodossiou and M.C. Constantinou, 6/10/91, (PB92-114602, A11, MF-A03).

NCEER-91-0016 "Closed-Loop Modal Testing of a 27-Story Reinforced Concrete Flat Plate-Core Building," by H.R. Somaprasad, T. Toksoy, H. Yoshiyuki and A.E. Aktan, 7/15/91, (PB92-129980, A07, MF-A02).

NCEER-91-0017 "Shake Table Test of a 1/6 Scale Two-Story Lightly Reinforced Concrete Building," by A.G. El-Attar, R.N. White and P. Gergely, 2/28/91, (PB92-222447, A06, MF-A02).

NCEER-91-0018 "Shake Table Test of a 1/8 Scale Three-Story Lightly Reinforced Concrete Building," by A.G. El-Attar, R.N. White and P. Gergely, 2/28/91, (PB93-116630, A08, MF-A02).

NCEER-91-0019 "Transfer Functions for Rigid Rectangular Foundations," by A.S. Veletsos, A.M. Prasad and W.H. Wu, 7/31/91, to be published.

NCEER-91-0020 "Hybrid Control of Seismic-Excited Nonlinear and Inelastic Structural Systems," by J.N. Yang, Z. Li and A. Danielians, 8/1/91, (PB92-143171, A06, MF-A02).

NCEER-91-0021 "The NCEER-91 Earthquake Catalog: Improved Intensity-Based Magnitudes and Recurrence Relations for U.S. Earthquakes East of New Madrid," by L. Seeber and J.G. Armbruster, 8/28/91, (PB92-176742, A06, MF-A02).

NCEER-91-0022 "Proceedings from the Implementation of Earthquake Planning and Education in Schools: The Need for Change - The Roles of the Changemakers," by K.E.K. Ross and F. Winslow, 7/23/91, (PB92-129998, A12, MF-A03).

NCEER-91-0023 "A Study of Reliability-Based Criteria for Seismic Design of Reinforced Concrete Frame Buildings," by H.H.M. Hwang and H-M. Hsu, 8/10/91, (PB92-140235, A09, MF-A02).

NCEER-91-0024 "Experimental Verification of a Number of Structural System Identification Algorithms," by R.G. Ghanem, H. Gavin and M. Shinozuka, 9/18/91, (PB92-176577, A18, MF-A04).

NCEER-91-0025 "Probabilistic Evaluation of Liquefaction Potential," by H.H.M. Hwang and C.S. Lee," 11/25/91, (PB92-143429, A05, MF-A01).

NCEER-91-0026 "Instantaneous Optimal Control for Linear, Nonlinear and Hysteretic Structures - Stable Controllers," by J.N. Yang and Z. Li, 11/15/91, (PB92-163807, A04, MF-A01).

NCEER-91-0027 "Experimental and Theoretical Study of a Sliding Isolation System for Bridges," by M.C. Constantinou, A. Kartoum, A.M. Reinhorn and P. Bradford, 11/15/91, (PB92-176973, A10, MF-A03).

NCEER-92-0001 "Case Studies of Liquefaction and Lifeline Performance During Past Earthquakes, Volume 1: Japanese Case Studies," Edited by M. Hamada and T. O'Rourke, 2/17/92, (PB92-197243, A18, MF-A04).

NCEER-92-0002 "Case Studies of Liquefaction and Lifeline Performance During Past Earthquakes, Volume 2: United States Case Studies," Edited by T. O'Rourke and M. Hamada, 2/17/92, (PB92-197250, A20, MF-A04).

NCEER-92-0003 "Issues in Earthquake Education," Edited by K. Ross, 2/3/92, (PB92-222389, A07, MF-A02).

NCEER-92-0004 "Proceedings from the First U.S. - Japan Workshop on Earthquake Protective Systems for Bridges," Edited by I.G. Buckle, 2/4/92, (PB94-142239, A99, MF-A06).

NCEER-92-0005 "Seismic Ground Motion from a Haskell-Type Source in a Multiple-Layered Half-Space," A.P. Theoharis, G. Deodatis and M. Shinozuka, 1/2/92, to be published.

NCEER-92-0006 "Proceedings from the Site Effects Workshop," Edited by R. Whitman, 2/29/92, (PB92-197201, A04, MF-A01).

NCEER-92-0007 "Engineering Evaluation of Permanent Ground Deformations Due to Seismically-Induced Liquefaction," by M.H. Baziar, R. Dobry and A-W.M. Elgamal, 3/24/92, (PB92-222421, A13, MF-A03).

NCEER-92-0008 "A Procedure for the Seismic Evaluation of Buildings in the Central and Eastern United States," by C.D. Poland and J.O. Malley, 4/2/92, (PB92-222439, A20, MF-A04).

NCEER-92-0009 "Experimental and Analytical Study of a Hybrid Isolation System Using Friction Controllable Sliding Bearings," by M.Q. Feng, S. Fujii and M. Shinozuka, 5/15/92, (PB93-150282, A06, MF-A02).

NCEER-92-0010 "Seismic Resistance of Slab-Column Connections in Existing Non-Ductile Flat-Plate Buildings," by A.J. Durrani and Y. Du, 5/18/92, (PB93-116812, A06, MF-A02).

NCEER-92-0011 "The Hysteretic and Dynamic Behavior of Brick Masonry Walls Upgraded by Ferrocement Coatings Under Cyclic Loading and Strong Simulated Ground Motion," by H. Lee and S.P. Prawel, 5/11/92, to be published.

NCEER-92-0012 "Study of Wire Rope Systems for Seismic Protection of Equipment in Buildings," by G.F. Demetriades, M.C. Constantinou and A.M. Reinhorn, 5/20/92, (PB93-116655, A08, MF-A02).

NCEER-92-0013 "Shape Memory Structural Dampers: Material Properties, Design and Seismic Testing," by P.R. Witting and F.A. Cozzarelli, 5/26/92, (PB93-116663, A05, MF-A01).

NCEER-92-0014 "Longitudinal Permanent Ground Deformation Effects on Buried Continuous Pipelines," by M.J. O'Rourke, and C. Nordberg, 6/15/92, (PB93-116671, A08, MF-A02).

NCEER-92-0015 "A Simulation Method for Stationary Gaussian Random Functions Based on the Sampling Theorem," by M. Grigoriu and S. Balopoulou, 6/11/92, (PB93-127496, A05, MF-A01).

NCEER-92-0016 "Gravity-Load-Designed Reinforced Concrete Buildings: Seismic Evaluation of Existing Construction and Detailing Strategies for Improved Seismic Resistance," by G.W. Hoffmann, S.K. Kunnath, A.M. Reinhorn and J.B. Mander, 7/15/92, (PB94-142007, A08, MF-A02).

NCEER-92-0017 "Observations on Water System and Pipeline Performance in the Limón Area of Costa Rica Due to the April 22, 1991 Earthquake," by M. O'Rourke and D. Ballantyne, 6/30/92, (PB93-126811, A06, MF-A02).

NCEER-92-0018 "Fourth Edition of Earthquake Education Materials for Grades K-12," Edited by K.E.K. Ross, 8/10/92, (PB93-114023, A07, MF-A02).

NCEER-92-0019 "Proceedings from the Fourth Japan-U.S. Workshop on Earthquake Resistant Design of Lifeline Facilities and Countermeasures for Soil Liquefaction," Edited by M. Hamada and T.D. O'Rourke, 8/12/92, (PB93-163939, A99, MF-E11).

NCEER-92-0020 "Active Bracing System: A Full Scale Implementation of Active Control," by A.M. Reinhorn, T.T. Soong, R.C. Lin, M.A. Riley, Y.P. Wang, S. Aizawa and M. Higashino, 8/14/92, (PB93-127512, A06, MF-A02).

NCEER-92-0021 "Empirical Analysis of Horizontal Ground Displacement Generated by Liquefaction-Induced Lateral Spreads," by S.F. Bartlett and T.L. Youd, 8/17/92, (PB93-188241, A06, MF-A02).

NCEER-92-0022 "IDARC Version 3.0: Inelastic Damage Analysis of Reinforced Concrete Structures," by S.K. Kunnath, A.M. Reinhorn and R.F. Lobo, 8/31/92, (PB93-227502, A07, MF-A02).

NCEER-92-0023 "A Semi-Empirical Analysis of Strong-Motion Peaks in Terms of Seismic Source, Propagation Path and Local Site Conditions, by M. Kamiyama, M.J. O'Rourke and R. Flores-Berrones, 9/9/92, (PB93-150266, A08, MF-A02).

NCEER-92-0024 "Seismic Behavior of Reinforced Concrete Frame Structures with Nonductile Details, Part I: Summary of Experimental Findings of Full Scale Beam-Column Joint Tests," by A. Beres, R.N. White and P. Gergely, 9/30/92, (PB93-227783, A05, MF-A01).

NCEER-92-0025 "Experimental Results of Repaired and Retrofitted Beam-Column Joint Tests in Lightly Reinforced Concrete Frame Buildings," by A. Beres, S. El-Borgi, R.N. White and P. Gergely, 10/29/92, (PB93-227791, A05, MF-A01).

NCEER-92-0026 "A Generalization of Optimal Control Theory: Linear and Nonlinear Structures," by J.N. Yang, Z. Li and S. Vongchavalitkul, 11/2/92, (PB93-188621, A05, MF-A01).

NCEER-92-0027 "Seismic Resistance of Reinforced Concrete Frame Structures Designed Only for Gravity Loads: Part I - Design and Properties of a One-Third Scale Model Structure," by J.M. Bracci, A.M. Reinhorn and J.B. Mander, 12/1/92, (PB94-104502, A08, MF-A02).

NCEER-92-0028 "Seismic Resistance of Reinforced Concrete Frame Structures Designed Only for Gravity Loads: Part II - Experimental Performance of Subassemblages," by L.E. Aycardi, J.B. Mander and A.M. Reinhorn, 12/1/92, (PB94-104510, A08, MF-A02).

NCEER-92-0029 "Seismic Resistance of Reinforced Concrete Frame Structures Designed Only for Gravity Loads: Part III - Experimental Performance and Analytical Study of a Structural Model," by J.M. Bracci, A.M. Reinhorn and J.B. Mander, 12/1/92, (PB93-227528, A09, MF-A01).

NCEER-92-0030 "Evaluation of Seismic Retrofit of Reinforced Concrete Frame Structures: Part I - Experimental Performance of Retrofitted Subassemblages," by D. Choudhuri, J.B. Mander and A.M. Reinhorn, 12/8/92, (PB93-198307, A07, MF-A02).

NCEER-92-0031 "Evaluation of Seismic Retrofit of Reinforced Concrete Frame Structures: Part II - Experimental Performance and Analytical Study of a Retrofitted Structural Model," by J.M. Bracci, A.M. Reinhorn and J.B. Mander, 12/8/92, (PB93-198315, A09, MF-A03).

NCEER-92-0032 "Experimental and Analytical Investigation of Seismic Response of Structures with Supplemental Fluid Viscous Dampers," by M.C. Constantinou and M.D. Symans, 12/21/92, (PB93-191435, A10, MF-A03). This report is available only through NTIS (see address given above).

NCEER-92-0033 "Reconnaissance Report on the Cairo, Egypt Earthquake of October 12, 1992," by M. Khater, 12/23/92, (PB93-188621, A03, MF-A01).

NCEER-92-0034 "Low-Level Dynamic Characteristics of Four Tall Flat-Plate Buildings in New York City," by H. Gavin, S. Yuan, J. Grossman, E. Pekelis and K. Jacob, 12/28/92, (PB93-188217, A07, MF-A02).

NCEER-93-0001 "An Experimental Study on the Seismic Performance of Brick-Infilled Steel Frames With and Without Retrofit," by J.B. Mander, B. Nair, K. Wojtkowski and J. Ma, 1/29/93, (PB93-227510, A07, MF-A02).

NCEER-93-0002 "Social Accounting for Disaster Preparedness and Recovery Planning," by S. Cole, E. Pantoja and V. Razak, 2/22/93, (PB94-142114, A12, MF-A03).

NCEER-93-0003 "Assessment of 1991 NEHRP Provisions for Nonstructural Components and Recommended Revisions," by T.T. Soong, G. Chen, Z. Wu, R-H. Zhang and M. Grigoriu, 3/1/93, (PB93-188639, A06, MF-A02).

NCEER-93-0004 "Evaluation of Static and Response Spectrum Analysis Procedures of SEAOC/UBC for Seismic Isolated Structures," by C.W. Winters and M.C. Constantinou, 3/23/93, (PB93-198299, A10, MF-A03).

NCEER-93-0005 "Earthquakes in the Northeast - Are We Ignoring the Hazard? A Workshop on Earthquake Science and Safety for Educators," edited by K.E.K. Ross, 4/2/93, (PB94-103066, A09, MF-A02).

NCEER-93-0006 "Inelastic Response of Reinforced Concrete Structures with Viscoelastic Braces," by R.F. Lobo, J.M. Bracci, K.L. Shen, A.M. Reinhorn and T.T. Soong, 4/5/93, (PB93-227486, A05, MF-A02).

NCEER-93-0007 "Seismic Testing of Installation Methods for Computers and Data Processing Equipment," by K. Kosar, T.T. Soong, K.L. Shen, J.A. HoLung and Y.K. Lin, 4/12/93, (PB93-198299, A07, MF-A02).

NCEER-93-0008 "Retrofit of Reinforced Concrete Frames Using Added Dampers," by A. Reinhorn, M. Constantinou and C. Li, to be published.

NCEER-93-0009 "Seismic Behavior and Design Guidelines for Steel Frame Structures with Added Viscoelastic Dampers," by K.C. Chang, M.L. Lai, T.T. Soong, D.S. Hao and Y.C. Yeh, 5/1/93, (PB94-141959, A07, MF-A02).

NCEER-93-0010 "Seismic Performance of Shear-Critical Reinforced Concrete Bridge Piers," by J.B. Mander, S.M. Waheed, M.T.A. Chaudhary and S.S. Chen, 5/12/93, (PB93-227494, A08, MF-A02).

NCEER-93-0011 "3D-BASIS-TABS: Computer Program for Nonlinear Dynamic Analysis of Three Dimensional Base Isolated Structures," by S. Nagarajaiah, C. Li, A.M. Reinhorn and M.C. Constantinou, 8/2/93, (PB94-141819, A09, MF-A02).

NCEER-93-0012 "Effects of Hydrocarbon Spills from an Oil Pipeline Break on Ground Water," by O.J. Helweg and H.H.M. Hwang, 8/3/93, (PB94-141942, A06, MF-A02).

NCEER-93-0013 "Simplified Procedures for Seismic Design of Nonstructural Components and Assessment of Current Code Provisions," by M.P. Singh, L.E. Suarez, E.E. Matheu and G.O. Maldonado, 8/4/93, (PB94-141827, A09, MF-A02).

NCEER-93-0014 "An Energy Approach to Seismic Analysis and Design of Secondary Systems," by G. Chen and T.T. Soong, 8/6/93, (PB94-142767, A11, MF-A03).

NCEER-93-0015 "Proceedings from School Sites: Becoming Prepared for Earthquakes - Commemorating the Third Anniversary of the Loma Prieta Earthquake," Edited by F.E. Winslow and K.E.K. Ross, 8/16/93, (PB94-154275, A16, MF-A02).

NCEER-93-0016 "Reconnaissance Report of Damage to Historic Monuments in Cairo, Egypt Following the October 12, 1992 Dahshur Earthquake," by D. Sykora, D. Look, G. Croci, E. Karaesmen and E. Karaesmen, 8/19/93, (PB94-142221, A08, MF-A02).

NCEER-93-0017 "The Island of Guam Earthquake of August 8, 1993," by S.W. Swan and S.K. Harris, 9/30/93, (PB94-141843, A04, MF-A01).

NCEER-93-0018 "Engineering Aspects of the October 12, 1992 Egyptian Earthquake," by A.W. Elgamal, M. Amer, K. Adalier and A. Abul-Fadl, 10/7/93, (PB94-141983, A05, MF-A01).

NCEER-93-0019 "Development of an Earthquake Motion Simulator and its Application in Dynamic Centrifuge Testing," by I. Krstelj, Supervised by J.H. Prevost, 10/23/93, (PB94-181773, A-10, MF-A03).

NCEER-93-0020 "NCEER-Taisei Corporation Research Program on Sliding Seismic Isolation Systems for Bridges: Experimental and Analytical Study of a Friction Pendulum System (FPS)," by M.C. Constantinou, P. Tsopelas, Y-S. Kim and S. Okamoto, 11/1/93, (PB94-142775, A08, MF-A02).

NCEER-93-0021 "Finite Element Modeling of Elastomeric Seismic Isolation Bearings," by L.J. Billings, Supervised by R. Shepherd, 11/8/93, to be published.

NCEER-93-0022 "Seismic Vulnerability of Equipment in Critical Facilities: Life-Safety and Operational Consequences," by K. Porter, G.S. Johnson, M.M. Zadeh, C. Scawthorn and S. Eder, 11/24/93, (PB94-181765, A16, MF-A03).

NCEER-93-0023 "Hokkaido Nansei-oki, Japan Earthquake of July 12, 1993, by P.I. Yanev and C.R. Scawthorn, 12/23/93, (PB94-181500, A07, MF-A01).

NCEER-94-0001 "An Evaluation of Seismic Serviceability of Water Supply Networks with Application to the San Francisco Auxiliary Water Supply System," by I. Markov, Supervised by M. Grigoriu and T. O'Rourke, 1/21/94, (PB94-204013, A07, MF-A02).

NCEER-94-0002 "NCEER-Taisei Corporation Research Program on Sliding Seismic Isolation Systems for Bridges: Experimental and Analytical Study of Systems Consisting of Sliding Bearings, Rubber Restoring Force Devices and Fluid Dampers," Volumes I and II, by P. Tsopelas, S. Okamoto, M.C. Constantinou, D. Ozaki and S. Fujii, 2/4/94, (PB94-181740, A09, MF-A02 and PB94-181757, A12, MF-A03).

NCEER-94-0003 "A Markov Model for Local and Global Damage Indices in Seismic Analysis," by S. Rahman and M. Grigoriu, 2/18/94, (PB94-206000, A12, MF-A03).

NCEER-94-0004 "Proceedings from the NCEER Workshop on Seismic Response of Masonry Infills," edited by D.P. Abrams, 3/1/94, (PB94-180783, A07, MF-A02).

NCEER-94-0005 "The Northridge, California Earthquake of January 17, 1994: General Reconnaissance Report," edited by J.D. Goltz, 3/11/94, (PB94-193943, A10, MF-A03).

NCEER-94-0006 "Seismic Energy Based Fatigue Damage Analysis of Bridge Columns: Part I - Evaluation of Seismic Capacity," by G.A. Chang and J.B. Mander, 3/14/94, (PB94-219185, A11, MF-A03).

NCEER-94-0007 "Seismic Isolation of Multi-Story Frame Structures Using Spherical Sliding Isolation Systems," by T.M. Al-Hussaini, V.A. Zayas and M.C. Constantinou, 3/17/94, (PB94-193745, A09, MF-A02).

NCEER-94-0008 "The Northridge, California Earthquake of January 17, 1994: Performance of Highway Bridges," edited by I.G. Buckle, 3/24/94, (PB94-193851, A06, MF-A02).

NCEER-94-0009 "Proceedings of the Third U.S.-Japan Workshop on Earthquake Protective Systems for Bridges," edited by I.G. Buckle and I. Friedland, 3/31/94, (PB94-195815, A99, MF-A06).

NCEER-94-0010 "3D-BASIS-ME: Computer Program for Nonlinear Dynamic Analysis of Seismically Isolated Single and Multiple Structures and Liquid Storage Tanks," by P.C. Tsopelas, M.C. Constantinou and A.M. Reinhorn, 4/12/94, (PB94-204922, A09, MF-A02).

NCEER-94-0011 "The Northridge, California Earthquake of January 17, 1994: Performance of Gas Transmission Pipelines," by T.D. O'Rourke and M.C. Palmer, 5/16/94, (PB94-204989, A05, MF-A01).

NCEER-94-0012 "Feasibility Study of Replacement Procedures and Earthquake Performance Related to Gas Transmission Pipelines," by T.D. O'Rourke and M.C. Palmer, 5/25/94, (PB94-206638, A09, MF-A02).

NCEER-94-0013 "Seismic Energy Based Fatigue Damage Analysis of Bridge Columns: Part II - Evaluation of Seismic Demand," by G.A. Chang and J.B. Mander, 6/1/94, (PB95-18106, A08, MF-A02).

NCEER-94-0014 "NCEER-Taisei Corporation Research Program on Sliding Seismic Isolation Systems for Bridges: Experimental and Analytical Study of a System Consisting of Sliding Bearings and Fluid Restoring Force/Damping Devices," by P. Tsopelas and M.C. Constantinou, 6/13/94, (PB94-219144, A10, MF-A03).

NCEER-94-0015 "Generation of Hazard-Consistent Fragility Curves for Seismic Loss Estimation Studies," by H. Hwang and J-R. Huo, 6/14/94, (PB95-181996, A09, MF-A02).

NCEER-94-0016 "Seismic Study of Building Frames with Added Energy-Absorbing Devices," by W.S. Pong, C.S. Tsai and G.C. Lee, 6/20/94, (PB94-219136, A10, A03).

NCEER-94-0017 "Sliding Mode Control for Seismic-Excited Linear and Nonlinear Civil Engineering Structures," by J. Yang, J. Wu, A. Agrawal and Z. Li, 6/21/94, (PB95-138483, A06, MF-A02).

NCEER-94-0018 "3D-BASIS-TABS Version 2.0: Computer Program for Nonlinear Dynamic Analysis of Three Dimensional Base Isolated Structures," by A.M. Reinhorn, S. Nagarajaiah, M.C. Constantinou, P. Tsopelas and R. Li, 6/22/94, (PB95-182176, A08, MF-A02).

NCEER-94-0019 "Proceedings of the International Workshop on Civil Infrastructure Systems: Application of Intelligent Systems and Advanced Materials on Bridge Systems," Edited by G.C. Lee and K.C. Chang, 7/18/94, (PB95-252474, A20, MF-A04).

NCEER-94-0020 "Study of Seismic Isolation Systems for Computer Floors," by V. Lambrou and M.C. Constantinou, 7/19/94, (PB95-138533, A10, MF-A03).

NCEER-94-0021 "Proceedings of the U.S.-Italian Workshop on Guidelines for Seismic Evaluation and Rehabilitation of Unreinforced Masonry Buildings," Edited by D.P. Abrams and G.M. Calvi, 7/20/94, (PB95-138749, A13, MF-A03).

NCEER-94-0022 "NCEER-Taisei Corporation Research Program on Sliding Seismic Isolation Systems for Bridges: Experimental and Analytical Study of a System Consisting of Lubricated PTFE Sliding Bearings and Mild Steel Dampers," by P. Tsopelas and M.C. Constantinou, 7/22/94, (PB95-182184, A08, MF-A02).

NCEER-94-0023 “Development of Reliability-Based Design Criteria for Buildings Under Seismic Load,” by Y.K. Wen, H. Hwang and M. Shinozuka, 8/1/94, (PB95-211934, A08, MF-A02).

NCEER-94-0024 “Experimental Verification of Acceleration Feedback Control Strategies for an Active Tendon System,” by S.J. Dyke, B.F. Spencer, Jr., P. Quast, M.K. Sain, D.C. Kaspari, Jr. and T.T. Soong, 8/29/94, (PB95-212320, A05, MF-A01).

NCEER-94-0025 “Seismic Retrofitting Manual for Highway Bridges,” Edited by I.G. Buckle and I.F. Friedland, published by the Federal Highway Administration (PB95-212676, A15, MF-A03).

NCEER-94-0026 “Proceedings from the Fifth U.S.-Japan Workshop on Earthquake Resistant Design of Lifeline Facilities and Countermeasures Against Soil Liquefaction,” Edited by T.D. O’Rourke and M. Hamada, 11/7/94, (PB95-220802, A99, MF-E08).

NCEER-95-0001 "Experimental and Analytical Investigation of Seismic Retrofit of Structures with Supplemental Damping: Part 1 - Fluid Viscous Damping Devices," by A.M. Reinhorn, C. Li and M.C. Constantinou, 1/3/95, (PB95-266599, A09, MF-A02).

NCEER-95-0002 "Experimental and Analytical Study of Low-Cycle Fatigue Behavior of Semi-Rigid Top-And-Seat Angle Connections," by G. Pekcan, J.B. Mander and S.S. Chen, 1/5/95, (PB95-220042, A07, MF-A02).

NCEER-95-0003 "NCEER-ATC Joint Study on Fragility of Buildings," by T. Anagnos, C. Rojahn and A.S. Kiremidjian, 1/20/95, (PB95-220026, A06, MF-A02).

NCEER-95-0004 "Nonlinear Control Algorithms for Peak Response Reduction," by Z. Wu, T.T. Soong, V. Gattulli and R.C. Lin, 2/16/95, (PB95-220349, A05, MF-A01).

NCEER-95-0005 "Pipeline Replacement Feasibility Study: A Methodology for Minimizing Seismic and Corrosion Risks to Underground Natural Gas Pipelines," by R.T. Eguchi, H.A. Seligson and D.G. Honegger, 3/2/95, (PB95-252326, A06, MF-A02).

NCEER-95-0006 "Evaluation of Seismic Performance of an 11-Story Frame Building During the 1994 Northridge Earthquake," by F. Naeim, R. DiSulio, K. Benuska, A. Reinhorn and C. Li, to be published.

NCEER-95-0007 "Prioritization of Bridges for Seismic Retrofitting," by N. Basöz and A.S. Kiremidjian, 4/24/95, (PB95-252300, A08, MF-A02).

NCEER-95-0008 "Method for Developing Motion Damage Relationships for Reinforced Concrete Frames," by A. Singhal and A.S. Kiremidjian, 5/11/95, (PB95-266607, A06, MF-A02).

NCEER-95-0009 "Experimental and Analytical Investigation of Seismic Retrofit of Structures with Supplemental Damping: Part II - Friction Devices," by C. Li and A.M. Reinhorn, 7/6/95, (PB96-128087, A11, MF-A03).

NCEER-95-0010 "Experimental Performance and Analytical Study of a Non-Ductile Reinforced Concrete Frame Structure Retrofitted with Elastomeric Spring Dampers," by G. Pekcan, J.B. Mander and S.S. Chen, 7/14/95, (PB96-137161, A08, MF-A02).

NCEER-95-0011 "Development and Experimental Study of Semi-Active Fluid Damping Devices for Seismic Protection of Structures," by M.D. Symans and M.C. Constantinou, 8/3/95, (PB96-136940, A23, MF-A04).

NCEER-95-0012 "Real-Time Structural Parameter Modification (RSPM): Development of Innervated Structures," by Z. Liang, M. Tong and G.C. Lee, 4/11/95, (PB96-137153, A06, MF-A01).

NCEER-95-0013 "Experimental and Analytical Investigation of Seismic Retrofit of Structures with Supplemental Damping: Part III - Viscous Damping Walls," by A.M. Reinhorn and C. Li, 10/1/95, (PB96-176409, A11, MF-A03).

NCEER-95-0014 "Seismic Fragility Analysis of Equipment and Structures in a Memphis Electric Substation," by J-R. Huo and H.H.M. Hwang, 8/10/95, (PB96-128087, A09, MF-A02).

NCEER-95-0015 "The Hanshin-Awaji Earthquake of January 17, 1995: Performance of Lifelines," Edited by M. Shinozuka, 11/3/95, (PB96-176383, A15, MF-A03).

NCEER-95-0016 "Highway Culvert Performance During Earthquakes," by T.L. Youd and C.J. Beckman, available as NCEER-96-0015.

NCEER-95-0017 "The Hanshin-Awaji Earthquake of January 17, 1995: Performance of Highway Bridges," Edited by I.G. Buckle, 12/1/95, to be published.

NCEER-95-0018 "Modeling of Masonry Infill Panels for Structural Analysis," by A.M. Reinhorn, A. Madan, R.E. Valles, Y. Reichmann and J.B. Mander, 12/8/95, (PB97-110886, MF-A01, A06).

NCEER-95-0019 "Optimal Polynomial Control for Linear and Nonlinear Structures," by A.K. Agrawal and J.N. Yang, 12/11/95, (PB96-168737, A07, MF-A02).

NCEER-95-0020 "Retrofit of Non-Ductile Reinforced Concrete Frames Using Friction Dampers," by R.S. Rao, P. Gergely and R.N. White, 12/22/95, (PB97-133508, A10, MF-A02).

NCEER-95-0021 "Parametric Results for Seismic Response of Pile-Supported Bridge Bents," by G. Mylonakis, A. Nikolaou and G. Gazetas, 12/22/95, (PB97-100242, A12, MF-A03).

NCEER-95-0022 "Kinematic Bending Moments in Seismically Stressed Piles," by A. Nikolaou, G. Mylonakis and G. Gazetas, 12/23/95, (PB97-113914, MF-A03, A13).

NCEER-96-0001 "Dynamic Response of Unreinforced Masonry Buildings with Flexible Diaphragms," by A.C. Costley and D.P. Abrams," 10/10/96, (PB97-133573, MF-A03, A15).

NCEER-96-0002 "State of the Art Review: Foundations and Retaining Structures," by I. Po Lam, to be published.

NCEER-96-0003 "Ductility of Rectangular Reinforced Concrete Bridge Columns with Moderate Confinement," by N. Wehbe, M. Saiidi, D. Sanders and B. Douglas, 11/7/96, (PB97-133557, A06, MF-A02).

NCEER-96-0004 "Proceedings of the Long-Span Bridge Seismic Research Workshop," edited by I.G. Buckle and I.M. Friedland, to be published.

NCEER-96-0005 "Establish Representative Pier Types for Comprehensive Study: Eastern United States," by J. Kulicki and Z. Prucz, 5/28/96, (PB98-119217, A07, MF-A02).

NCEER-96-0006 "Establish Representative Pier Types for Comprehensive Study: Western United States," by R. Imbsen, R.A. Schamber and T.A. Osterkamp, 5/28/96, (PB98-118607, A07, MF-A02).

NCEER-96-0007 "Nonlinear Control Techniques for Dynamical Systems with Uncertain Parameters," by R.G. Ghanem and M.I. Bujakov, 5/27/96, (PB97-100259, A17, MF-A03).

NCEER-96-0008 "Seismic Evaluation of a 30-Year Old Non-Ductile Highway Bridge Pier and Its Retrofit," by J.B. Mander, B. Mahmoodzadegan, S. Bhadra and S.S. Chen, 5/31/96, (PB97-110902, MF-A03, A10).

NCEER-96-0009 "Seismic Performance of a Model Reinforced Concrete Bridge Pier Before and After Retrofit," by J.B. Mander, J.H. Kim and C.A. Ligozio, 5/31/96, (PB97-110910, MF-A02, A10).

NCEER-96-0010 "IDARC2D Version 4.0: A Computer Program for the Inelastic Damage Analysis of Buildings," by R.E. Valles, A.M. Reinhorn, S.K. Kunnath, C. Li and A. Madan, 6/3/96, (PB97-100234, A17, MF-A03).

NCEER-96-0011 "Estimation of the Economic Impact of Multiple Lifeline Disruption: Memphis Light, Gas and Water Division Case Study," by S.E. Chang, H.A. Seligson and R.T. Eguchi, 8/16/96, (PB97-133490, A11, MF-A03).

NCEER-96-0012 "Proceedings from the Sixth Japan-U.S. Workshop on Earthquake Resistant Design of Lifeline Facilities and Countermeasures Against Soil Liquefaction, Edited by M. Hamada and T. O'Rourke, 9/11/96, (PB97-133581, A99, MF-A06).

NCEER-96-0013 "Chemical Hazards, Mitigation and Preparedness in Areas of High Seismic Risk: A Methodology for Estimating the Risk of Post-Earthquake Hazardous Materials Release," by H.A. Seligson, R.T. Eguchi, K.J. Tierney and K. Richmond, 11/7/96, (PB97-133565, MF-A02, A08).

NCEER-96-0014 "Response of Steel Bridge Bearings to Reversed Cyclic Loading," by J.B. Mander, D-K. Kim, S.S. Chen and G.J. Premus, 11/13/96, (PB97-140735, A12, MF-A03).

NCEER-96-0015 "Highway Culvert Performance During Past Earthquakes," by T.L. Youd and C.J. Beckman, 11/25/96, (PB97-133532, A06, MF-A01).

NCEER-97-0001 "Evaluation, Prevention and Mitigation of Pounding Effects in Building Structures," by R.E. Valles and A.M. Reinhorn, 2/20/97, (PB97-159552, A14, MF-A03).

NCEER-97-0002 "Seismic Design Criteria for Bridges and Other Highway Structures," by C. Rojahn, R. Mayes, D.G. Anderson, J. Clark, J.H. Hom, R.V. Nutt and M.J. O'Rourke, 4/30/97, (PB97-194658, A06, MF-A03).

NCEER-97-0003 “Proceedings of the U.S.-Italian Workshop on Seismic Evaluation and Retrofit,” Edited by D.P. Abrams and G.M. Calvi, 3/19/97, (PB97-194666, A13, MF-A03).

NCEER-97-0004 "Investigation of Seismic Response of Buildings with Linear and Nonlinear Fluid Viscous Dampers," by A.A. Seleemah and M.C. Constantinou, 5/21/97, (PB98-109002, A15, MF-A03).

NCEER-97-0005 "Proceedings of the Workshop on Earthquake Engineering Frontiers in Transportation Facilities," edited by G.C. Lee and I.M. Friedland, 8/29/97, (PB98-128911, A25, MR-A04).

NCEER-97-0006 "Cumulative Seismic Damage of Reinforced Concrete Bridge Piers," by S.K. Kunnath, A. El-Bahy, A. Taylor and W. Stone, 9/2/97, (PB98-108814, A11, MF-A03).

NCEER-97-0007 "Structural Details to Accommodate Seismic Movements of Highway Bridges and Retaining Walls," by R.A. Imbsen, R.A. Schamber, E. Thorkildsen, A. Kartoum, B.T. Martin, T.N. Rosser and J.M. Kulicki, 9/3/97, (PB98-108996, A09, MF-A02).

NCEER-97-0008 "A Method for Earthquake Motion-Damage Relationships with Application to Reinforced Concrete Frames," by A. Singhal and A.S. Kiremidjian, 9/10/97, (PB98-108988, A13, MF-A03).

NCEER-97-0009 "Seismic Analysis and Design of Bridge Abutments Considering Sliding and Rotation," by K. Fishman and R. Richards, Jr., 9/15/97, (PB98-108897, A06, MF-A02).

NCEER-97-0010 "Proceedings of the FHWA/NCEER Workshop on the National Representation of Seismic Ground Motion for New and Existing Highway Facilities," edited by I.M. Friedland, M.S. Power and R.L. Mayes, 9/22/97, (PB98-128903, A21, MF-A04).

NCEER-97-0011 "Seismic Analysis for Design or Retrofit of Gravity Bridge Abutments," by K.L. Fishman, R. Richards, Jr. and R.C. Divito, 10/2/97, (PB98-128937, A08, MF-A02).

NCEER-97-0012 "Evaluation of Simplified Methods of Analysis for Yielding Structures," by P. Tsopelas, M.C. Constantinou, C.A. Kircher and A.S. Whittaker, 10/31/97, (PB98-128929, A10, MF-A03).

NCEER-97-0013 "Seismic Design of Bridge Columns Based on Control and Repairability of Damage," by C-T. Cheng and J.B. Mander, 12/8/97, (PB98-144249, A11, MF-A03).

NCEER-97-0014 "Seismic Resistance of Bridge Piers Based on Damage Avoidance Design," by J.B. Mander and C-T. Cheng, 12/10/97, (PB98-144223, A09, MF-A02).

NCEER-97-0015 “Seismic Response of Nominally Symmetric Systems with Strength Uncertainty,” by S. Balopoulou and M. Grigoriu, 12/23/97, (PB98-153422, A11, MF-A03).

NCEER-97-0016 “Evaluation of Seismic Retrofit Methods for Reinforced Concrete Bridge Columns,” by T.J. Wipf, F.W. Klaiber and F.M. Russo, 12/28/97, (PB98-144215, A12, MF-A03).

NCEER-97-0017 “Seismic Fragility of Existing Conventional Reinforced Concrete Highway Bridges,” by C.L. Mullen and A.S. Cakmak, 12/30/97, (PB98-153406, A08, MF-A02).

NCEER-97-0018 “Loss Asssessment of Memphis Buildings,” edited by D.P. Abrams and M. Shinozuka, 12/31/97, (PB98-144231, A13, MF-A03).

NCEER-97-0019 “Seismic Evaluation of Frames with Infill Walls Using Quasi-static Experiments,” by K.M. Mosalam, R.N. White and P. Gergely, 12/31/97, (PB98-153455, A07, MF-A02).

NCEER-97-0020 “Seismic Evaluation of Frames with Infill Walls Using Pseudo-dynamic Experiments,” by K.M. Mosalam, R.N. White and P. Gergely, 12/31/97, (PB98-153430, A07, MF-A02).

NCEER-97-0021 “Computational Strategies for Frames with Infill Walls: Discrete and Smeared Crack Analyses and Seismic Fragility,” by K.M. Mosalam, R.N. White and P. Gergely, 12/31/97, (PB98-153414, A10, MF-A02).

NCEER-97-0022 "Proceedings of the NCEER Workshop on Evaluation of Liquefaction Resistance of Soils," edited by T.L. Youd and I.M. Idriss, 12/31/97, (PB98-155617, A15, MF-A03).

MCEER-98-0001 "Extraction of Nonlinear Hysteretic Properties of Seismically Isolated Bridges from Quick-Release Field Tests," by Q. Chen, B.M. Douglas, E.M. Maragakis and I.G. Buckle, 5/26/98, (PB99-118838, A06, MF-A01).

MCEER-98-0002 "Methodologies for Evaluating the Importance of Highway Bridges," by A. Thomas, S. Eshenaur and J. Kulicki, 5/29/98, (PB99-118846, A10, MF-A02).

MCEER-98-0003 "Capacity Design of Bridge Piers and the Analysis of Overstrength," by J.B. Mander, A. Dutta and P. Goel, 6/1/98, (PB99-118853, A09, MF-A02).

MCEER-98-0004 "Evaluation of Bridge Damage Data from the Loma Prieta and Northridge, California Earthquakes," by N. Basoz and A. Kiremidjian, 6/2/98, (PB99-118861, A15, MF-A03).

MCEER-98-0005 "Screening Guide for Rapid Assessment of Liquefaction Hazard at Highway Bridge Sites," by T. L. Youd, 6/16/98, (PB99-118879, A06, not available on microfiche).

MCEER-98-0006 "Structural Steel and Steel/Concrete Interface Details for Bridges," by P. Ritchie, N. Kauhl and J. Kulicki, 7/13/98, (PB99-118945, A06, MF-A01).

MCEER-98-0007 "Capacity Design and Fatigue Analysis of Confined Concrete Columns," by A. Dutta and J.B. Mander, 7/14/98, (PB99-118960, A14, MF-A03).

MCEER-98-0008 "Proceedings of the Workshop on Performance Criteria for Telecommunication Services Under Earthquake Conditions," edited by A.J. Schiff, 7/15/98, (PB99-118952, A08, MF-A02).

MCEER-98-0009 "Fatigue Analysis of Unconfined Concrete Columns," by J.B. Mander, A. Dutta and J.H. Kim, 9/12/98, (PB99-123655, A10, MF-A02).

MCEER-98-0010 "Centrifuge Modeling of Cyclic Lateral Response of Pile-Cap Systems and Seat-Type Abutments in Dry Sands," by A.D. Gadre and R. Dobry, 10/2/98, (PB99-123606, A13, MF-A03).

MCEER-98-0011 "IDARC-BRIDGE: A Computational Platform for Seismic Damage Assessment of Bridge Structures," by A.M. Reinhorn, V. Simeonov, G. Mylonakis and Y. Reichman, 10/2/98, (PB99-162919, A15, MF-A03).

MCEER-98-0012 "Experimental Investigation of the Dynamic Response of Two Bridges Before and After Retrofitting with Elastomeric Bearings," by D.A. Wendichansky, S.S. Chen and J.B. Mander, 10/2/98, (PB99-162927, A15, MF-A03).

MCEER-98-0013 "Design Procedures for Hinge Restrainers and Hinge Sear Width for Multiple-Frame Bridges," by R. Des Roches and G.L. Fenves, 11/3/98, (PB99-140477, A13, MF-A03).

MCEER-98-0014 "Response Modification Factors for Seismically Isolated Bridges," by M.C. Constantinou and J.K. Quarshie, 11/3/98, (PB99-140485, A14, MF-A03).

MCEER-98-0015 "Proceedings of the U.S.-Italy Workshop on Seismic Protective Systems for Bridges," edited by I.M. Friedland and M.C. Constantinou, 11/3/98, (PB2000-101711, A22, MF-A04).

MCEER-98-0016 "Appropriate Seismic Reliability for Critical Equipment Systems: Recommendations Based on Regional Analysis of Financial and Life Loss," by K. Porter, C. Scawthorn, C. Taylor and N. Blais, 11/10/98, (PB99-157265, A08, MF-A02).

MCEER-98-0017 "Proceedings of the U.S. Japan Joint Seminar on Civil Infrastructure Systems Research," edited by M. Shinozuka and A. Rose, 11/12/98, (PB99-156713, A16, MF-A03).

MCEER-98-0018 "Modeling of Pile Footings and Drilled Shafts for Seismic Design," by I. PoLam, M. Kapuskar and D. Chaudhuri, 12/21/98, (PB99-157257, A09, MF-A02).

MCEER-99-0001 "Seismic Evaluation of a Masonry Infilled Reinforced Concrete Frame by Pseudodynamic Testing," by S.G. Buonopane and R.N. White, 2/16/99, (PB99-162851, A09, MF-A02).

MCEER-99-0002 "Response History Analysis of Structures with Seismic Isolation and Energy Dissipation Systems: Verification Examples for Program SAP2000," by J. Scheller and M.C. Constantinou, 2/22/99, (PB99-162869, A08, MF-A02).

MCEER-99-0003 "Experimental Study on the Seismic Design and Retrofit of Bridge Columns Including Axial Load Effects," by A. Dutta, T. Kokorina and J.B. Mander, 2/22/99, (PB99-162877, A09, MF-A02).

MCEER-99-0004 "Experimental Study of Bridge Elastomeric and Other Isolation and Energy Dissipation Systems with Emphasis on Uplift Prevention and High Velocity Near-source Seismic Excitation," by A. Kasalanati and M. C. Constantinou, 2/26/99, (PB99-162885, A12, MF-A03).

MCEER-99-0005 "Truss Modeling of Reinforced Concrete Shear-flexure Behavior," by J.H. Kim and J.B. Mander, 3/8/99, (PB99-163693, A12, MF-A03).

MCEER-99-0006 "Experimental Investigation and Computational Modeling of Seismic Response of a 1:4 Scale Model Steel Structure with a Load Balancing Supplemental Damping System," by G. Pekcan, J.B. Mander and S.S. Chen, 4/2/99, (PB99-162893, A11, MF-A03).

MCEER-99-0007 "Effect of Vertical Ground Motions on the Structural Response of Highway Bridges," by M.R. Button, C.J. Cronin and R.L. Mayes, 4/10/99, (PB2000-101411, A10, MF-A03).

MCEER-99-0008 "Seismic Reliability Assessment of Critical Facilities: A Handbook, Supporting Documentation, and Model Code Provisions," by G.S. Johnson, R.E. Sheppard, M.D. Quilici, S.J. Eder and C.R. Scawthorn, 4/12/99, (PB2000-101701, A18, MF-A04).

MCEER-99-0009 "Impact Assessment of Selected MCEER Highway Project Research on the Seismic Design of Highway Structures," by C. Rojahn, R. Mayes, D.G. Anderson, J.H. Clark, D'Appolonia Engineering, S. Gloyd and R.V. Nutt, 4/14/99, (PB99-162901, A10, MF-A02).

MCEER-99-0010 "Site Factors and Site Categories in Seismic Codes," by R. Dobry, R. Ramos and M.S. Power, 7/19/99, (PB2000-101705, A08, MF-A02).

MCEER-99-0011 "Restrainer Design Procedures for Multi-Span Simply-Supported Bridges," by M.J. Randall, M. Saiidi, E. Maragakis and T. Isakovic, 7/20/99, (PB2000-101702, A10, MF-A02).

MCEER-99-0012 "Property Modification Factors for Seismic Isolation Bearings," by M.C. Constantinou, P. Tsopelas, A. Kasalanati and E. Wolff, 7/20/99, (PB2000-103387, A11, MF-A03).

MCEER-99-0013 "Critical Seismic Issues for Existing Steel Bridges," by P. Ritchie, N. Kauhl and J. Kulicki, 7/20/99, (PB2000-101697, A09, MF-A02).

MCEER-99-0014 "Nonstructural Damage Database," by A. Kao, T.T. Soong and A. Vender, 7/24/99, (PB2000-101407, A06, MF-A01).

MCEER-99-0015 "Guide to Remedial Measures for Liquefaction Mitigation at Existing Highway Bridge Sites," by H.G. Cooke and J. K. Mitchell, 7/26/99, (PB2000-101703, A11, MF-A03).

MCEER-99-0016 "Proceedings of the MCEER Workshop on Ground Motion Methodologies for the Eastern United States," edited by N. Abrahamson and A. Becker, 8/11/99, (PB2000-103385, A07, MF-A02).

MCEER-99-0017 "Quindío, Colombia Earthquake of January 25, 1999: Reconnaissance Report," by A.P. Asfura and P.J. Flores, 10/4/99, (PB2000-106893, A06, MF-A01).

MCEER-99-0018 "Hysteretic Models for Cyclic Behavior of Deteriorating Inelastic Structures," by M.V. Sivaselvan and A.M. Reinhorn, 11/5/99, (PB2000-103386, A08, MF-A02).

MCEER-99-0019 "Proceedings of the 7th U.S.- Japan Workshop on Earthquake Resistant Design of Lifeline Facilities and Countermeasures Against Soil Liquefaction," edited by T.D. O'Rourke, J.P. Bardet and M. Hamada, 11/19/99, (PB2000-103354, A99, MF-A06).

MCEER-99-0020 "Development of Measurement Capability for Micro-Vibration Evaluations with Application to Chip Fabrication Facilities," by G.C. Lee, Z. Liang, J.W. Song, J.D. Shen and W.C. Liu, 12/1/99, (PB2000-105993, A08, MF-A02).

MCEER-99-0021 "Design and Retrofit Methodology for Building Structures with Supplemental Energy Dissipating Systems," by G. Pekcan, J.B. Mander and S.S. Chen, 12/31/99, (PB2000-105994, A11, MF-A03).

MCEER-00-0001 "The Marmara, Turkey Earthquake of August 17, 1999: Reconnaissance Report," edited by C. Scawthorn; with major contributions by M. Bruneau, R. Eguchi, T. Holzer, G. Johnson, J. Mander, J. Mitchell, W. Mitchell, A. Papageorgiou, C. Scaethorn, and G. Webb, 3/23/00, (PB2000-106200, A11, MF-A03).

MCEER-00-0002 "Proceedings of the MCEER Workshop for Seismic Hazard Mitigation of Health Care Facilities," edited by G.C. Lee, M. Ettouney, M. Grigoriu, J. Hauer and J. Nigg, 3/29/00, (PB2000-106892, A08, MF-A02).

MCEER-00-0003 "The Chi-Chi, Taiwan Earthquake of September 21, 1999: Reconnaissance Report," edited by G.C. Lee and C.H. Loh, with major contributions by G.C. Lee, M. Bruneau, I.G. Buckle, S.E. Chang, P.J. Flores, T.D. O'Rourke, M. Shinozuka, T.T. Soong, C-H. Loh, K-C. Chang, Z-J. Chen, J-S. Hwang, M-L. Lin, G-Y. Liu, K-C. Tsai, G.C. Yao and C-L. Yen, 4/30/00, (PB2001-100980, A10, MF-A02).

MCEER-00-0004 "Seismic Retrofit of End-Sway Frames of Steel Deck-Truss Bridges with a Supplemental Tendon System: Experimental and Analytical Investigation," by G. Pekcan, J.B. Mander and S.S. Chen, 7/1/00, (PB2001-100982, A10, MF-A02).

MCEER-00-0005 "Sliding Fragility of Unrestrained Equipment in Critical Facilities," by W.H. Chong and T.T. Soong, 7/5/00, (PB2001-100983, A08, MF-A02).

MCEER-00-0006 "Seismic Response of Reinforced Concrete Bridge Pier Walls in the Weak Direction," by N. Abo-Shadi, M. Saiidi and D. Sanders, 7/17/00, (PB2001-100981, A17, MF-A03).

MCEER-00-0007 "Low-Cycle Fatigue Behavior of Longitudinal Reinforcement in Reinforced Concrete Bridge Columns," by J. Brown and S.K. Kunnath, 7/23/00, (PB2001-104392, A08, MF-A02).

MCEER-00-0008 "Soil Structure Interaction of Bridges for Seismic Analysis," I. PoLam and H. Law, 9/25/00, (PB2001-105397, A08, MF-A02).

MCEER-00-0009 "Proceedings of the First MCEER Workshop on Mitigation of Earthquake Disaster by Advanced Technologies (MEDAT-1), edited by M. Shinozuka, D.J. Inman and T.D. O'Rourke, 11/10/00, (PB2001-105399, A14, MF-A03).

MCEER-00-0010 "Development and Evaluation of Simplified Procedures for Analysis and Design of Buildings with Passive Energy Dissipation Systems," by O.M. Ramirez, M.C. Constantinou, C.A. Kircher, A.S. Whittaker, M.W. Johnson, J.D. Gomez and C. Chrysostomou, 11/16/01, (PB2001-105523, A23, MF-A04).

MCEER-00-0011 "Dynamic Soil-Foundation-Structure Interaction Analyses of Large Caissons," by C-Y. Chang, C-M. Mok, Z-L. Wang, R. Settgast, F. Waggoner, M.A. Ketchum, H.M. Gonnermann and C-C. Chin, 12/30/00, (PB2001-104373, A07, MF-A02).

MCEER-00-0012 "Experimental Evaluation of Seismic Performance of Bridge Restrainers," by A.G. Vlassis, E.M. Maragakis and M. Saiid Saiidi, 12/30/00, (PB2001-104354, A09, MF-A02).

MCEER-00-0013 "Effect of Spatial Variation of Ground Motion on Highway Structures," by M. Shinozuka, V. Saxena and G. Deodatis, 12/31/00, (PB2001-108755, A13, MF-A03).

MCEER-00-0014 "A Risk-Based Methodology for Assessing the Seismic Performance of Highway Systems," by S.D. Werner, C.E. Taylor, J.E. Moore, II, J.S. Walton and S. Cho, 12/31/00, (PB2001-108756, A14, MF-A03).

MCEER-01-0001 "Experimental Investigation of P-Delta Effects to Collapse During Earthquakes," by D. Vian and M. Bruneau, 6/25/01, (PB2002-100534, A17, MF-A03).

MCEER-01-0002 "Proceedings of the Second MCEER Workshop on Mitigation of Earthquake Disaster by Advanced Technologies (MEDAT-2)," edited by M. Bruneau and D.J. Inman, 7/23/01, (PB2002-100434, A16, MF-A03).

MCEER-01-0003 "Sensitivity Analysis of Dynamic Systems Subjected to Seismic Loads," by C. Roth and M. Grigoriu, 9/18/01, (PB2003-100884, A12, MF-A03).

MCEER-01-0004 "Overcoming Obstacles to Implementing Earthquake Hazard Mitigation Policies: Stage 1 Report," by D.J. Alesch and W.J. Petak, 12/17/01, (PB2002-107949, A07, MF-A02).

MCEER-01-0005 "Updating Real-Time Earthquake Loss Estimates: Methods, Problems and Insights," by C.E. Taylor, S.E. Chang and R.T. Eguchi, 12/17/01, (PB2002-107948, A05, MF-A01).

MCEER-01-0006 "Experimental Investigation and Retrofit of Steel Pile Foundations and Pile Bents Under Cyclic Lateral Loadings," by A. Shama, J. Mander, B. Blabac and S. Chen, 12/31/01, (PB2002-107950, A13, MF-A03).

MCEER-02-0001 "Assessment of Performance of Bolu Viaduct in the 1999 Duzce Earthquake in Turkey" by P.C. Roussis, M.C. Constantinou, M. Erdik, E. Durukal and M. Dicleli, 5/8/02, (PB2003-100883, A08, MF-A02).

MCEER-02-0002 "Seismic Behavior of Rail Counterweight Systems of Elevators in Buildings," by M.P. Singh, Rildova and L.E. Suarez, 5/27/02. (PB2003-100882, A11, MF-A03).

MCEER-02-0003 "Development of Analysis and Design Procedures for Spread Footings," by G. Mylonakis, G. Gazetas, S. Nikolaou and A. Chauncey, 10/02/02, (PB2004-101636, A13, MF-A03, CD-A13).

MCEER-02-0004 "Bare-Earth Algorithms for Use with SAR and LIDAR Digital Elevation Models," by C.K. Huyck, R.T. Eguchi and B. Houshmand, 10/16/02, (PB2004-101637, A07, CD-A07).

MCEER-02-0005 "Review of Energy Dissipation of Compression Members in Concentrically Braced Frames," by K.Lee and M. Bruneau, 10/18/02, (PB2004-101638, A10, CD-A10).

MCEER-03-0001 "Experimental Investigation of Light-Gauge Steel Plate Shear Walls for the Seismic Retrofit of Buildings" by J. Berman and M. Bruneau, 5/2/03, (PB2004-101622, A10, MF-A03, CD-A10).

MCEER-03-0002 "Statistical Analysis of Fragility Curves," by M. Shinozuka, M.Q. Feng, H. Kim, T. Uzawa and T. Ueda, 6/16/03, (PB2004-101849, A09, CD-A09).

MCEER-03-0003 "Proceedings of the Eighth U.S.-Japan Workshop on Earthquake Resistant Design f Lifeline Facilities and Countermeasures Against Liquefaction," edited by M. Hamada, J.P. Bardet and T.D. O'Rourke, 6/30/03, (PB2004-104386, A99, CD-A99).

MCEER-03-0004 "Proceedings of the PRC-US Workshop on Seismic Analysis and Design of Special Bridges," edited by L.C. Fan and G.C. Lee, 7/15/03, (PB2004-104387, A14, CD-A14).

MCEER-03-0005 "Urban Disaster Recovery: A Framework and Simulation Model," by S.B. Miles and S.E. Chang, 7/25/03, (PB2004-104388, A07, CD-A07).

MCEER-03-0006 "Behavior of Underground Piping Joints Due to Static and Dynamic Loading," by R.D. Meis, M. Maragakis and R. Siddharthan, 11/17/03, (PB2005-102194, A13, A03, CD-A00).

MCEER-03-0007 "Seismic Vulnerability of Timber Bridges and Timber Substructures," by A.A. Shama, J.B. Mander, I.M. Friedland and D.R. Allicock, 12/15/03.

MCEER-04-0001 "Experimental Study of Seismic Isolation Systems with Emphasis on Secondary System Response and Verification of Accuracy of Dynamic Response History Analysis Methods," by E. Wolff and M. Constantinou, 1/16/04 (PB2005-102195, A99, E08, CD-A00).

MCEER-04-0002 "Tension, Compression and Cyclic Testing of Engineered Cementitious Composite Materials," by K. Kesner and S.L. Billington, 3/1/04, (PB2005-102196, A08, CD-A08).

MCEER-04-0003 "Cyclic Testing of Braces Laterally Restrained by Steel Studs to Enhance Performance During Earthquakes," by O.C. Celik, J.W. Berman and M. Bruneau, 3/16/04, (PB2005-102197, A13, A03, CD-A00).

MCEER-04-0004 "Methodologies for Post Earthquake Building Damage Detection Using SAR and Optical Remote Sensing: Application to the August 17, 1999 Marmara, Turkey Earthquake," by C.K. Huyck, B.J. Adams, S. Cho, R.T. Eguchi, B. Mansouri and B. Houshmand, 6/15/04.

MCEER-04-0005 "Nonlinear Structural Analysis Towards Collapse Simulation: A Dynamical Systems Approach," by M.V. Sivaselvan and A.M. Reinhorn, 6/16/04.

MCEER-04-0006 "Proceedings of the Second PRC-US Workshop on Seismic Analysis and Design of Special Bridges," edited by G.C. Lee and L.C. Fan, 6/25/04.

MCEER-04-0007 "Seismic Vulnerability Evaluation of Axially Loaded Steel Built-up Laced Members," by K. Lee and M. Bruneau, 6/30/04.

MCEER-04-0008 "Evaluation of Accuracy of Simplified Methods of Analysis and Design of Buildings with Damping Systems for Near-Fault and for Soft-Soil Seismic Motions," by E.A. Pavlou and M.C. Constantinou, 8/16/04.

MCEER-04-0009 "Assessment of Geotechnical Issues in Acute Care Facilities in California," by M. Lew, T.D. O'Rourke, R. Dobry and M. Koch, 9/15/04.

MCEER-04-0010 "Scissor-Jack-Damper Energy Dissipation System," by A.N. Sigaher-Boyle and M.C. Constantinou, 12/1/04.

MCEER-04-0011 "Seismic Retrofit of Bridge Steel Truss Piers Using a Controlled Rocking Approach," by M. Pollino and M. Bruneau, 12/20/04.

MCEER-05-0001 "Experimental and Analytical Studies of Structures Seismically Isolated with an Uplift-Restraint Isolation System," by P.C. Roussis and M.C. Constantinou, 1/10/05.

MCEER-05-0002 "A Versatile Experimentation Model for Study of Structures Near Collapse Applied to Seismic Evaluation of Irregular Structures," by D. Kusumastuti, A.M. Reinhorn and A. Rutenberg, 3/31/05.

MCEER-05-0003 "Proceedings of the Third PRC-US Workshop on Seismic Analysis and Design of Special Bridges," edited by L.C. Fan and G.C. Lee, 4/20/05.

MCEER-05-0004 "Approaches for the Seismic Retrofit of Braced Steel Bridge Piers and Proof-of-Concept Testing of an Eccentrically Braced Frame with Tubular Link," by J.W. Berman and M. Bruneau, 4/21/05.

MULTIDISCIPLINARY CENTER FOR EARTHQUAKE ENGINEERING RESEARCH

A National Center of Excellence in Advanced Technology Applications

University at Buffalo, State University of New York
Red Jacket Quadrangle ▪ Buffalo, New York 14261
Phone: (716) 645-3391 ▪ Fax: (716) 645-3399
E-mail: *mceer@mceermail.buffalo.edu* ▪ WWW Site *http://mceer.buffalo.edu*

University at Buffalo *The State University of New York*

ISSN 1520-295X